

# **Microwave UWB sensors for measurements under non-stationary conditions: detection of human being beneath rubble for rescue applications**

Der Fakultät für Elektrotechnik und Informationstechnik der Technische Universität  
Ilmenau zur Erlangung des akademischen Grades Doktor-Ingenieur vorgelegte  
Dissertation

von  
Dipl.-Ing. Yahor Zaikou

geboren am 04.01.1982  
in Minsk, Weißrussland

1. Gutachter: Univ.-Prof. Dr.-Ing. habil. R. Thomä
2. Gutachter: Prof. Ing. D. Kocur
3. Gutachter: Prof. Dr.-Ing. habil. U. Pliquett

Tag der Einreichung: 21.02.1017

Tag der wissenschaftlichen Aussprache: 11.12.1017

## **Erklärung**

Ich versichere, dass ich die vorliegende Arbeit ohne unzulässige Hilfe Dritter und ohne Benutzung anderer als der angegebenen Hilfsmittel angefertigt habe. Die aus anderen Quellen direkt oder indirekt übernommenen Daten und Konzepte sind unter Angabe der Quelle gekennzeichnet.

Bei der Auswahl und Auswertung folgenden Materials haben mir die nachstehend aufgeführten Personen in der jeweils beschriebenen Weise entgeltlich/unentgeltlich geholfen:

Dr.-Ing. Jürgen Sachs

Weitere Personen waren an der inhaltlich-materiellen Erstellung der vorliegenden Arbeit nicht beteiligt. Insbesondere habe ich hierfür nicht die entgeltliche Hilfe von Vermittlungs- bzw. Beratungsdiensten (Promotionsberater oder anderer Personen) in Anspruch genommen. Niemand hat von mir unmittelbar oder mittelbar geldwerte Leistungen für Arbeiten erhalten, die im Zusammenhang mit dem Inhalt der vorgelegten Dissertation stehen.

Die Arbeit wurde bisher weder im In- noch im Ausland in gleicher oder ähnlicher Form einer Prüfungsbehörde vorgelegt.

Ich bin darauf hingewiesen worden, dass die Unrichtigkeit der vorstehenden Erklärung als Täuschungsversuch bewertet wird und gemäß § 7 Abs. 10 der Promotionsordnung den Abbruch des Promotionsverfahrens zur Folge hat.

*(Ort, Datum)*

*(Unterschrift)*

# Contents

Zusammenfassung.....	4
Abstract .....	5
1 Introduction.....	6
1.1 Search and Rescue in the disaster area.....	6
1.2 Classical equipment for Search in the disaster area .....	7
1.3 Narrowband radar for Search in the disaster area and its limitations.....	9
1.4 UWB radar for Search in the disaster area.....	10
1.5 Thesis outline and novelties of this work.....	12
2 Weakly moving object in radar response.....	14
2.1 Physical principle of radar motion detection .....	14
2.2 Graphical representation of moving object as seen by UWB radar.....	17
2.3 Minor motion in radar response and random perturbations .....	19
2.4 Minor motion detectability .....	29
2.5 Averaging in slow time and stepwise continuous motion compensation .....	32
3 Respiratory motion in noise and its enhancement .....	41
3.1 Periodical motion as seen by radar .....	41
3.2 Respiratory motion in the measured data .....	48
3.3 Spectral estimation methods and detection of periodical motion.....	52
3.3.1 Welch method in application to breathing detection.....	56
3.3.2 Bispectrum slice method .....	60
3.4 Breathing detection based on the properties of main tone respiration signature.....	62
3.4.1 FIR filtering in range direction .....	62
3.4.2 Statement of the problem of respiratory motion enhancement due to respiratory signature being range-spread.....	63
3.4.3 Optimal detection by means of correlation detector as a boundary for SNR improvement. Correlation processing with measured reference signature. ....	64
3.4.4 Energy detector (incoherent summation).....	68
3.4.5 Breathing signature enhancement via slow-time cross-correlation functions.....	69
3.5 Welch method modification.....	75
3.6 SVD-based breathing detection in the clutter-free case (reference method).....	75
3.7 Evaluation from modeling .....	77
3.7.1 Test scenarios .....	78
3.7.2 Simulation: results and discussion .....	82
3.8 Breathing detection through the heap of rubble, online measurement results .....	85
4 Clutter .....	90
4.1 Stationary clutter.....	91

4.2 Non- Stationary clutter .....	91
4.3 Simulated dataset to demonstrate algorithms that remove non-stationary clutter.....	93
4.4 SVD-based clutter removal .....	96
4.5 Clutter localization from ‘slow’ variation .....	100
4.6 Clutter removal by means of SVD after localizing it in low-frequency variation .....	102
5 Person localization by respiratory motion .....	105
5.1 Localization principle. Time of arrival and time difference of arrival estimates.....	105
5.2 Localization algorithm .....	107
5.3 Measurement results .....	108
6 Radar unit for breathing detection.....	110
6.1 SNR of the radar unit and different ways to increase target detection range .....	112
Summary.....	115
List of symbols .....	117
Reference list.....	121

## Zusammenfassung

UWB (Ultra-Wide Band) -Radar ist eine vielversprechende Möglichkeit, Menschen unter eingestürzten Gebäuden zu lokalisieren. Diese Arbeit widmet sich unterschiedlichen Wegen diese Anwendung zu verbessern.

Zu Beginn wird umfassend analysiert, wie kleine unregelmäßige Bewegungen vom Radar erfasst werden. Es wird festgestellt, dass minimale Objektbewegungen im Bereich weniger Mikrometer detektierbar sind, was viel weniger ist, als die Atembewegung eines Menschen. Weiterhin wird dargestellt, dass für die Erfassung von sehr kleinen Objektbewegungen ein sehr geringer Jitter notwendig ist. Daher wird in dieser Arbeit ein MLBS (Maximum Length Binary Sequence) Radar mit sehr geringem Jitter verwendet. Zusätzlich wird eine quantitative Bewertung der Durchschnittswertbildung vorgenommen. Als ein Hauptergebnis wurden die genauen Bedingungen für die Geschwindigkeit der Datenerfassung ermittelt, die notwendig sind, um bei gegebener Objektgeschwindigkeit die blockweise Durchschnittswertbildung für die Erfassung kleiner Objektbewegungen zu verbessern.

Eine Analyse, wie kleine periodische Bewegungen sich äußern wird gegeben. Die mathematischen Betrachtungen bestätigen, dass die menschliche Atmung vorwiegend Sinusanteile enthält, die hauptsächlich an den Taktflanken auftreten. Daher ist der Stand der Technik zur Erfassung von Atembewegungen gerechtfertigt. Analysen zeigen aber, dass Signaleigenschaften existieren, die eine Verbesserung gegenüber dem Stand der Technik zulassen. Weitergehend wird dargestellt, dass theoretisch zwei Typen von Harmonischen in den Radardaten vorhanden sind, die von der Standard-FFT nicht berücksichtigt werden. Diese Harmonischen werden genutzt, um mittels der Bispectrum-Slice – Technik das Signal zu verstärken. Es wird der Schluss gezogen, dass dieser Ansatz in der Praxis die Detektierbarkeit nur verbessert, wenn die Level der Harmonischen groß genug sind.

Eine weitere Signaleigenschaft, die in der horizontalen Standard FFT (Fast Fourier Transform) Technik nicht berücksichtigt wird, ist die Spreizung der Laufzeit in der Atmungssignatur. Es werden Algorithmen vorgestellt, die dieses Phänomen nutzen, um das Auffinden verschütteter Personen zu verbessern. Es wird die Leistungsfähigkeit dieser Algorithmen theoretisch analysiert und praktisch mit simulierten und gemessenen Radardaten überprüft. Es zeigt sich, dass sich der Störabstand durch diesen Ansatz gegenüber den Standardtechniken um mehrere dB verbessert.

Eines der Hauptprobleme beim Suchen von Überlebenden sind bewegte Objekte im Strahlengang der Antenne. In dieser Arbeit werden zwei Algorithmen zur Beseitigung dieser Störung vorgeschlagen. Beide Methoden nutzen die Tatsache dass Atembewegungen im Radargramm sehr spezifisch ausgeprägt sind und sich daher sehr gut von anderen Signalkomponenten unterscheiden lassen. Beide Algorithmen funktionieren sehr gut mit simulierten und gemessenen Radardaten.

Abschließend wird die Positionsbestimmung einer verschütteten Person beschrieben. Es wird ein entsprechender Algorithmus dargestellt und mit Messdaten in 2D und 3D getestet. Es kann der Schluss gezogen werden, dass die Positionsbestimmung erfolgreich durchgeführt werden kann, indem die Methoden der Ankunftszeitbestimmung und Differenzankunftszeitbestimmung kombiniert werden.

## **Abstract**

UWB (Ultra-Wide Band) radar is a promising tool for finding victims beneath collapsed buildings. Therefore, this thesis concentrates on different ways of improving the performance of abovementioned device.

At first thorough theoretical analysis of how minor irregular motion is seen by radar is given. It is concluded that minimal object shift detectable via radar device is in the order of dozens of micrometers, which is much lower than the amplitude of human respiration. It is also derived that in case of detecting minor motion low jitter is a key to successful performance and thus, radar unit with minimal jitter has to be used (like MLBS (Maximum Length Binary Sequence) radar considered in this thesis). Besides, the effect of averaging is analyzed quantitatively. As a main result precise condition is established on how fast we need to acquire data so that blockwise averaging would improve detectability of target displacement.

Analysis of how minor periodical motion manifests itself in the radargram is presented. It is confirmed by our mathematical considerations that respiration is to high extent sinusoidal and that it mainly appears at the pulse edge. That is, state-of-the art technique for detecting respiratory motion (FFT (Fast Fourier Transform) and maximum search) is justified. However, analysis also shows signal features that allow improvement in comparison with state of the art technique. In particular, it is derived theoretically that harmonics of two different types are present in the measured radar data (which is not respected in standard FFT data processing). These harmonics are used to amplify useful signal by means of bispectrum-slice technique. The conclusion is made that in practice this approach improves the detectability only when level of harmonics is high enough.

Another signal feature that was not respected in standard horizontal FFT technique is that respiratory signature is spread in propagation time. I propose algorithms that help to improve victim detectability via making use of this phenomenon. Performance of these algorithms is analyzed both theoretically and by means of experiments with simulated and measured radar data. It is concluded that SNR (Signal to Noise Ratio) improvement introduced via this approach over standard technique is in the order of several dB.

With respect to radar as a tool for search and rescue, major problem is identified as strongly moving objects within antenna beam. In this thesis, two original algorithms for removing this perturbation are proposed. Both methods make use of respiratory motion looking very specific in the radargram which fact helps to separate it from other signal components. Algorithms show high performance in tests both with simulated and measured datasets.

At the end problem of finding the person position is addressed. I present localization algorithm and test it with experimental radar data both in 2D and in 3D .It can be concluded that localization can be performed successfully we combining TOA/TDOA (Time of Arrival/ Time Difference of Arrival) estimates.

# 1 Introduction

According to [26] more than 800 000 deaths occurred worldwide in 2000 through 2012 due to the earthquakes while the number of major earthquakes remains relatively constant. Thus, increasing the survivability rate among the people trapped beneath the collapsed building remains an important issue.

## 1.1 Search and Rescue in the disaster area

Information in this part is given according to the description from [4]. Urban search and rescue in progress is shortly sketched in figure 1.1

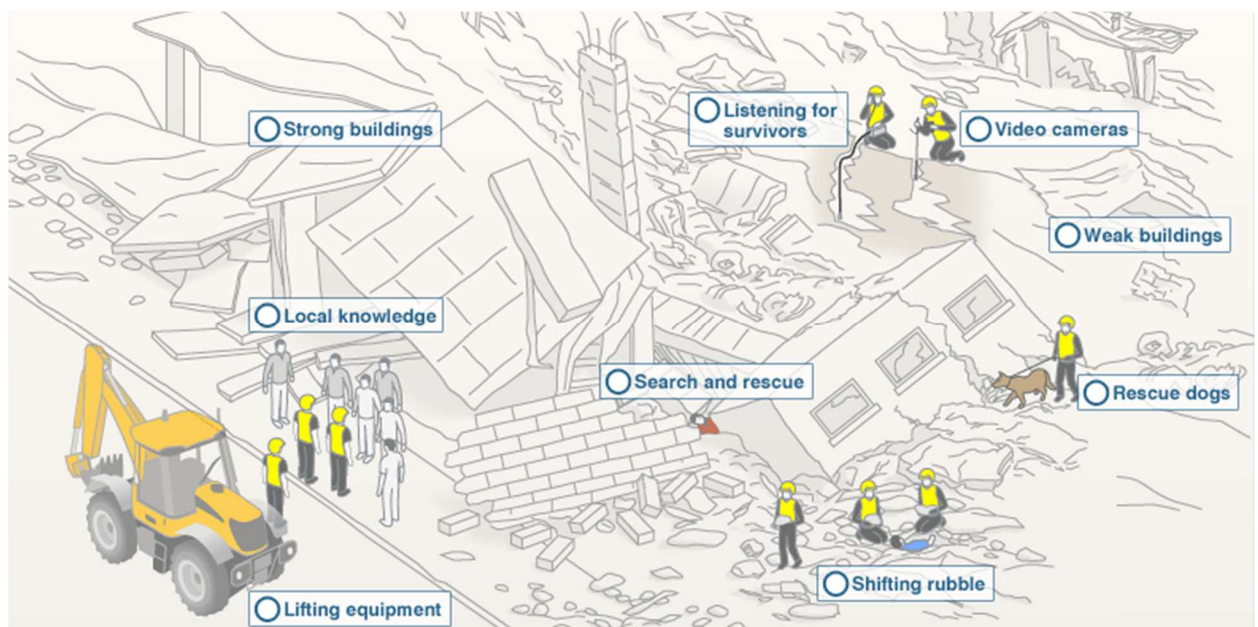


Figure 1.1 Urban Search and Rescue (courtesy of BBC)

The procedure starts with gathering the local information in order to define the most promising locations for the search. Another type of useful information is connected with the type and structure of collapsed buildings: the building is not always completely destroyed and in the case of remaining building structure there are certain places like stairwells that produce voids. Inside such voids people are more likely to be found alive than in other places. The time factor to detect such people is absolutely crucial at this stage.

In order to remove the rubble, rescuers use heavy machinery (diggers and hydraulic jacks) how it is shown in figure 1.2. However, the situations of shifting the rubble by softer means (shovels for example) are not uncommon. In this case, chainsaws and

disc-cutters can be used to tackle the reinforced concrete. The reason might be not only the absence of heavy machinery in the disaster area, but also the fear to harm trapped people by incautious rubble shift.



Figure 1.2 Different types of collapsed buildings

The difficult decision that rescuers should switch to another location where there is bigger probability to find the survivors is usually taken between five and seven days after starting the operation, although there is a case known when person was saved after being trapped for 13 days.

### ***1.2 Classical equipment for Search in the disaster area***

The problem of rescuing people from beneath the collapsed buildings does not have an ultimate technical solution that would guarantee efficient detection and localization of victims. After determining the prospective locations, search is committed with the help of following technical means (here they are listed alongside the factors limiting their performance):

- Cameras with long optical fibers that are injected into the holes or fissures in the collapsed buildings (shown in figure 1.3). Often such device can sense in infrared. This broadens their detection ability, since person outside rescuers line of sight heats the surrounding material. This heated area can be detected by infrared imaging. The usability of such devices and their efficiency depend on the structure of collapsed building and besides, when the victim is detected it is difficult in the most cases to determine its actual position.
- Sledge hammers are used to give a signal to potential victims, and rescuers with microphones are waiting for hearing the response (such set of equipment is shown in figure 1.4). Microphones used for this purpose are sensitive enough to



catch the slightest sound within several meters. Obvious limitation of this method is that unconscious people cannot be detected. Localization of victims is a problem as well. Besides, this method requires complete silence in the disaster area. This is often hard to reach in practice.

### Thermal imaging camera & video camera with flexible pole

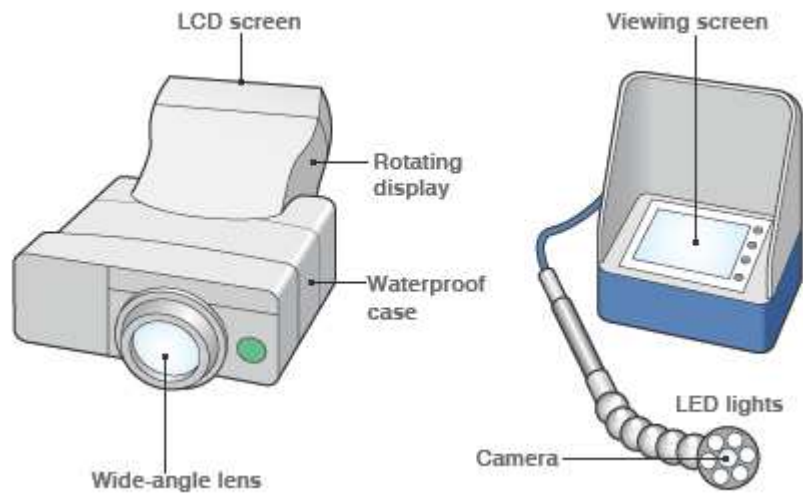


Figure 1.3 Video camera designed for survivor search (courtesy of BBC)

### Listening equipment and carbon dioxide detector

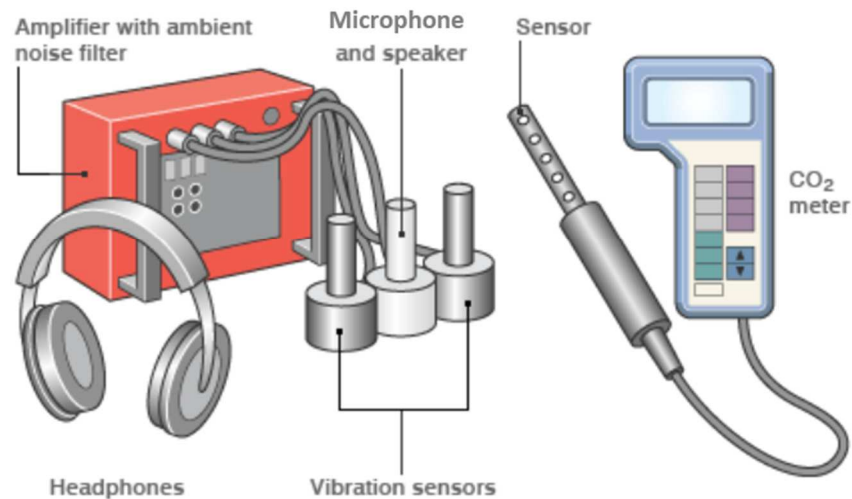


Figure 1.4 Listening equipment and carbon dioxide detector for survivor search (courtesy of BBC)

- Carbon dioxide detectors can be used to find the unconscious victims (figure 1.4). However, they work best in confined spaces where they detect the greater CO<sub>2</sub> concentration in the air exhaled by those still breathing. Besides,

performance of such sensors is obviously limited by the necessity to have the airflow between the sensor and a victim.

- Search dogs are deployed in the disaster area (figure 1.5). They detect presence of victims efficiently by smell, but information about their actual positions or quantity cannot be indicated. Moreover, dog is likely to indicate the presence of dead person which distracts rescuers from locations where living people can still be found. Obvious advantage of the search dogs is that they complete search in the wide area within a short time.



Figure 1.5 Search dog in the disaster area

This set of equipment represents state of the art of technique for Urban Search and Rescue

### ***1.3 Narrowband radar for Search in the disaster area and its limitations***

Historically interferometric and Doppler radars were the first radar sensors used for breathing activity monitoring. First experiments were carried out as early as the first half of 70s. Later narrowband systems were developed and tested with respect to urban search and rescue (USAR) scenarios. To name a few:

- In [2] prototype radar device is described, which is capable of detecting human breathing through at least 2 meters of diverse debris. Operating frequency is 1.2 GHz.
- Commercial Bioradar BR402 by BOS - Sondermaschinenbau GmbH is a narrowband device with operating frequency 1 299 MHz. According to its

description 'is able to detect objects through dielectric materials like normal brick walls or concrete walls (even adjacent walls), layers of sand, rubble, soil and snow up to thickness of several metres or other nonmetallic obstacles to visibility. Metal parts (e.g. steel reinforcements of concrete) always reduce the sensitivity depending on the quantity of metal' [6]. Remarkable penetration ranges are mentioned:" 3-8 m with brick walls, 1 m with concrete, 3-4 m through debris and rubble, (BOS - Sondermaschinenbau GmbH).



Figure 1.6 Bioradar BR402 by BOS - Sondermaschinenbau GmbH, [6]

In general we can state that reported depth were breathing is detected with narrowband radar is higher than that for UWB radars. This can be explained by notion that radar electronics in the case of narrowband device produces less noise in comparison with UWB radar (due to applying sub-sampling in the latter). However, narrowband radars have poor resolution capacity and that is, they do not provide sufficient abilities to detect multiple persons or, most importantly, to determine the position of trapped victim. Besides, there are much more possibilities for cancellation of clutter arising from moving surrounding in UWB radar.

#### ***1.4 UWB radar for Search in the disaster area***

Like in many other applications of short-range radars the main advantage of using them in Search&Rescue arises from ability of electromagnetic waves to penetrate obstacles

(building materials in our case) and significant range resolution. More specifically, with relation to state of the art techniques the main benefits expected from UWB radar are following:

- *Ability to localize trapped victims.* Techniques used by rescue services at present mostly do not provide reliable information about actual location of trapped person, although some of them a priori outperform UWB radar in terms of penetration depth in many scenarios (narrowband radars, search dogs, sledge hammers). UWB system is expected to bring ability to localize person due to remarkable range precision in order of few centimetres.
- *Detection of unconscious victims.* Some conventional methods (like sledge hammers) rely on response from trapped person. However, unconsciousness of person (or his/her inaptness to act in a certain way) should not be an obstacle for rescuing him or her. For this reason, we describe a device here that detects victims by their breathing and provide measurement examples and system parameters with respect to breathing only.
- *Detection of multiple persons.* In order to let rescuers evaluate the situation in disaster area, UWB radar brings abilities to detect multiple victims both by breathing rate and because of different positions of victims. Again, this can hardly be reached by techniques in use.
- *Detection through at least 1—2 meters of rubble.* Penetration depth has to be high enough in order to make all abovementioned points useful in practice.

It should be mentioned, that most of the early research in the area of breathing-detecting UWB radar was concentrated on ability to detect one person through wall in GHz range. Diverse hardware and algorithms taking into account periodicity of respiration are proposed for this purpose in [7], [13], [21] along with measurement examples. However, we could find out that in much earlier research [9] real through-rubble breathing detection was attempted (in the most cases successfully). Rubble consisted of one/two (depending on particular scenario) concrete slabs and concrete tube. In this work significant efficiency of FFT in amplifying breathing in noisy surrounding is demonstrated. Besides, strong dependency of breathing visibility on the magnitude of respiratory motion is shown.

Importantly, in [14] ability to detect multiple breathing persons is proven experimentally. Later, extensive experimental study of this topic with dozens of people under test and wall/no wall measurement scenarios confirmed high ability of UWB radar to detect multiple victims in [34].

Although most of the researches use FFT to treat the periodicity of breathing, in [27] the example of using MUSIC (Multiple Signal Classification) spectral estimate is given. In signal processing non-stationarity of breathing received considerable attention recently [17] and earlier in [19]. In [16] tracking algorithm for varying breathing frequency is proposed. In general, non-stationarity of respiratory activity is a major topic for health-monitoring microwave systems.

Besides, an interesting approach is presented in [15]: slowly moving object is detected with moving antenna array by means of Fourier Processing and Principal Component Analysis (PCA). Thorough research on our topic is given in the PHD thesis [35]. In this work we often use methods from these thesis as a reference technique.

Last but not least, there is a commercially available device for detecting people beneath the rubble: LifeLocator™ by UltraVision Security Systems, Inc. Citation from [25]: ‘Detection Distance through Debris Pile: Up to 15’ (4.6 meters) for breathing , up to 20’ (6.4 meters) for motion ’. Rubble type for these particular rubble sizes is not specified.

### ***1.5 Thesis outline and novelties of this work***

As we have seen above, previously reported research in breathing detection with UWB radar was mainly concentrated on detection and enhancement of useful signal. While viable data processing methods proposed are diverse, according to [28], the fact that UWB radar allows for positioning of trapped victim have not been proven experimentally. The problems of multiple victims and clutter did not receive much attention as well.

This thesis is organized in the following way:

- In chapter 2 we consider minor motion in general and address the question about how small is the motion that can be detected by radar device and discuss how different types of UWB radar compare to one another with respect to the topic of this thesis. Also, we consider quantitatively the efficiency of averaging as a tool of making minor motion more visible. Some considerations given in this chapter were published beforehand in [22], [23] and [24]
- In chapter 3 we present original investigation into how respiratory motion looks on the radar screen and why. After that based on this investigation we discuss the efficiency of different techniques (both commonly used and original ones) for enhancing the respiratory motion in comparison with noise. Our conclusions are supported both with theoretical considerations and with practical results.

- In chapter 4 we discuss how to detect respiratory motion in the presence of strongly moving unwanted objects. We present our own techniques previously reported in [30], [32] that are based on a priori information about the unwanted motion and compare them with reference method from [35], [20]
- In chapter 5 we briefly present our approach to localization of trapped people by their respiratory motion. First results on this topic were published in [30], [31] and to our knowledge it was a first example of such results reported in literature.
- Even though in this thesis we are mainly dealing with algorithm for respiratory motion enhancement and localization (and thus our main results are applicable in combination with any UWB radar system), all experiments were carried out with high-precision low-jitter M-sequence radar unit. Its characteristics are given in chapter 6.

## 2 Weakly moving object in radar response

In this chapter at first it is mathematically described why how moving objects are seen by the radar. After that, radar sensitivity to weak object motion in presence of random perturbations (noise and jitter) is considered. In the end, we discuss averaging and how it affects object detectability.

### 2.1 Physical principle of radar motion detection

Let us consider how object of interest (person under test, PUT) is detected by means of UWB radar. Basic measurement scenario is sketched in figure 2.1. Probing time signal  $A(t)$  generated by means of radar electronics and converted into electromagnetic waves via antenna system in this form propagates (partly) in the direction of test person. Due to dielectric contrast between the medium and biological tissue electromagnetic waves are (partly) reflected and after propagating back they reach antenna system once again. Further they are converted into signal  $W(t)$  which is captured by the receiver part of radar electronics.

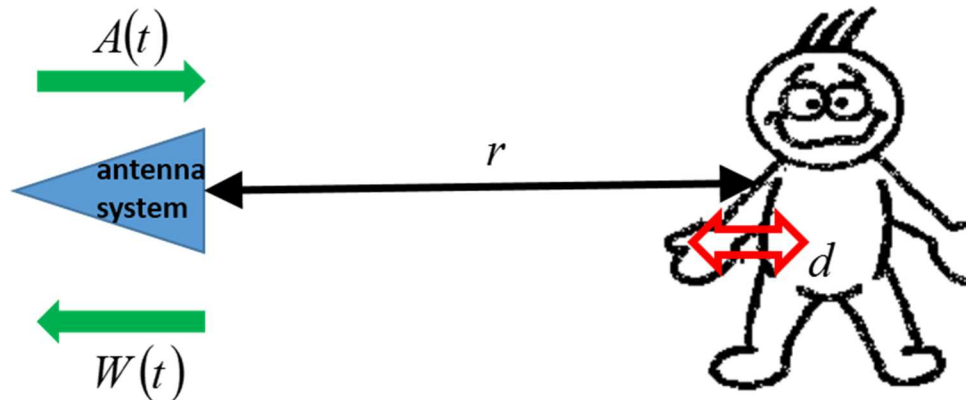


Figure 2.1: Basic scenario for radar measurements with one PUT

In what follows we suppose  $B_1(t)$  and  $B_2(t)$  to be IRFs (impulse response functions) of the antenna system in receive and transmit mode. Reflection from the person is characterized by  $C(t)$ . Under some omissions (we suppose at this stage no propagation loss, no antenna reflections, omitting angular dependencies, no noise) we can reconstruct the received signal  $W(t)$  by consequently convolving all the transfer functions described above:

$$W(t) = \frac{A(t) * B_1(t) * \delta\left(t - \frac{r}{c}\right) * C(t) * \delta\left(t - \frac{r}{c}\right) * B_2(t)}{2r \dots r^2} \quad (2.1)$$

Two terms  $\delta\left(t - \frac{r}{c}\right)$  in equation 2.1 represent delay of spherical electromagnetic waves due to propagation from antennas towards PUT and back.  $r$  is the distance from antenna system to the chest of test person.

Of course, reflection from any particular target depends on its shape. Shapes of real measurement objects (like human chest in this work) are complicated and there is no precise knowledge about how they affect received signal and its dependency on  $r$ . In equation 2.1 we suppose two possible geometrical shapes of the object for which  $W(r)$  dependencies are known:

- A sphere, the only object of finite dimensions whose scattering is analytically modelled [23], is often used as a model that approximates scattering behaviour of more complex shapes. It is shown in [23] that given radar frequency range of  $\Delta F \approx 2$  GHz, denominator in equation 2.1 is  $r^2$  in case sphere is a measurement object
- A large plane and a corresponding to it denominator in equation 2.1  $2r$  (this is shown in [11])

For the typical measurement object of this work (human chest), there seems to be no reason to suppose that with  $r$  decreasing amplitude of the object response as seen by the radar will decay slower than in the case of large plane. Actually, our measurement object resembles the sphere much more.

After grouping up some terms inside  $W_0(t)$  in order to simplify the expression, we can rewrite equation 2.1 in the following form:

$$W(t) = W_0(t) * \frac{\delta\left(t - \frac{2r}{c}\right)}{2r \dots r^2} \quad (2.2)$$

In this work we detect PUT due to his/her motion. That is we do not consider  $r$  constant it depends on time:

$$r(\tau) = r_0 + d(\tau) \quad (2.3)$$

Here  $\tau$  is the time instant when particular radar impulse response function (IRF) was collected. In this work  $\tau$  is referred as observation time (or slow time, in the range of seconds) in contrast to propagation time  $t$  (or fast time since its typical values are in the



range of nanoseconds) related to propagation of electromagnetic waves. In 2.3  $r_0$  is initial distance between PUT and antennas ( $r_0 = r(0)$ ) and  $d(\tau)$  is an object displacement.

After introducing PUT motion in 2.3 we come to ‘fast time’—‘slow time’ representation of object motion as seen by radar device:

$$W(t, \tau) = W_0(t) * \frac{\delta\left(t - \frac{2r(\tau)}{c}\right)}{2r(\tau) \dots r^2(\tau)} \quad (2.4)$$

In this work we are especially interested in weak, or minor motion. Condition for target displacement being minor can be formulated in the following way:

$$d \ll r_0 \quad (2.5)$$

Expression 2.5 holds for the typical measurement scenarios of this work: trapped person is separated from antennas by at least several dozens of centimetres of building material.

After applying geometric series to the denominator in 2.4

$$\frac{1}{r(\tau)} = \frac{1}{r_0 + d(\tau)} = \frac{1}{r_0} \left( 1 + \left( -\frac{d}{r_0} \right) + \left( -\frac{d}{r_0} \right)^2 + \dots \right) \quad (2.6)$$

$$\frac{1}{r^2(\tau)} = \frac{1}{(r_0 + d(\tau))^2} = \frac{1}{r_0^2} \left( 1 + \left( -\frac{2d}{r_0} - \frac{d^2}{r_0^2} \right) + \left( -\frac{2d}{r_0} - \frac{d^2}{r_0^2} \right)^2 + \dots \right)$$

and using  $\delta$  properties 2.4 becomes:

$$W(t, \tau) \approx \left[ \frac{W_0(t) * \delta\left(t - \frac{2r_0}{c}\right)}{2r_0 \dots r_0^2} * \delta\left(t - \frac{2d(\tau)}{c}\right) \right] \left( 1 - (1 \dots 2) \frac{d(\tau)}{r_0} \right) \quad (2.7)$$

As it can be seen in 2.7, breathing modulates received radar signal in two ways. First, there is amplitude modulation with a term  $\left( 1 - (1 \dots 2) \frac{d(\tau)}{r_0} \right)$ . However, given equation

2.5, this is a minor effect.

Much more importantly, received signal is modulated in propagation time and this type of modulation serves as a basis for the detection of minor motion in radar data. In order to underline this, we rewrite equation 2.7 after amplitude modulation is ignored:

$$W(t, \tau) \approx \frac{W_0(t)}{2r_0 \dots r_0^2} * \delta\left(t - 2 \frac{r_0 + d(\tau)}{c}\right) \quad (2.8)$$

And, finally, we can rewrite 2.8 in a shorter form which is convenient to use in further discussions:

$$W(t, \tau) \approx \frac{W_0(t) * \delta\left(t - 2\frac{r_0}{c}\right)}{2r_0 \dots r_0^2} * \delta\left(t - 2\frac{d(\tau)}{c}\right) = W_s(t) * \delta\left(t - 2\frac{d(\tau)}{c}\right) = W_s\left(t - 2\frac{d(\tau)}{c}\right) \quad (2.9)$$

$W_s$  is a radar pulse  $W$  shifted to the target initial position  $r_0$ . Values  $t$  and  $\tau$  can be interpreted as discrete variables  $t = l\Delta t$  and  $\tau = m\Delta \tau$  where  $\Delta t$  and  $\Delta \tau$  represent sampling intervals in fast time and slow time,  $l$  and  $m$  are corresponding indices. In this case we deal with matrix  $\mathbf{W}(\mathbf{t}, \boldsymbol{\tau})$

## 2.2 Graphical representation of moving object as seen by UWB radar

At every  $\tau$  instant radar device collects an IRF that may contain reflection from one or more objects. In case UWB radar is used each of these reflections is represented as a short pulse (shown, for example, in figure 2.2).

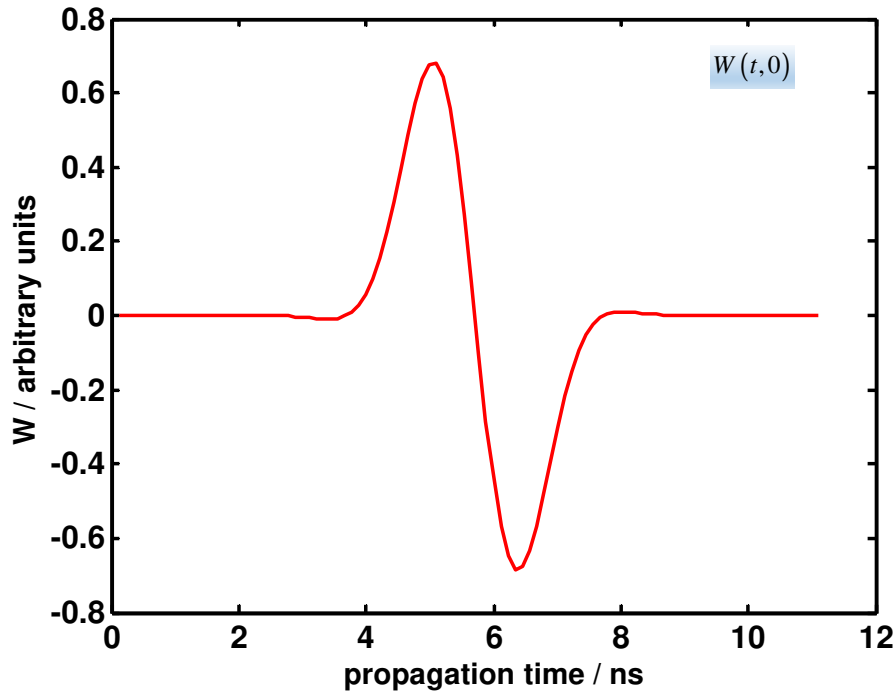


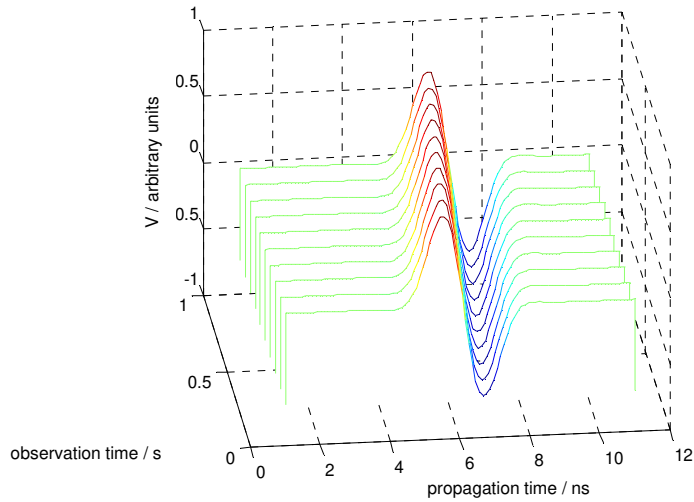
Figure 2.2: Simulated object reflection in the radar data

With the observation time going, we consequently acquire a number of IRFs and as a result we have a set of radar responses (in this work this set is denoted as radargram).

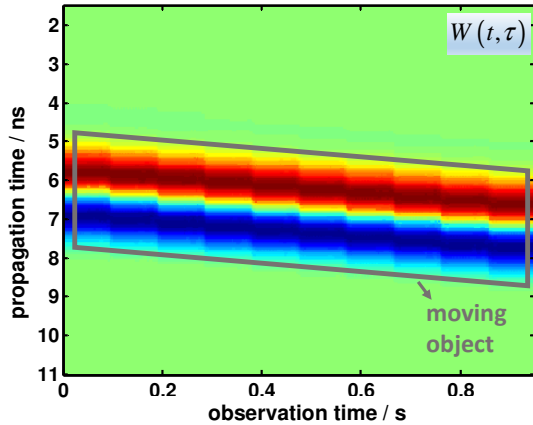
In case object was moving corresponding pulse in this set of IRFs is changed (more particular, in case of minor motion it is shifted according to expression 2.9).

Example of representing radargram as a set of IRFs is shown in figure 2.3, A. In this case object was moving with constant velocity.

**A**



**B**



**C**

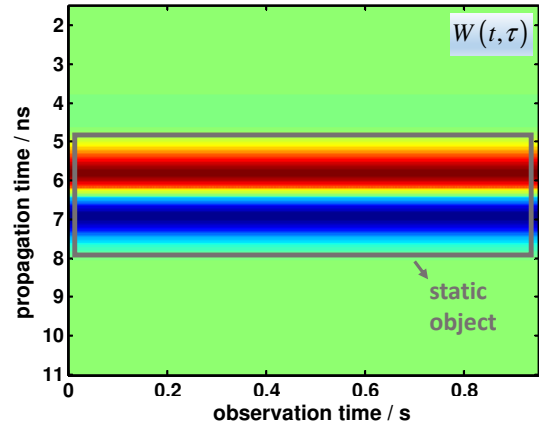


Figure 2.3: Modelled target radargrams: A, B: forwardly moving target and C: motionless target.

Though it is the most complete one, representation shown in figure 2.3 A is, however, not the best in terms of minor motion visibility. Thus, in order to show the target motion in this work two-dimensional images constructed from the set of radar responses are used. Color of each particular image bin is determined by the voltage value collected by the radar device. In such 2d image all necessary information about target motion, noise, clutter, etc is presumed and represented. Two examples of such images are shown in

figure 2.3: the object is moving forwardly from the antennas (B) and standing still (C). Difference in motion character in this two images is visible.

In some cases we are interested in underlining how radar data changes at certain instants of fast time. In this case we use horizontal line lookup like in figure 2.4.. Target object gradually ‘disappears’ (signal value approaches zero) for the earlier fast-time instant and the target gradually ‘appears’ for the later fast-time as it should be for the object moving away from antennas.

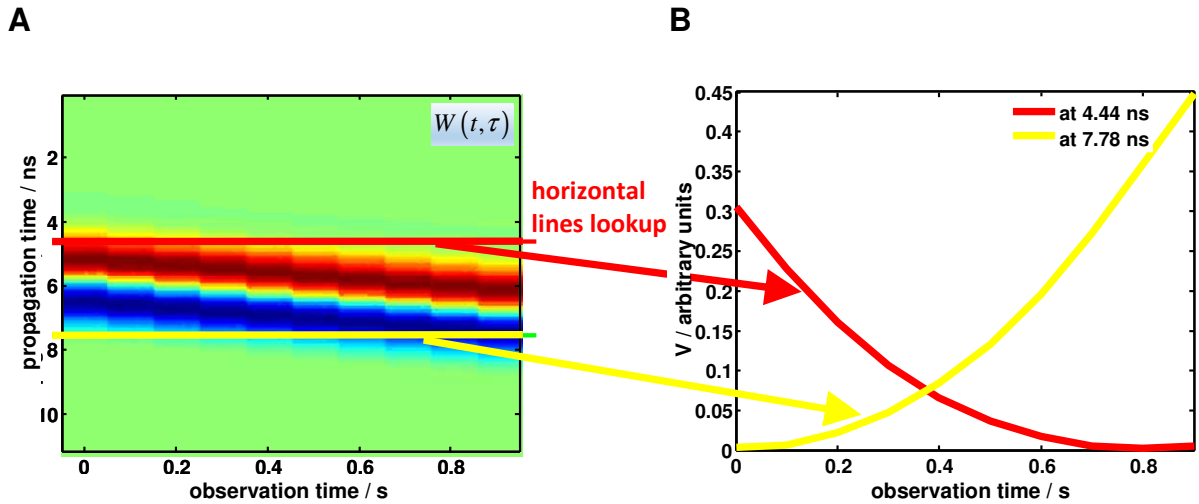


Figure 2.4: Forwardly moving target radargram (A) and as seen at two particular fast-time instants (B)

### 2.3 Minor motion in radar response and random perturbations

Most of this thesis is dealing with different methods that alleviate negative effect of random perturbations on the detectability of useful signal. At first, however, these perturbations have to be described. Essentially, in the radar data we can encounter following random contributors:

1. Additive noise. The dominant additive noise component is thermal (or Johnson-Nyquist) noise in the receiving part of radar electronics. Its source is thermal agitation of free charges and it is well-known that thermal noise  $n_T$  is Gaussian distributed ( $N$ ) with zero mean and standard deviation  $\sigma_T$  :

$$n_T(t, \tau) \sim N(0, \sigma_T^2) \quad (2.10)$$

2. Quantization noise. This error is produced due to transforming continuous signal into a discrete one by means of ADC. For obvious reasons this transformation is only possible with the precision of ADC step  $\mu$ . Thus, as it is shown in many

sources, quantization error of an ideal ADC  $n_\mu$  is uniformly distributed over interval  $\left[-\frac{\mu}{2}, \frac{\mu}{2}\right]$ . The variance of such distribution is given by:

$$\sigma_\mu^2 = \frac{\mu^2}{12} \quad (2.11)$$

Given ADC choice for the radar used in this work, we can safely suppose that following inequality is fulfilled:

$$\sigma_\mu^2 \leq \sigma_T^2 \quad (2.12)$$

Due to expression 2.12 deviation of total additive noise from being Gaussian is negligible. Thus, we suppose that in total additive noise is Gaussian and zero-mean:

$$n = n_\mu + n_T \sim N(0, \sigma^2) \quad (2.13)$$

3. Sampling jitter. In general, sampling jitter  $\Delta\psi(t, \tau)$  can be defined as a random perturbation a radargram sampling instances. We consider normally distributed sampling jitter with standard deviation  $\sigma_j$  and zero mean:

$$\Delta\psi(t, \tau) \sim N(0, \sigma_j^2) \quad (2.14)$$

4. Besides, typically there are multiple unwanted reflecting objects to be found in the area where radar is used. In general, their contribution into radargram is referred to as clutter. We make difference between reflections from static objects (stationary clutter) and reflections from moving background (non-stationary clutter).

In order to investigate how abovementioned perturbations affect radargram  $W(t, \tau)$ , let us introduce its 'randomized' version  $\widehat{W}(t, \tau)$ .  $\widehat{W}(t, \tau)$  includes additive noise and jitter:

$$\widehat{W}(t, \tau) = W(t + \Delta\psi(t, \tau), \tau) + n(t + \Delta\psi(t, \tau), \tau) \quad (2.15)$$

In order to get explicit dependency of  $\widehat{W}$  on  $\Delta\psi$  we can develop equation (2.15) in Taylor series. If we take into account noise ergodicity and suppose that random effects are small and thus neglect their terms of the order higher than one we get:

$$\widehat{W}(t, \tau) \approx W(t, \tau) + \dot{W}(t, \tau)\Delta\psi(t, \tau) + n(t, \tau) \quad (2.16)$$

Equation 2.16 is illustrated in figure 2.5: we see, that since jitter is proportional to  $\dot{W}(t, \tau)$  it has big influence on the signal edge and it is almost zero when  $W(t, \tau)$  tends to be constant.

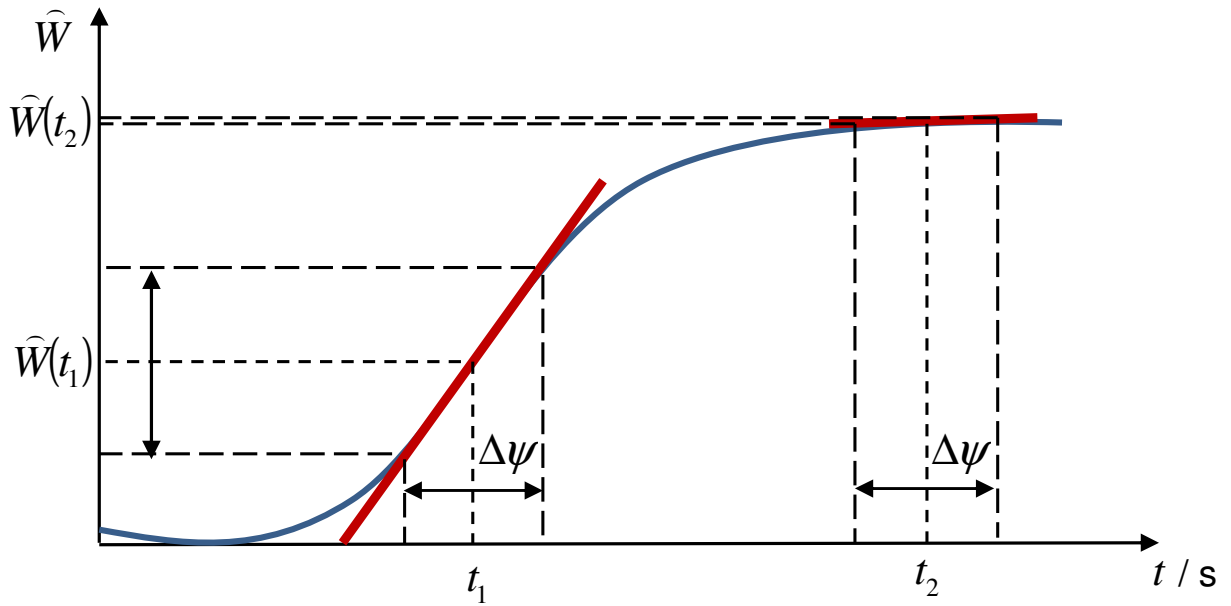


Figure 2.5: influence of jitter in the radar IRF

Jitter is a very ‘unpleasant’ perturbation of the radar data for anybody oriented at detecting minor motion. The very fact that jitter-induced noise depends on the signal shape (as it is seen in eq. 2.15) makes it hard to treat it properly in terms of increasing the detectability of useful signal component. Moreover, jitter manifests itself in the radar data exactly the same way as minor motion does, since the target motion might also be seen as a change in the sampling instances. This fact makes it virtually impossible to unambiguously separate jittering waveform from the moving object (if no a priori information about the character of object trajectory is available).

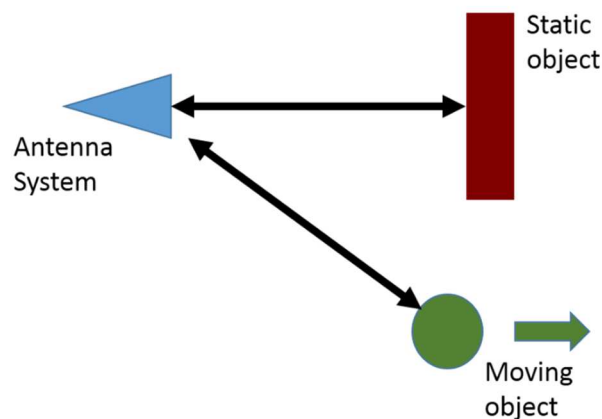


Figure 2.6: Measurement scenario corresponding to equation 2.17

In order to discuss additional problems arising due to the jitter presence, let us consider particular measurement scenario (shown in figure 2.6): strongly reflecting static object

(its response in the measured data is  $W_1(t, \tau) = W_1(t)$ ) is shadowing moving object ( $W_2(t, \tau)$ ).

Such scenario is often met in practice, unwanted static object being stationary clutter: air-rubble interface, wall, or any reflecting object. Moving object represents target of interest. This scenario is also considered in [38]. Here, however, we make emphasizes on weak and periodical motion. Radargram, corresponding to the scenario, with noise and jitter included is given by:

$$\widehat{W}(t, \tau) = W_1(t + \Delta\psi(t, \tau), \tau) + W_2(t + \Delta\psi(t, \tau), \tau) + n(t + \Delta\psi(t, \tau), \tau) \quad (2.17)$$

In this work, we are interested in moving objects only; stationary background(clutter) has to be removed. The standard way to do this in practise is to calculate average in slow time and to subtract result from the measured data:

$$\widehat{W}_{rb}(t, \tau) = \widehat{W}(t, \tau) - \overline{\widehat{W}(t, \tau)} \quad (2.18)$$

Here we suppose that object motion and noise is mainly suppressed by averaging,  $\overline{\widehat{W}_2(t, \tau)} \approx 0$ . How efficient was our background subtraction we can determine by analysing expected value and variance of a time-variable radargram, random process  $\widehat{W}_{rb}(t, \tau) = [\widehat{W}_{rb}^{(1)}(t, \tau), \widehat{W}_{rb}^{(2)}(t, \tau), \dots, \widehat{W}_{rb}^{(n)}(t, \tau), \dots]$  consisted of numerous realizations of  $\widehat{W}_{rb}^{(n)}(t, \tau)$ :

$$\begin{aligned} \mathbb{E}\{\widehat{W}_{rb}(t, \tau)\} &= \lim_{N \rightarrow \infty} \frac{1}{N} \sum_{n=1}^N \widehat{W}_{rb}^{(n)}(t, \tau) \\ \text{var}\{\widehat{W}_{rb}(t, \tau)\} &= \mathbb{E}\{\widehat{W}_{rb}^2(t, \tau)\} - (\mathbb{E}\{\widehat{W}_{rb}(t, \tau)\})^2 \end{aligned} \quad (2.19)$$

In order to calculate 2.19 we will need approximations for expected value and variance of arbitrary function  $f$  of a random variable  $x$  with  $\mathbb{E}\{x\} = \mu_x$  and  $\text{var}\{x\} = \sigma_x^2$  in the vicinity of  $\mu_x$ . In order to derive this expressions we first use Taylor series expansion and cut the terms of an order higher than two:

$$f(x) \approx f(\mu_x) + \dot{f}(\mu_x)(x - \mu_x) + \frac{\ddot{f}(\mu_x)}{2}(x - \mu_x)^2 \quad (2.20)$$

Now we can put down expected value of this function:

$$\mathbb{E}\{f(x)\} \approx \mathbb{E}\left\{f(\mu_x) + \dot{f}(\mu_x)(x - \mu_x) + \frac{\ddot{f}(\mu_x)}{2}(x - \mu_x)^2\right\} = f(\mu_x) + \frac{\ddot{f}(\mu_x)}{2}\sigma_x^2 \quad (2.21)$$

Here we have taken into account that  $E\{x - \mu_x\} = 0$  by definition of expected value and  $E\{(x - \mu_x)^2\} = \sigma_x^2$  by definition of variance.

In order to calculate  $\text{var}\{f(x)\}$  we use Taylor series expansion and limit ourselves to terms of an order lower than two:

$$f(x) \approx f(\mu_x) + \dot{f}(\mu_x)(x - \mu_x) \quad (2.22)$$

When we apply this approximation and simplify expressions the same way as in (2.21), we get:

$$E\{f^2(x)\} \approx E\{f^2(\mu_x) + \dot{f}^2(\mu_x)(x - \mu_x)^2 + f(\mu_x)\dot{f}(\mu_x)(x - \mu_x)\} = f^2(\mu_x) + \dot{f}^2(\mu_x)\sigma_x^2 \quad (2.23)$$

And

$$E^2\{f(x)\} \approx f^2(\mu_x) \quad (2.24)$$

As a result, expression for variance is given by:

$$\text{var}(f(x)) = E\{f^2(x)\} - E^2\{f(x)\} \approx \dot{f}^2(\mu_x)\sigma_x^2 \quad (2.25)$$

In what follows we consider  $\widehat{W}_1(t + \Delta\psi)$  as a function of random variable  $x := t + \Delta\psi$ . That is,  $E\{x\} = t$  and  $\text{var}\{x\} = \sigma_j^2$ . In line with 2.21 we can state for horizontally averaged time- variable waveform that:

$$\overline{\widehat{W}_1(t, \tau)} \approx E\{\widehat{W}_1(x)\} \approx W_1(t) + \frac{\ddot{W}_1(t)}{2}\sigma_j^2 \quad (2.26)$$

Now let us calculate expected value of time-variant waveform after subtracting horizontally averaged signal. For this purpose we use result from 2.26 and apply 2.21 again:

$$E\{\widehat{W}_1(t, \tau) - \overline{\widehat{W}_1(t, \tau)}\} \approx E\left\{\widehat{W}_1(x) - W_1(t) - \frac{\ddot{W}_1(t)}{2}\sigma_j^2\right\} + W_2(t, \tau) \approx W_2(t, \tau) \quad (2.27)$$

As for estimating the variance of time-variant waveform with high precision, we can use Bienayme equality, (it states that variance of the sum of uncorrelated variables equals sum of their variances). Accordingly:

$$\text{var}\{\widehat{W}_1(t, \tau) - \overline{\widehat{W}_1(t, \tau)} + n(t, \tau)\} \approx \text{var}\{\widehat{W}_1(t, \tau)\} + \text{var}\{\overline{\widehat{W}_1(t, \tau)}\} + \sigma^2 \quad (2.28)$$

It follows from Bienayme equality that  $\text{var}\{\overline{\widehat{W}_1(t, \tau)}\} = \frac{1}{K}\text{var}\{\widehat{W}_1(t, \tau)\}$  and in equation 2.25, we see that  $\text{var}\{\widehat{W}_1(t, \tau)\} = \dot{W}_1^2(t)\sigma_j^2$ . Therefore, 2.28 can be rewritten like:



$$\text{var}\left\{\widehat{W}_1(t, \tau) - \overline{\widehat{W}_1(t, \tau)} + n(t, \tau)\right\} \approx \left(1 + \frac{1}{K}\right) \dot{W}_1^2(t) \sigma_j^2 + \sigma^2 \quad (2.29)$$

We can see in equation 2.29 that it is impossible to get rid of the static reflection  $W_1(t)$  by subtracting it from the radar data in case jitter is not negligible since jitter causes noise increase at the propagation time where static object is situated. In order for target reflection  $W_2(t, \tau)$  to be detected its magnitude must of course be significantly higher

than standard deviation of the false target  $\sqrt{\dot{W}_1^2(t) \left(1 + \frac{1}{K}\right) \sigma_j^2}$ . Thus, radar performance

degrades in the case when object of interest is shadowed by clutter even when this clutter is stationary.

In order to demonstrate how jitter affects radar data in practice, two simple simulations were done. In the first case (figures 2.7 and 2.8) forward motion is simulated with velocity 3.8 cm/s.

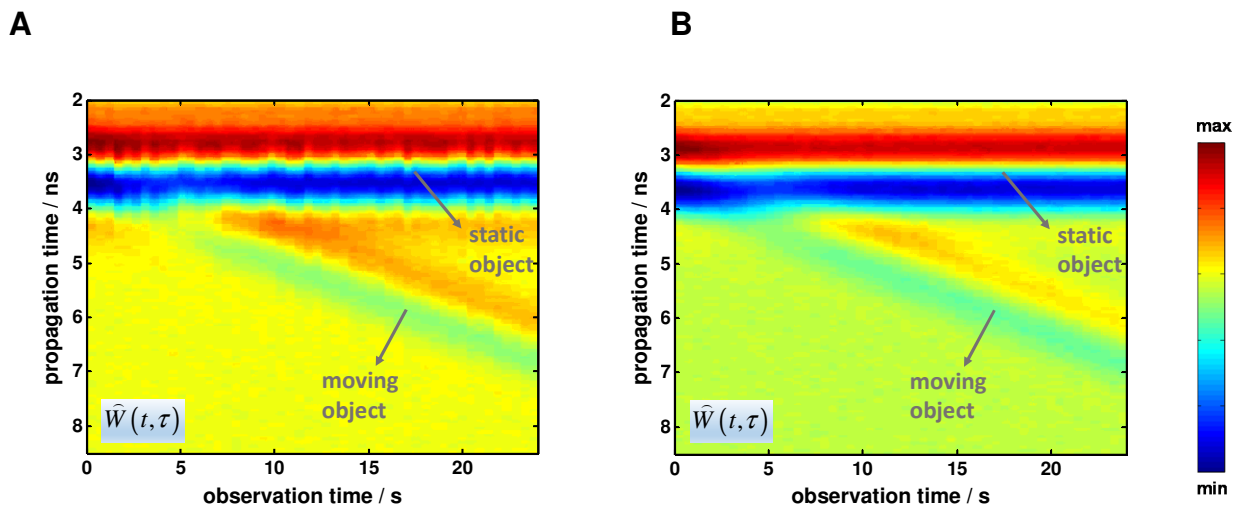


Figure 2.7: Simulated radargram of forwardly moving object in the presence of static reflector: without jitter (A) and with jitter (B)

We can see in figure 2.7, A that reflection from moving object was weaker than from the static one (how it is supposed in our scenario). In figure 2.7, B we can already mention how jitter influenced radargram: object reflections become blurred. However, most interesting effect is observed after subtracting horizontal average (figure 2.8). As predicted, along with moving target we see elevated noise due to jitter in the vicinity of static object (2.5—4.5 ns in propagation time). This jitter-induced noise can be interpreted as a false target that occasionally starts and stops moving. Moreover, for the first five seconds, when static object and moving target were close, we have no way to

separate one from another and we cannot say if there was a moving object, or was it jitter only.

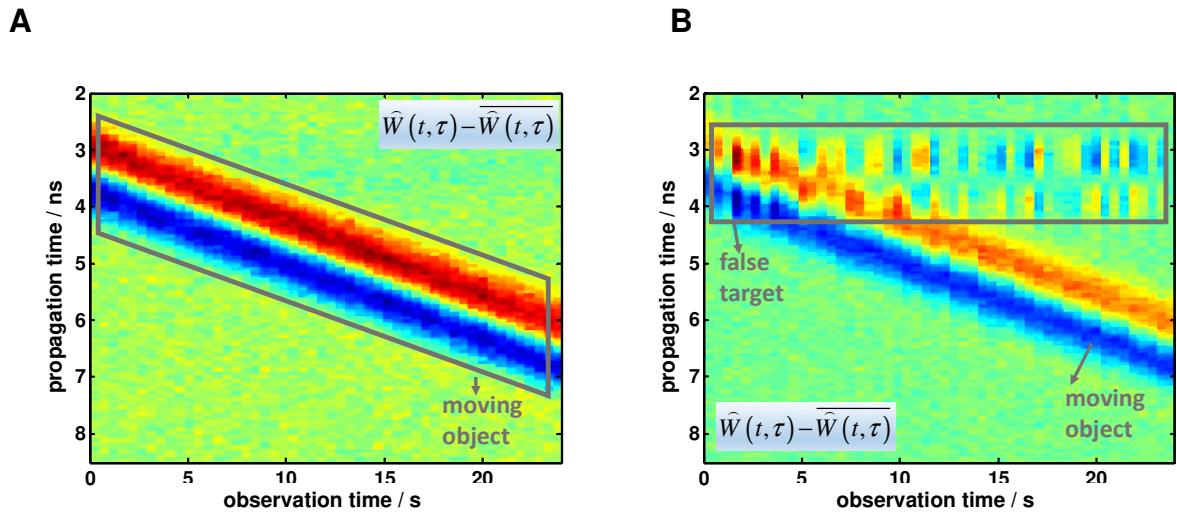


Figure 2.8: Simulated radargram of forwardly moving object after subtraction of horizontal averaged in the presence of static reflector: without jitter (A) and with jitter (B)

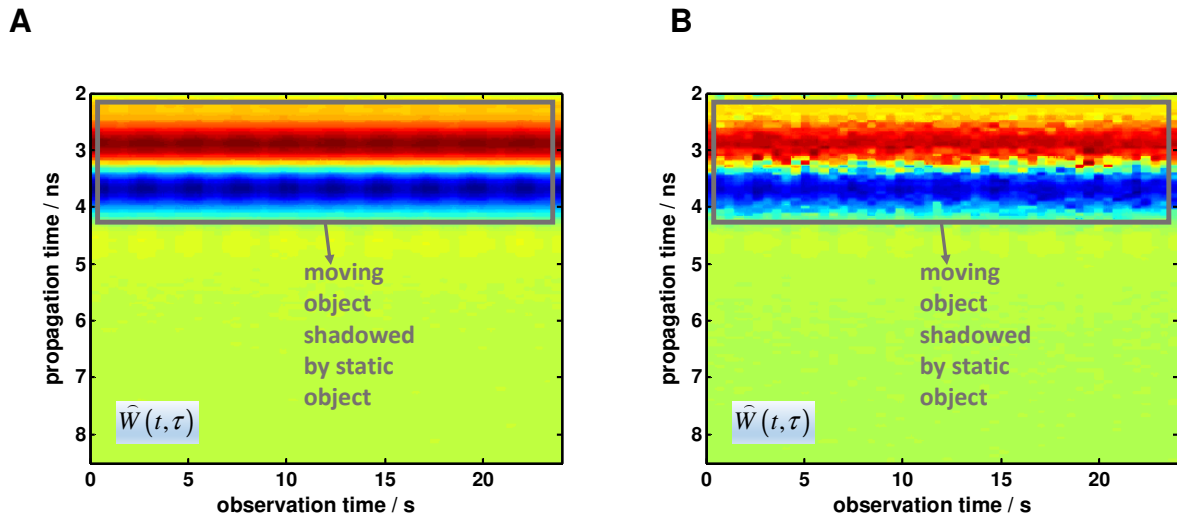


Figure 2.9: Simulated radargram of periodically moving object in the presence of static reflector: without jitter (left) and with jitter (right)

In the second example we simulated sinusoidal shift of a waveform that resembles respiratory motion (with the frequency 0.4 Hz and amplitude 2 cm) appearing close to static object. Again, as in case of forwardly moving object, we can see some blurring due to jitter before stationary clutter is removed by subtraction (figure 2.9). After performing this subtraction however, in 'jittered' case (figure 2.10, B), we can hardly say that we detect moving target in presence of false target. It looks more like we see false target only even though when jitter is absent (figure 2.10, A) periodical variation of

the radargram is obvious. This is the consequence of useful signal appearing close to the static reflection over whole observation time interval. Therefore, in presence of strong static reflector jitter is especially dangerous for detecting minor motion, when object does not relocate itself further than a couple of centimetres. Such situation is not uncommon in case of search for survivals in the disaster area: trapped and probably unconscious person does not change his/her position and there is a plenty of clutter sources around.

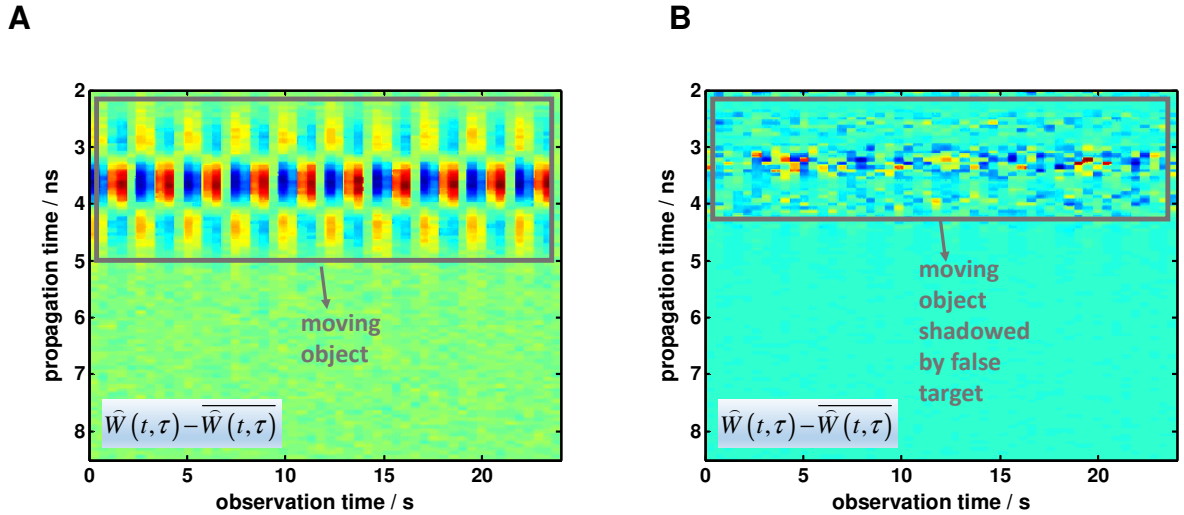


Figure 2,10: Simulated radargram of periodically moving object after subtraction of horizontal averaged in the presence of static reflector: without jitter (left) and with jitter (right)

However, how big jitter can be depends on radar electronics and by choosing certain radar sensing principles it can be minimized. Let us consider this issue in more details. Jitter phenomenon appears exactly as described above in pulse radar systems. That is, according to 2.16 jitter is the strongest on the signal edge. In this work, however, MLBS radar was used and probing signal is an M-sequence  $W_M(t)$ . Pulse-like radar signal in this case is restored via pulse compression by correlation:

$$\widehat{X}_M(t) = \widehat{W}_M(t) * W_M(-t) \quad (2.30)$$

At this stage we are interested in jitter only. For this reason we suppose that measured signal  $\widehat{W}_M(t)$  is 'randomized' by jitter only, additive noise is ignored.

Now, in order to evaluate jitter influence, we need to calculate variance of  $\widehat{X}_M(t)$ . For this purpose, however, it is convenient to substitute expression 2.30 with

$$\widehat{X}_{M1}(t) = (\widehat{W}_M(t) - W_M(t)) * W_M(-t) \quad (2.31)$$

This value is easier to interpret in case of considering M-sequence and at the same time since difference between  $\widehat{X}_M(t)$  and  $\widehat{X}_{M1}(t)$  is deterministic, we can state that

$$\text{var}\{\widehat{X}_M(t)\} = \text{var}\{\widehat{X}_{M1}(t)\} \quad (2.32)$$

How it is shown in figure 2.11, function  $\widehat{W}_M(t) - W_M(t)$  equals zero everywhere except for the short time period in the vicinity of transition ('step') where it equals  $-\Delta V$  or, with equal probability,  $2\Delta V$  (where  $\Delta V$  is M-sequence 'amplitude').

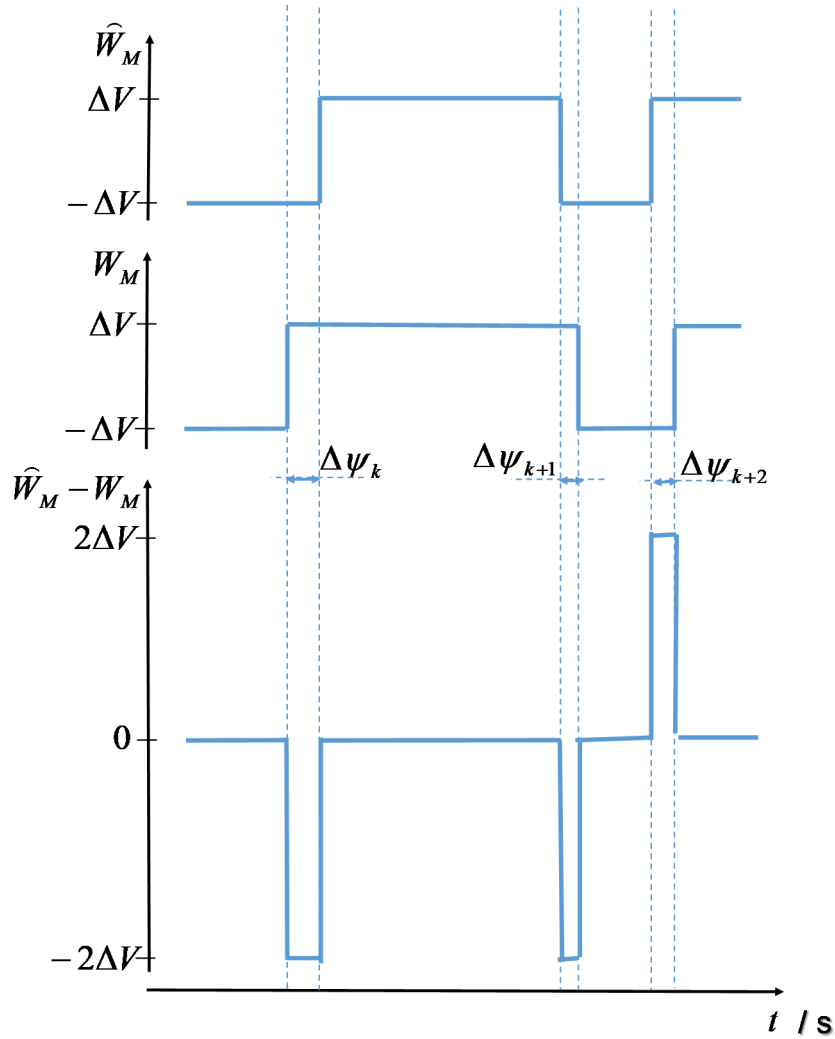


Figure 2.11: Part of M-sequence affected by jitter

Duration of these abovementioned periods is a jitter random variable  $\Delta\psi_k \sim N(0, \sigma_j^2)$ .

All areas beneath  $\widehat{W}_M(t) - W_M(t)$  graph via convolution in (2.31) are multiplied by  $-\Delta V$  or  $\Delta V$  with equal probability and added up:

$$\widehat{X}_{M1}(t) = 2\Delta V^2 \sum_{k=1}^{N_r} \Delta\psi_k \quad (2.33)$$

where  $N_T$  is the number of transitions in M-sequence. Accordingly, we can state about the variance:

$$\text{var}\{\widehat{X}_{M1}(t)\} = 4\Delta V^4 N_T \sigma_j^2 \quad (2.34)$$

We see in 2.34 that in case of M-sequence radar variance caused by jitter does not depend on  $t$  and that is, jitter is not localized on the signal edge as it happens with pulse radars. Signal power (maximum of autocorrelation function) in case of M-sequence radar can be calculated as following:

$$\|X_M(t)\|_{\infty} = \int_{-Nt_c/2}^{Nt_c/2} W_M^2(t) dt = \Delta V^2 N_M t_c \quad (2.35)$$

Here  $t_c$  is the length of one data chip (elementary pulse of M-sequence) and  $N_M$  is the number of such chips. The number of chips and the number of transitions are connected with the order of M-sequence  $\chi$ :

$$N_M = 2^\chi - 1, \quad N_T = 2^{\chi-1} \quad (2.36)$$

As a result of using (2-34—2.36), we can put down SNR value in case of M-sequence radar:

$$SNR_{M\text{-sequence}} = \frac{\|X_M(t)\|_{\infty}^2}{\text{var}\{\widehat{X}_M(t)\}} = \left(\frac{t_c}{2\sigma_j}\right)^2 \frac{N_M^2}{N_T} \approx \left(\frac{t_c}{\sigma_j}\right)^2 2^{\chi-1} \quad (2.37)$$

Here we have taken into account that in the radar device used in this work  $\chi=10$  and thus  $N_M \approx 2^\chi$ .

Let us now consider radar in which Gaussian pulse with maximal value  $V_G$  and pulse width  $t_w$  is used as a probing signal:

$$X_G(t) = V_G \exp\left(-\pi\left(\frac{t}{t_w}\right)^2\right) \quad (2.38)$$

Performing pulse compression (like we did it in expression 2.30 in case of M-sequence radar) would not make much sense in case of pulse radar, since autocorrelation function of  $X_G(t)$  is a short pulse as well. Therefore, jitter would still be concentrated on the signal edge. According to (2.25) we can put down variance of jittered Gaussian pulse defined in 2.38 (after ignoring additive noise how we did it when considering M-sequence radar):

$$\text{var}\{\widehat{X}_G(t)\} = \dot{X}_G^2(t) \sigma_j^2 \quad (2.39)$$

That is, jitter influence on the signal edge is determined by slew rate. For Gaussian pulse slew rate equals ([23]):

$$\|\dot{V}_G(t)\|_{\infty} = \sqrt{2\pi}e^{-0.5} \frac{V_G}{t_w} = 1.52 \frac{V_G}{t_w} \quad (2.40)$$

From 2.39 and 2.40, we see that jitter-induced variance at signal edge equals:

$$\text{var}\{X_G(t)\} = 2.31 \left( \sigma_j \frac{V_G}{t_w} \right)^2 \quad (2.41)$$

Now, like in 2.37, we can introduce SNR value with respect to jitter for the radar with Gaussian pulse as a probing signal:

$$SNR_{gauss} = \frac{\|X_G(t)\|^2}{\text{var}\{X_G(t)\}} = \left( \frac{t_w}{\sigma_j} \right)^2 \frac{1}{2.31} \approx 0.43 \left( \frac{t_w}{\sigma_j} \right)^2 \quad (2.42)$$

As a result, let us calculate the coefficient that reflects difference in susceptibility to jitter between M-sequence radar and pulse radar:

$$\frac{SNR_{M-sequence}}{SNR_{gauss}} \approx \left( \frac{t_w}{t_c} \right)^2 \frac{2^{\chi-1}}{0,87} \quad (2.43)$$

Typically  $t_c$  and  $t_w$  are of one order and therefore, we can state that susceptibility to jitter of M-sequence radar is some hundreds of times lower than for the pulse radar (with hardware parameters as used in this work). This was one of the reasons for choosing M-sequence radar as a main tool in this thesis.

Given that in M-sequence radar used in this work jitter is a minor effect, further in the text it is ignored and we regard additive noise as a dominant random perturbation (until non-stationary clutter is included in signal model)

$$\sigma^2 \approx \sigma_T^2 \quad (2.44)$$

As a result, 'randomized' radargram  $\widehat{W}(t, \tau)$  will not include jitter further in this work.

Total radar noise being additive white Gaussian noise is an important development, since noise distribution determines development of SNR-enhancing algorithms further in this work.

## **2.4 Minor motion detectability**

Let us consider important question about how small is the motion that can still be detected by radar device.

Difference, introduced into randomized radargram by minor motion during  $\Delta\tau$  can be expressed as following:

$$\widehat{W}(t, \tau) - \widehat{W}(t, \tau + \Delta\tau) = W(t, \tau) - W(t, \tau + \Delta\tau) + n(t, \tau) - n(t, \tau + \Delta\tau) \quad (2.45)$$

According to 2.45 we need to consider the problem of detecting 'signal' difference  $W(t, \tau) - W(t, \tau + \Delta\tau)$  in presence of AWGN (Additive white Gaussian noise)  $n(t, \tau) - n(t, \tau + \Delta\tau)$  how it is illustrated in figure 2.12. Due to the noise ergodicity we can state that,

$$n(t, \tau) - n(t, \tau + \Delta\tau) \sim N(0, 2\sigma^2) \quad (2.46)$$

In order for the object motion to be detected, maximal difference caused by target position change in the radar response has to be greater than  $k_\sigma$  times noise standard deviation.

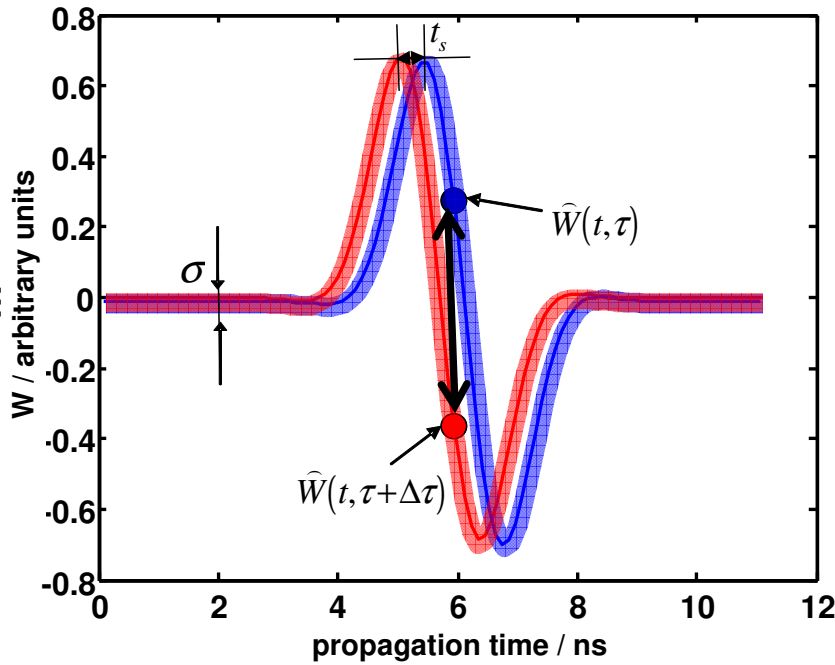


Figure 2.12: Illustration of detection problem (expression 2.47)

Now let us formulate two hypothesis and detection problem:

- $H_1$ : motion happened
- $H_0$ : motion did not happen

$$\|W(t, \tau) - W(t, \tau + \Delta\tau)\|_\infty \begin{cases} > k_\sigma \sqrt{2}\sigma : H_1 \\ \leq k_\sigma \sqrt{2}\sigma : H_0 \end{cases} \quad (2.47)$$

Here  $k_\sigma \sigma$  is a tolerance interval that determines the false-alarm rate we are ready to tolerate. According to the well-known rule in the case  $k_\sigma = 3$  in 99.7% of cases

detection according to (2.47) will happen due to the target motion, and all others due to noise. The higher  $k_\sigma$  the less false alarm probability.

Since motion is seen by radar device as a shift  $t_s$  in fast time, we can write:

$$W(t, \tau) - W(t, \tau + \Delta\tau) = W(t) - W(t - t_s) \quad (2.48)$$

Here fast-time pulse shift can be simply expressed through the object shift in distance  $\Delta d$ :

$$t_s = 2 \frac{\Delta d}{c} \quad (2.49)$$

Then equation that needs to be solved for 2.47 can be written like

$$\|W(t) - W(t - t_s)\|_\infty = k_\sigma \sqrt{2} \sigma \quad (2.50)$$

In the left part of eq. 2.50 we apply Taylor series and limit it to the linear term:

$$\|\dot{W}\|_\infty t_s = k_\sigma \sqrt{2} \sigma \quad (2.51)$$

From eq. 2.51, minimum motion visible for the radar is expressed as

$$t_s = \frac{k_\sigma \sqrt{2} \sigma}{\|\dot{W}\|_\infty} \quad (2.52)$$

Since with respect to motion distance is more illustrative than propagation time we are rather interested in the minimum shift expressed in the distance units and thus, after using 2.49 rewrite 2.52 in the following form:

$$\Delta d = \frac{k_\sigma c \sigma}{\sqrt{2} \|\dot{W}\|_\infty} \quad (2.53)$$

In this work we will often evaluate radar performance (including software techniques targeted at the amplification of useful signal) based on signal to noise ratio (SNR). We define it broadly as the square of expected value of a certain dataset divided by the variance of this dataset. Given the definition, SNR of a radar unit is given by:

$$SNR = \left( \frac{\|W\|_\infty}{\sigma} \right)^2 \quad (2.54)$$

Where  $\|W\|_\infty$  is a maximum of expected value (expected value being the whole radar IRF). Equation 2.53 now becomes:

$$\Delta d = \frac{k_\sigma c}{\sqrt{2} SNR} \frac{\|W\|_\infty}{\|\dot{W}\|_\infty} \quad (2.55)$$



Slew rate  $\|\dot{W}\|_\infty$  can be defined via pulse duration  $t_p$  (in case of M-sequence radar  $t_p$  is interpreted as coherence interval) and frequency bandwidth  $B$  of the radar unit as follows:

$$\|\dot{W}\|_\infty = \frac{\|W\|_\infty}{t_p} = \|W\|_\infty B \quad (2.56)$$

Accordingly, we can rewrite expression 2.55 like:

$$\Delta d = \frac{k_\sigma c}{B\sqrt{2SNR}} \quad (2.57)$$

For the radar unit used in this work  $B = 2.25$  GHz and SNR was measured to be 80 dB (or  $10^8$  in the units to be used in equation 2.57) at the maximal available data acquisition rate of 67 IRFs per second (technical details are given in chapter 6). If we suppose  $k_\sigma = 3$  (0.003 false alarm rate) than equation 2.57 gives us remarkable theoretical sensitivity:  $\Delta d = 9.4$  micrometers. This is an upper limit, however, since under real conditions both SNR and the waveform shape are affected by antenna transfer function, attenuation of the material, propagation losses etc.

### 2.5 Averaging in slow time and stepwise continuous motion compensation

With observation time going person that we need to detect is moving continuously. However, radar electronic is fetching finite number of impulse response functions (IRFs) within observation time interval. How it is shown in figure 2.13, every discrete IRF contains finite number of continuous signal values acquired at equidistantly spread propagation time instants (discretization interval being denoted as  $\Delta t$ ).

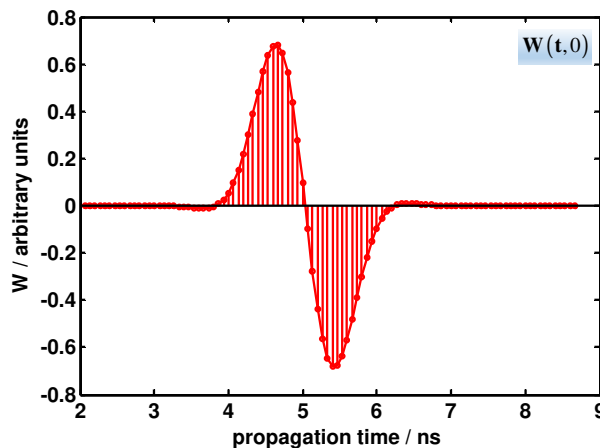


Figure 2.13: Sampled signal pulse

In observation time discretization means that impulse response function contains horizontal averages of the moving object reflections within discretization interval  $\Delta\tau$ . Let us concentrate on horizontal averaging and write an expression for radargram matrix  $\mathbf{W}$  (vertical averaging is done in the same way):

$$\mathbf{W}(\mathbf{t}, \boldsymbol{\tau}) = \frac{1}{\Delta\tau} \int_{(m-1)\Delta\tau}^{m\Delta\tau} W(\mathbf{t}, \tau) d\tau = \frac{1}{\Delta\tau} \int_{(m-1)\Delta\tau}^{m\Delta\tau} W_1\left(\mathbf{t} - \frac{2s}{c}\tau\right) d\tau \quad (2.58)$$

Here  $\mathbf{t} = l\Delta t$  is discrete propagation time,  $\boldsymbol{\tau} = m\Delta\tau$  is discrete observation time,  $s$  is the velocity of moving object.

Let us discuss how motion affects signal level (and, accordingly, SNR) in the radargram. In case measurement object is static maximal signal level in the radargram is determined by one value of  $W$ , taken at the instant  $\mathbf{t} = t_m$  when pulse reaches its maximum:

$$\|\mathbf{W}\|_{\infty} = |W(t_m, 0)| \quad (2.59)$$

When measurement object is moving such a high  $\|\mathbf{W}\|_{\infty}$  value is not reachable (since there is no such horizontal line where we can average only maximums of the reflected pulse). At this point we can introduce coefficient that characterizes signal degradation due to compensating continuous motion stepwisely and takes values between zero and one:

$$k_d = 1 - \frac{\|\mathbf{W}\|_{\infty}}{|W(t_m, 0)|} \quad (2.60)$$

No degradation ( $k_d = 0$ ) is only reached when object of interest is static. Slowly moving objects (or objects that shifted fast, but whose shift was much less than the pulse length) would produce low degradation values close to zero. Unfortunately, situation of complete degradation when  $k_d = 1$  and signal value equals zero is also realistic. Signal pulse itself tends to have zero mean (since working frequencies of the radar do not include zero frequency). That is, if we average along the whole observation time when motion happened fast enough and shift was big enough,  $\|\mathbf{W}\|_{\infty}$  will tend to become 0. For example, this would happen in radargram shown in figure 2.14 if we average over the whole observation period. This phenomenon sets the limit on how fast the object can move so that it is still seen in radar response: during measurement interval  $\Delta\tau$  shift of the object should not exceed the pulse length  $\frac{c}{2B}$ .

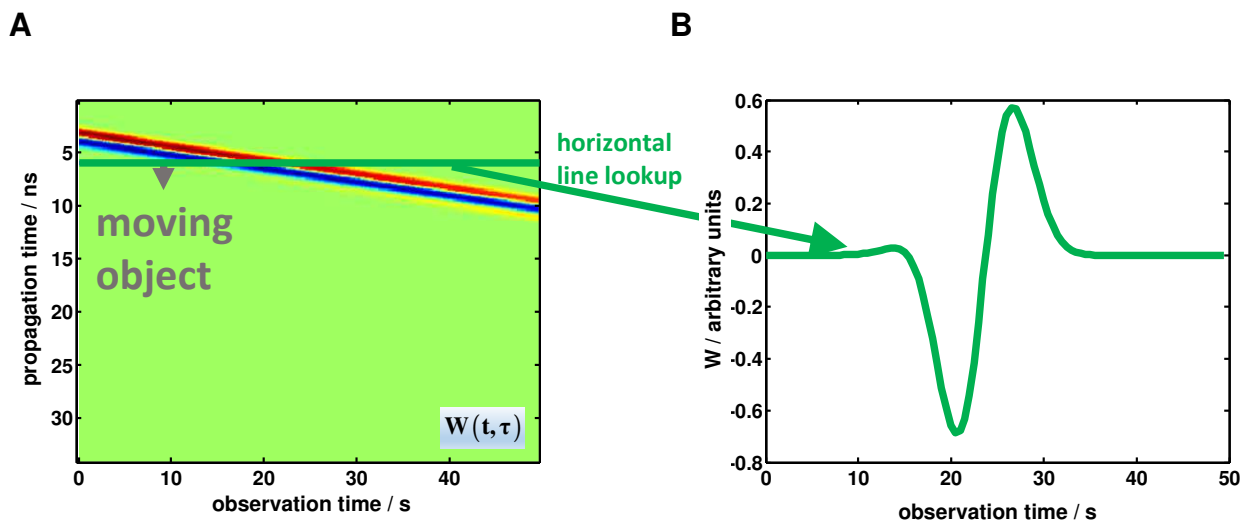


Figure 2.14: Motion with constant velocity as seen by radar. Radargram (A) and its horizontal line (B)

In this work, however, we concentrate on minor motion, when object shift is much less than  $\frac{c}{2B}$ . Therefore, regarding averaging we are interested if we should apply additional horizontal averaging in order to improve moving object detectability or not. Let us now consider this issue.

Optimal SNR improvement by coherent averaging in slow time might be reached if the motion trajectory is precisely known. In this case we could simply compensate the motion by the process that we can call alignment as it is given in equation 2.61 and illustrated in figure 2.15:

$$\widehat{W}_a(t, \tau) = \widehat{W}\left(t + \frac{2s}{c} \tau, \tau\right) \quad (2.61)$$

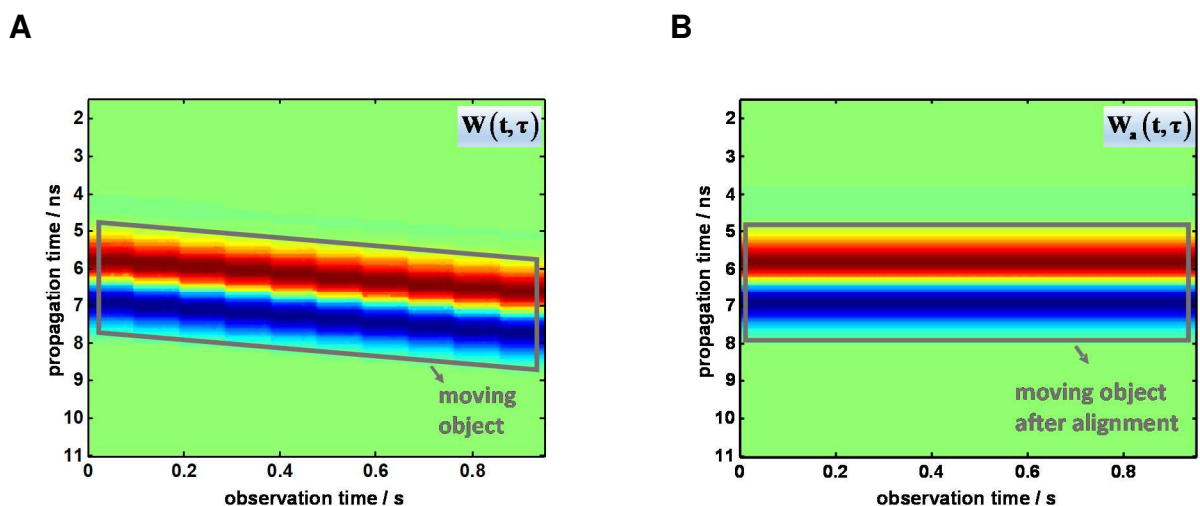


Figure 2.15: Radargram without alignment to compensate motion (A) and with it (B)

After aligning the scans according to the motion trajectory SNR is improved by horizontal averaging:

$$\overline{\widehat{\mathbf{W}}}_a(\mathbf{t}) = \frac{1}{M} \sum_{m=0}^{M-1} \widehat{\mathbf{W}}_a(\mathbf{t}, m\Delta\tau) \quad (2.62)$$

By definition, SNR in radargram without using averaging as described in eq. 2.62 is given by:

$$SNR_0 = \left( \frac{\mathbf{W}(t_m, 0)}{\sigma} \right)^2 \quad (2.63)$$

Using Bienayme equality in (2.62) leads to the expression of SNR after averaging the aligned radargram:

$$SNR_a = M \left( \frac{\mathbf{W}(t_m, 0)}{\sigma} \right)^2 \quad (2.64)$$

Therefore, SNR improvement in the case of horizontal averaging after alignment is given by:

$$\frac{SNR_a}{SNR_0} = M \quad (2.65)$$

However, in our task target trajectory is never known and thus, SNR improvement up to (2.65) is not reachable. Moreover, we should detect the object due to its motion rather than due to its (target) existence. This is the case because there is a plenty of reflecting static objects in the disaster area and we have no choice except for filtering out everything that is not moving.

Let us now consider in more details how horizontal averaging affects our ability to detect target minor motion with constant velocity  $s_0$ . We define motion being minor when it shifts signal pulse less than pulse rise time  $t_r$ . Motion with constant velocity is an important case for practice, since we can consider forward minor motion as a first order approximation of different motion types that can be encountered at disaster area: single hand waving, body relocation etc.

When dealing with minor motion we do not observe complete waveform in slow time how it is shown in figure 2.14, we rather observe its parts as in figure 2.16. If in figure 2.16, B we look at signal amplitude close to the end of observation time interval we can mention that signal becomes nonlinear, and, moreover, its first derivative at a certain instant changes its sign as if motion direction was changed to the opposite. It is discussed in details in the next chapter how these nonlinearities distort respiratory

motion in radargram. Now, however, let us concentrate on how horizontal averaging affects sensitivity in important edge region of signal pulse where how we have already seen minor motion produces maximal signal difference.

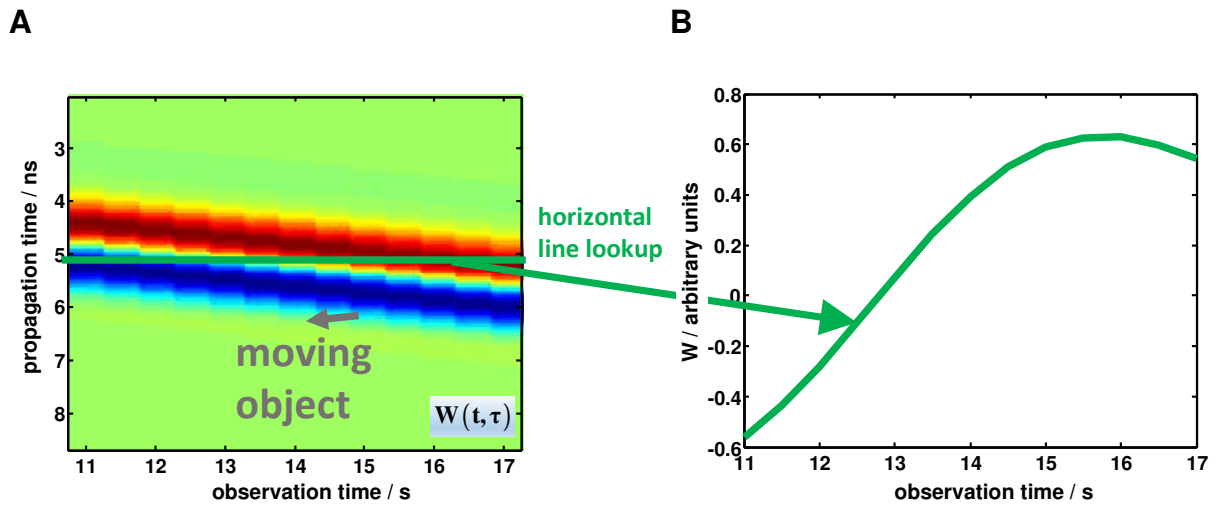


Figure 2.16: Minor motion with constant velocity as seen by radar. Radargram (A) and its horizontal line (B)

Radargram  $W(t, \tau)$  at signal edge ( $t = t_e$ ) for object moving with constant velocity is shown as a blue line in figure 2.17.

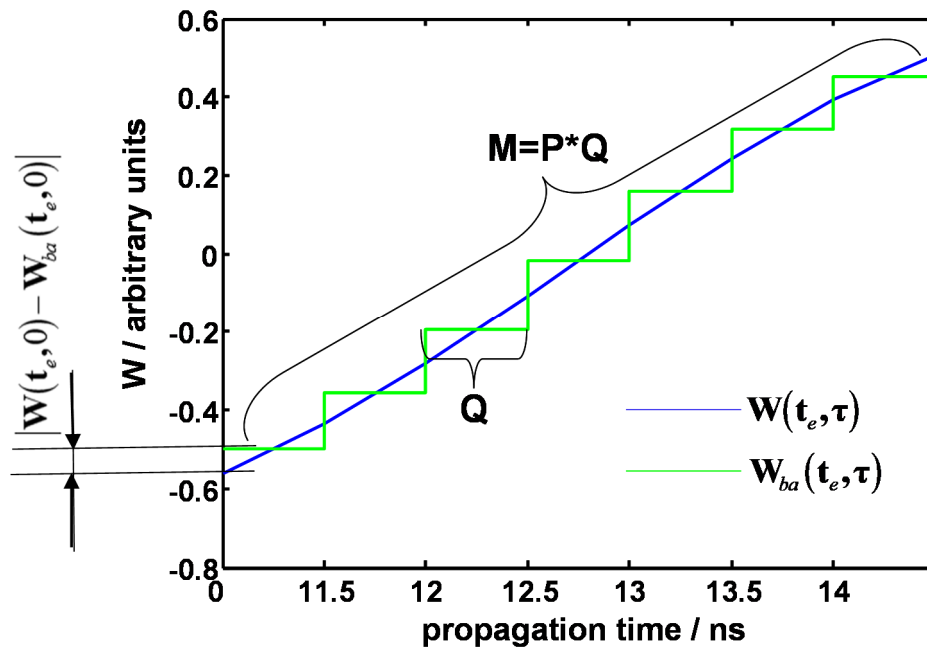


Figure 2.17: Motion with constant velocity as seen by radar: linear region with and without horizontal averaging

Let  $\mathbf{W}(\mathbf{t}, \tau)$  contain  $M = PQ$  IRFs. If we split the radargram into  $P$  consecutive blocks,  $Q$  consecutive scans inside each block and average inside every block, as a result we receive ‘block-averaged’ radargram (shown in green in figure 2.17):

$$\mathbf{W}_{ba}(\mathbf{t}_e, ((p-1)Q + q)\Delta\tau) = \frac{1}{Q} \sum_{n=(p-1)Q}^{pQ-1} \mathbf{W}(\mathbf{t}_e, n\Delta\tau) \quad (2.66)$$

Here  $p = \overline{1, P}$  is the number of block and  $q = \overline{0, Q}$  determines the position of averaged radargram value inside each block.

Regarding sensitivity, the effect of averaging according to 2.66 is twofold:

- Noise variance is reduced by averaging and thus, sensitivity is increased
- It can be seen in figure 2.17 that for radargram considered at signal edge difference between first and last values is bigger in case no blockwise averaging was used. That is, if we denote the length of observation time interval as  $\tau_{obs}$  we can state that:

$$|\mathbf{W}_{ba}(\mathbf{t}_e, \tau_{obs}) - \mathbf{W}_{ba}(\mathbf{t}_e, 0)| < |\mathbf{W}(\mathbf{t}_e, \tau_{obs}) - \mathbf{W}(\mathbf{t}_e, 0)| \quad (2.67)$$

Expression 2.67 signals reduction of sensitivity due to blockwise averaging.

Let us consider differences from 2.67 quantitatively. We can see it in figure 2.17 that  $\mathbf{W}_{ba}(\mathbf{t}, \tau)$  is a stepped function. Since in our example motion happens with constant velocity, height of the step equals  $2|\mathbf{W}(\mathbf{t}, 0) - \mathbf{W}_{ba}(\mathbf{t}, 0)|$ . Now we can calculate maximal difference caused by motion among signal values in block-averaged radargram (in case of forward motion this is the difference between the first and the last values). Such difference is related to sensitivity and it is given by

$$|\mathbf{W}_{ba}(\mathbf{t}, \tau_{obs}) - \mathbf{W}_{ba}(\mathbf{t}, 0)| = 2(P-1)|\mathbf{W}(\mathbf{t}, 0) - \mathbf{W}_{ba}(\mathbf{t}, 0)| \quad (2.68)$$

Accordingly, in case no blockwise averaging is used corresponding difference can be written like:

$$|\mathbf{W}(\mathbf{t}, \tau_{obs}) - \mathbf{W}(\mathbf{t}, 0)| = 2P|\mathbf{W}(\mathbf{t}, 0) - \mathbf{W}_{ba}(\mathbf{t}, 0)| \quad (2.69)$$

As a measure of sensitivity we introduce SNR values of ‘differential’ signals (we denote them as DSNR). For those signals expected values are given in equations 2.68 and 2.69. According to the properties of normally distributed random variables variance of differential averaged signal is  $\frac{2\sigma^2}{Q}$  while for differential signal without averaging it is just

$2\sigma^2$ . Therefore, we can put down DSNR in case block averaging was used,  $DSNR_{ba}$  and in case no additional averaging was used,  $DSNR_0$ :

$$DSNR_{ba} = \frac{2Q(P-1)^2 |\mathbf{W}(\mathbf{t}, \mathbf{0}) - \mathbf{W}_{ba}(\mathbf{t}, \mathbf{0})|^2}{\sigma^2} \quad (2.70)$$

$$DSNR_0 = \frac{2P^2 |\mathbf{W}(\mathbf{t}, \mathbf{0}) - \mathbf{W}_{ba}(\mathbf{t}, \mathbf{0})|^2}{\sigma^2} \quad (2.71)$$

In order to evaluate the efficiency of block averaging we consider the ratio of given SNR measures:

$$\frac{DSNR_{ba}}{DSNR_0} = \frac{Q(P-1)^2}{P^2} \quad (2.72)$$

First of all, we can see in (2.72) that slow-time averaging does not guarantee any SNR improvement at all. Actually, if we substitute  $P$  and  $Q$  in (2.72) with small numbers ( $P, Q=1,2,3$ ) we mention that  $\frac{DSNR_{ba}}{DSNR_0}$  can only exceed one when the number of collected IRFs satisfies:

$$PQ > 8 \quad (2.73)$$

In case motion was so short that 2.73 was not satisfied, we cannot improve its detectability via slow time averaging.

When target is moving slower more IRFs are collected on one signal edge,  $\frac{DSNR_{ba}}{DSNR_0}$  exceeds one and according to (2.72) starts to grow with increasing the number of averages  $Q$ . This trend, however, does not continue until the maximal possible value of  $Q$  is reached and  $\frac{DSNR_{ba}}{DSNR_0}$  peaks before starting to decrease. See figure 2.18 where this dependency is given for 300 collected IRFs (300 was an arbitrary choice).

Let us find out what is the optimal number of software averages  $Q$  given the total number of collected waveforms is fixed at  $M = PQ$ . In this case equation 2.72 is rewritten as a function of  $Q$ :

$$g(Q) = \left(1 - \frac{Q}{M}\right)^2 Q \quad (2.74)$$

The condition for finding a maximum then looks like:

$$\frac{dg}{dQ} = 1 - \frac{4Q}{M} + \frac{3Q^2}{M^2} = 0 \quad (2.75)$$

And its solution is given by:

$$Q_{opt} = \frac{M}{3} \quad (2.76)$$

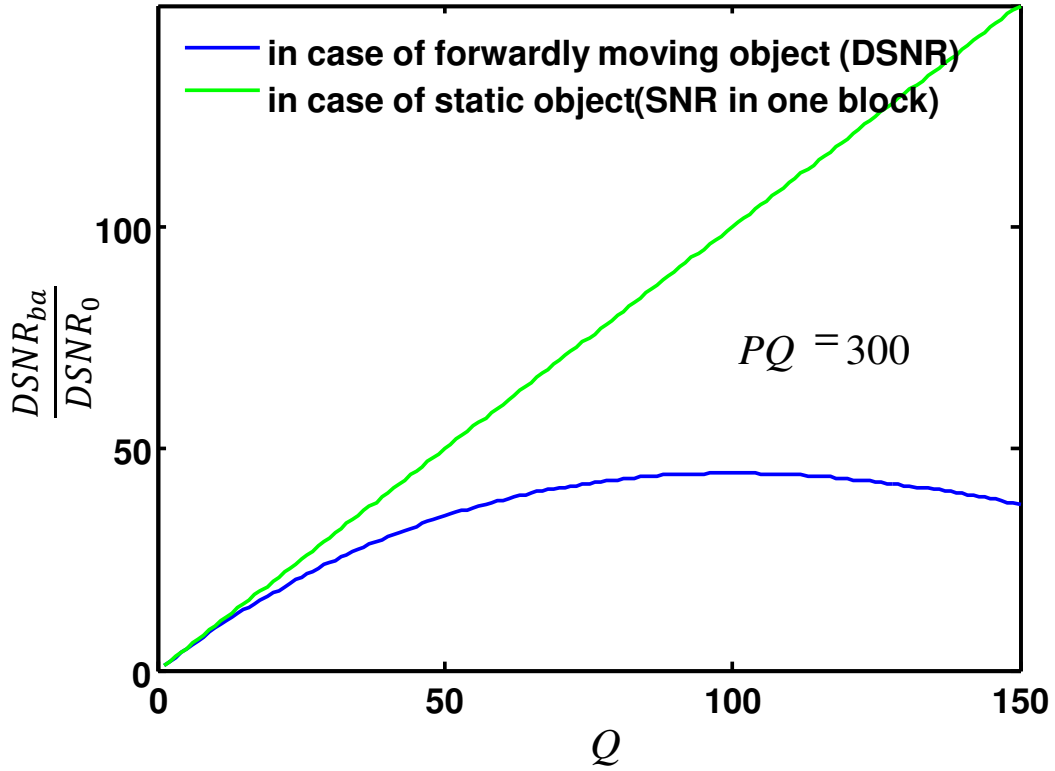


Figure 2.18: Differential SNR improvement due to the slow-time averaging when 300 IRFs are collected.

That is, the maximum  $\frac{DSNR_{ba}}{DSNR_0}$  is reached when the collected IRFs are split into three blocks and then averaged. We can also assert that if (2.73) is satisfied, splitting a set of collected IRFs into two blocks and averaging inside every block improves SNR. Thus, we can write the maximal slow-time averaging parameter that still guarantees SNR improvement:

$$Q_{\max} = \frac{M}{2} \quad (2.77)$$

Let us now derive the conditions for improving SNR by slow time averaging in our particular case. We consider minor motion with velocity  $s_0$  that in its magnitude does not exceed pulse rise time  $t_r$ , which can be formulated as following:

$$\frac{s_0 \tau_{obs}}{c} = \frac{s_0 PQ \Delta \tau}{c} \leq t_r \quad (2.78)$$



Pulse rise time typically equals some dozens of percent pulse length  $\frac{1}{B}$ . Let us take as an example pulse rise time of Gaussian pulse  $t_r \approx \frac{1}{2B}$ . Now we can rewrite 2.78 in the following form:

$$s_0 \leq \frac{c}{2PQB\Delta\tau} \quad (2.79)$$

If we now take  $PQ$  value from 2.73 we get precise condition on how fast we need to acquire data given the target velocity so that slow time blockwise averaging would improve detectability of small target displacement with constant speed:

$$s_0 \leq \frac{c}{16B\Delta\tau} \quad (2.80)$$

### 3 Respiratory motion in noise and its enhancement

In this chapter I first introduce inherent features of respiratory motion as seen by UWB radar. Then we move from the description of phenomena towards practical algorithms that can improve detectability of useful signal. Different approaches are evaluated theoretically and/or by means of processing simulated and measured radar data.

After introducing breathing motion as seen by radar, we first consider breathing signature at one fixed instant in propagation time  $t_0$  in order to discuss spectral methods suitable for breathing detection. Then the discussion of SNR improvement is finalized by considering breathing person as a range-spread target (e.g. we consider combining several respiratory motion traces appearing at different instants  $t = t_0 \in [t_{\min}, t_{\max}]$ ).

#### 3.1 Periodical motion as seen by radar

At this point we start to consider respiratory motion within radar aperture. For now we view it as periodic variation with repetition rate  $\nu_0$ . Therefore we can write a general expression for chest position variation (motion profile) when person is situated  $r_0 + d$  meters from antennas:

$$d(\tau) = \sum_k d_k \sin(2\pi k \nu_0 \tau + \varphi_k) \quad (3.1)$$

It should be noted that in practice breathing motion profile most often does not deviate a lot from  $d_1 \sin(2\pi \nu_0 \tau + \varphi_k)$  [22]. That is, all other terms in comparison with main breathing rate component are minor and can be considered as harmonics (we call them first type harmonics). We keep to eq. 3.1 for now though in order not to lose generality.

According to expression 2.9 signal received by the radar in this case can be written like

$W(t, \tau) = W_s \left( t - 2 \frac{d(\tau)}{c} \right)$ , where  $W_s$  is already shifted by  $2 \frac{r_0}{c}$  to the position of breathing person.

Given that the magnitude of respiratory motion  $\|d(\tau)\|_{\infty}$  is minor (does not exceed a couple of centimetres) shift  $2 \frac{d(\tau)}{c}$  is limited and at every  $t_0$  instant of a radargram

$W(t_0, \tau)$  we can only observe values from a short part of reflected pulse. In general due to its shortness this pulse part can contain at maximum one extremum. Thus, as a function of respiration-caused shift  $\xi$ ,  $W_s$  can be precisely approximated by Taylor

series truncated after third term with higher-order effects being minor (like it is illustrated for example in figure 3.1):

$$W_s(\xi) \approx A_2(t_0)\xi^2 + A_1(t_0)\xi + A_0(t_0), \quad (3.2)$$

Where  $\xi = \frac{2d(\tau)}{c}$ ,  $A_2 = \frac{1}{2} \frac{d^2 W_s}{d\xi^2} \Big|_{\xi=0}$ ,  $A_1 = \frac{dW_s}{d\xi} \Big|_{\xi=0}$ ,  $A_0 = W_s \Big|_{\xi=0}$

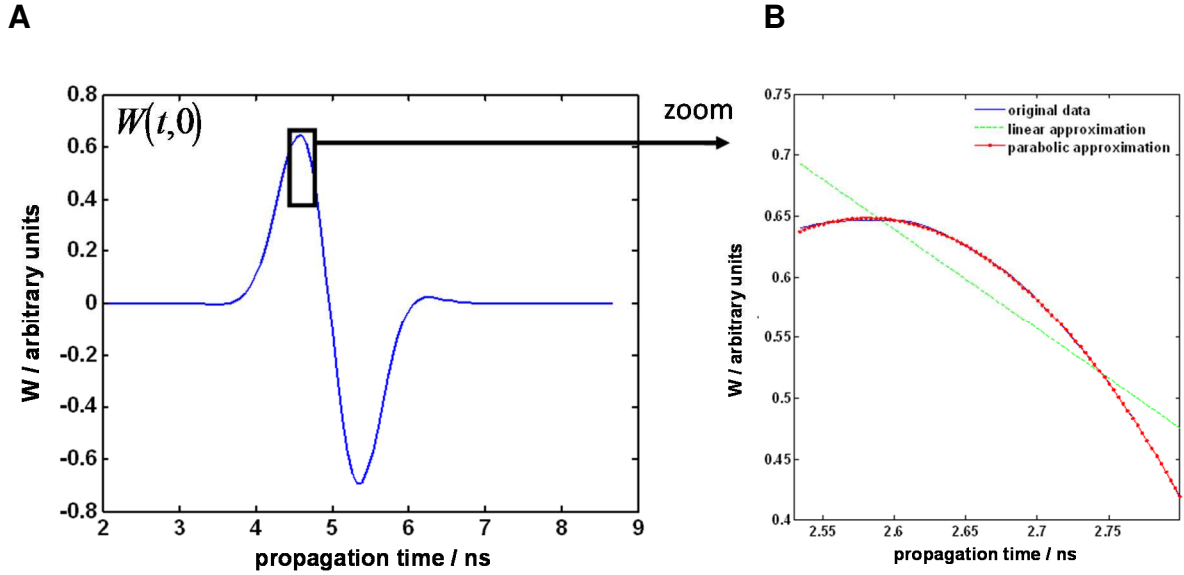


Figure 3.1:  $W(t,0)$ , its part observed close to the pulse extremum marked (A) and zoomed (B).

At the same time we see in figure 3.1 that in case of considering breathing close to the pulse extremum we cannot limit approximation in equation 3.2 to the first-order polynomial since linear approximation in this case is too rough and it significantly deviates from original signal shape.

Let us rewrite equation 3.2 in the form that directly includes motion profile  $d(\tau)$ :

$$W_s(\tau) = A_2 \left( \frac{2d(\tau)}{c} \right)^2 + A_1 \left( \frac{2d(\tau)}{c} \right) + A_0 \quad (3.3)$$

We can see in 3.3 that in general case respiratory motion causes nonlinear behaviour of the observed radargram and we can consider separately linear and nonlinear parts of  $W_s$ :

$$W_s(\tau) = \underbrace{A_2 \left( \frac{\sum_k d_k \sin(2\pi k v_0 \tau + \phi_k)}{c} \right)^2}_{W_{nl}, \text{ nonlinear part}} + \underbrace{A_1 \left( \frac{\sum_k d_k \sin(2\pi k v_0 \tau + \phi_k)}{c} \right)}_{W_l, \text{ linear part}} + A_0 \quad (3.4)$$

Term  $A_0$  does not depend on  $\tau$  and as such further data processing it is removed from the radargram along with all stationary reflections. How breathing signal looks at particular fast time instant depends on how  $A_2$  and  $A_1$  compare to one another.

Let us first consider important case when  $A_2 = 0$  and thus we have  $W_s$  as a linear function of  $\xi$  in equation 3.2. This is valid when we observe oscillations on the signal edge only. We can see it in figure 3.2: signal edge as it is to be expected was approximated by linear function almost as good as by the parabola, which signals that non-linear term can be neglected.

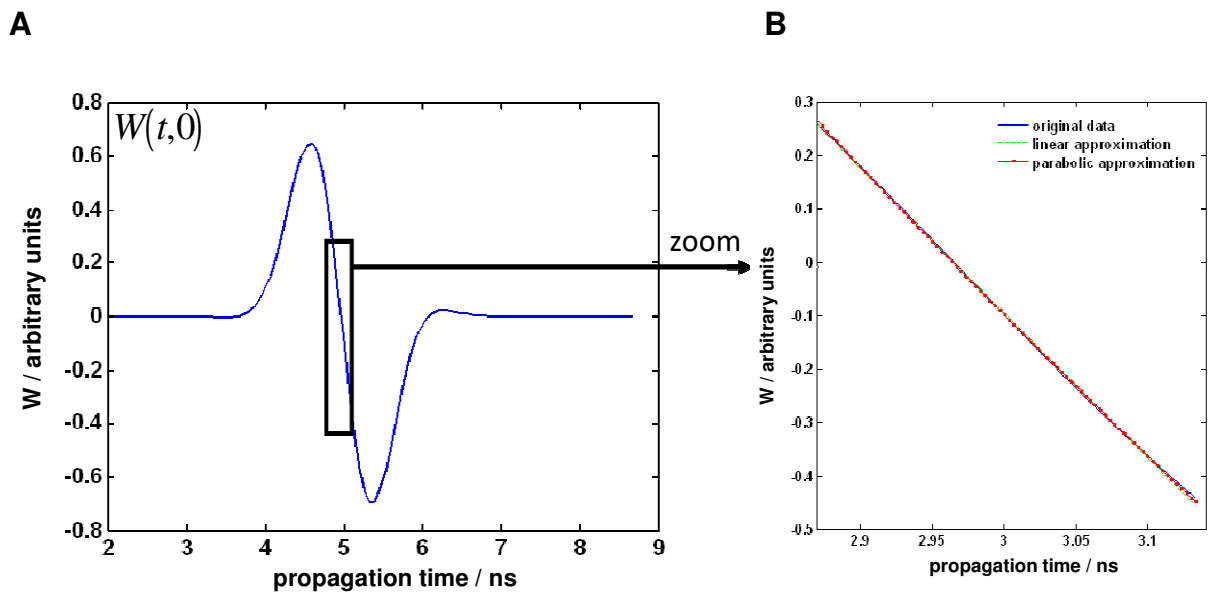


Figure 3.2:  $W(t,0)$ , its part observed at the pulse edge marked (A) and zoomed (B).

According to equation 3.4, in this case only signal components of respiratory rate  $\nu_0$  as well as zero-rate components are observable.

The situation when  $A_2 = 0$  is the most important for this work since, how it was shown in the previous chapter, among all motion-affected radargram instants motion signature is the strongest at the fast-time instant  $t = t_0$  when  $\|\dot{W}(t)\|_\infty$  is maximal. This happens at the signal edges and thus we can already state that in breathing-containing radargram non-linear terms are minor in comparison with main-rate peaks that can be found at the waveform edges.

Let us now consider the general case when both linear and nonlinear parts are significant. We can put down nonlinear part as following:

$$W_{nl}(\tau) = \frac{4A_2}{c^2} \sum_l \sum_m d_l d_m \sin(2\pi l v_0 \tau + \phi_l) \sin(2\pi m v_0 \tau + \phi_m) \quad (3.5)$$

After using trigonometric equalities terms summed up in equation 3.5 can be rewritten like:

$$d_l d_m \sin(2\pi l v_0 \tau + \phi_l) \sin(2\pi m v_0 \tau + \phi_m) = \frac{\cos(2\pi(l-m)v_0\tau + \phi_l - \phi_m) + \cos(2\pi(l+m)v_0\tau + \phi_l + \phi_m)}{2} \quad (3.6)$$

As it follows from equations 3.5 and 3.6 when significant first type harmonics are present, they cause additional harmonic perturbations both at higher frequencies than first type harmonics and at the frequencies of first-type harmonics themselves. Amount of these perturbations is, however, limited by their magnitude  $d_l d_m$  and typically the higher  $l, m$  the lower  $d_l, d_m$ .

Let us consider important case when

$$d_k \ll d_1 \quad (3.7)$$

for  $k > 1$ .

This is the case of purely sinusoidal breathing motion. Even though simple, in practice this is a good approximation of respiratory motion in the most circumstances. Given 3.7 equation 3.5 after taking into account 3.6 becomes:

$$W_{nl}(\tau) = \frac{4A_2}{c^2} \left( \frac{1}{2} + \frac{\cos(4\pi v_0 \tau + 2\phi_1)}{2} \right) \quad (3.8)$$

Thus, perturbation due to nonlinearity contributes into stationary component in radargram, but more importantly, it causes harmonic at the rate of  $2v_0$  (second harmonic) and has no effect on main tone component. Let us call it second type harmonic (in contrast to the first type harmonics that arise due to respiratory motion being non-sinusoidal). One of the important questions about this harmonic is: how big is it in comparison with linear part on the right in equation 3.4? In case of observing respiratory variation on the pulse edge answer is obvious:  $A_2 = 0$  and according to expression 3.8 second type harmonic is not observed. For other cases answer is given by the following equation:

$$\left| \frac{A_1}{A_2} \right| = 2h \quad (3.9)$$

Here  $h = \xi_{ver}$  is the x-coordinate of the vertex of parabola defined by equation 3.5. The closer this vertex is to the instant where we observe breathing the more second type harmonic is in comparison with linear part. It follows immediately from equation 3.9 that

in case  $h = 0$ ,  $A_1 = 0$  as well. This situation is shown in figure 3.3: pulse extremum and the vertex of the second order approximation are situated in the middle of the interval defined by breathing amplitude  $\|d(\tau)\|_\infty$  (this corresponds to  $h = 0$ ) and, as predicted by equation 3.9 we can see that linear approximation in this case contains only constant component.

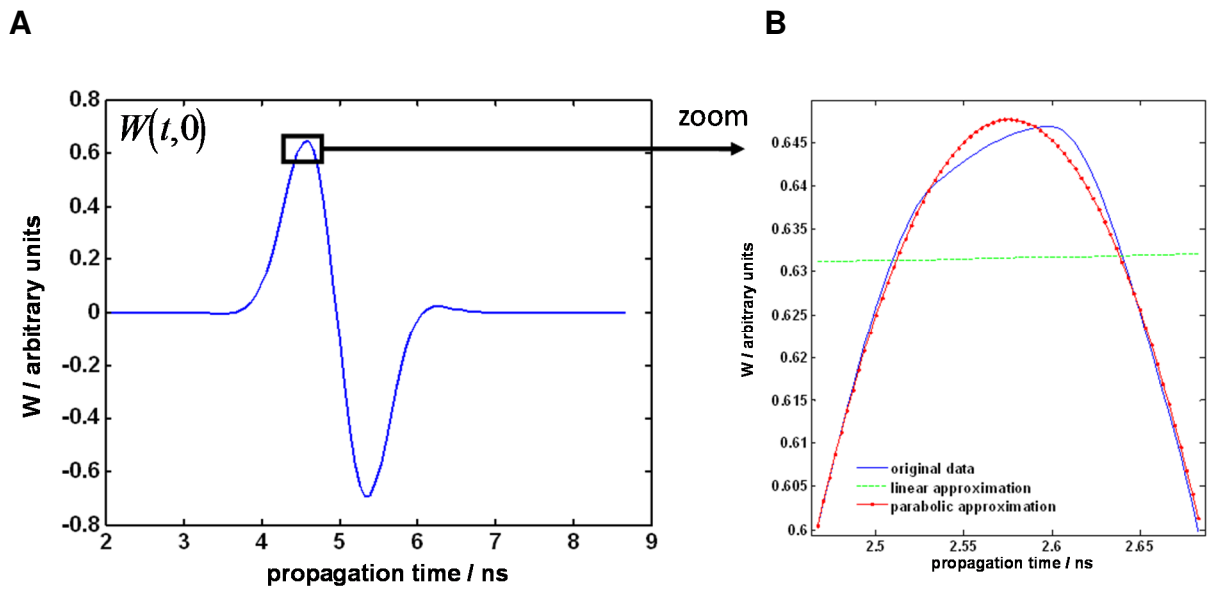


Figure 3.3:  $W(t,0)$ , its part observed strictly at the pulse extremum marked (A) and zoomed (B).

That is, when we observe at  $t_0$  symmetrical oscillations of the signal peak position,  $A_1 = 0$  and we see no signal component at the respiration rate  $\nu_0$ . Instead, all signal energy leaks into harmonic oscillating with the rate  $2\nu_0$  described by expression 3.8. Since parabola is in this case symmetrical around zero harmonic function of it is also symmetrical and period of observed oscillations is decreased two times in comparison with all other instances.

But how does the respiration amplitude affects this relation between different-rate components? How visible is motion at particular  $t_0$  is determined by the difference between maximal and minimal values of  $W(t_0, \tau)$ . This visibility we can estimate by considering  $W_s$  derivative by motion-related shift  $\xi$ . According to expression 3.2:

$$\left| \frac{dW_s}{d\xi} \right| = |2A_2\xi + A_1| \quad (3.10)$$

At the signal edge  $A_2 = 0$ , accordingly, in case of very weak breathing this sensitivity remains equal to the slew rate:

$$\lim_{\xi \rightarrow 0} \left| \frac{dW_s}{d\xi} \right|_{t=t_0} = |A_1| \quad (3.11)$$

And in opposite, at the signal peak we can state (since  $A_1 = 0$ ):

$$\lim_{\xi \rightarrow 0} \left| \frac{dW_s}{d\xi} \right|_{t=t_0} = 0 \quad (3.12)$$

Thus, the weaker the breathing (and very weak breathing is characteristic for unconscious victims) the more second type harmonics are minimized in comparison with main-tone components. Accordingly we can expect that to the very high extent energy of respiratory motion in the radagram appears at respiration rate. In addition as it follows from equation 3.11, increasing the slew rate leads to increasing the detectability of respiratory motion. We have seen in the previous chapter that slew rate is proportional to the frequency bandwidth. However, when bandwidth is fixed slew-rate depends on the shape of probing signal (on the shape of its autocorrelation function in case of M-sequence radar). One of the reasons why M-sequence radar is chosen for this work is that the auto-correlation function of M-sequence, has relatively high slew-rate among other possible probing signals.

Radagram of simulated respiratory motion (with purely sinusoidal motion and no harmonics of the first type) is shown in figure 3.4, A. We can see that this is a very specific pattern. That is, from the first view it has no similarity to radar noise or typical clutter. It is important, since under realistic conditions we need to perform detection in the presence of strong noise and clutter (and thus, it is good to be able to discriminate between useful signal and other contributors).

Subtle features connected with respiratory motion are good visible in horizontal (slow-time) spectrum after calculating Fourier transform:

$$\underline{Z}(t, \nu) = \int_{-\infty}^{+\infty} W(t, \tau) e^{-2\pi i \nu \tau} d\tau \quad (3.13)$$

Here I should make a short explanation of terminology. For the value  $\nu$  we use term 'sinusoidal micro-Doppler rate' (not to be confused with Doppler frequency), since breathing-like harmonic variations are often called in radar literature 'micro-Doppler effect'. In this case breathing would be seen as frequency modulations of the returned signal which generate sidebands about the target's body return Doppler frequency [37]. In our case of ultrawideband radar (which implies short target response in fast time),

more information is available in comparison with Doppler radar. One of the consequences is that UWB signals are not subjected to Doppler ambiguity due to the properties their ambiguity function [23]. Thus, it was more convenient to derive how respiration is seen in radargram in  $(t, \tau)$  domain instead of considering corresponding Doppler shifts.

In practice we are dealing with randomized discrete radargram  $\widehat{W}(l\Delta t, m\Delta \tau)$  and its spectrum  $\widehat{Z}(l\Delta t, k\Delta \nu)$  is calculated via discrete Fourier transform. This is considered in more details in chapter 3.3. For now, let us check whether we see respiration in simulated radar data in the same way how we predicted above.

Amplitude of discrete Fourier transform of the radargram containing single tone respiratory signal is shown in the figure 3.4B. First, we see very strong constant (zero sinusoidal micro-Doppler rate) component. In our theoretical considerations it is represented as  $A_0$  in equation 3.4. This component arises due to presence of the object rather than due to its motion (all static reflectors are represented with such peak only). Some researchers have developed algorithms for detecting breathing based on using this static component along with main-tone component (for example, [14]). This approach makes sense, however, only under conditions that it is guaranteed that breathing person is separated in distance from any stationary clutter source (like if it was situated in the free space). Eventually in this work we are not detecting breathing person in the open space (in fact, we are doing in the very different conditions in the sense of homogeneity: typical disaster area is full of diverse materials including air. Every border between two materials produces stationary reflection in the radar data). And unfortunately, there is no reason for the reflection from breathing person to be stronger than this type of stationary clutter. Still, breathing as such is distinct from unwanted components, but big part of the potentially useful signal energy has to be lost due to filtering it out together with stationary clutter.

Second, in figure 3.4 there is main-tone peak in the spectrum at about 0.3 Hz. When we remove constant component by subtracting horizontal mean value (resulting radargram  $W_{rb}$  and its horizontal amplitude spectrum  $|\underline{Z}_{rb}|$  are shown in figure 3.5) we can see that the strongest signal peak is produced at the breathing rate. This peak is crucial for detecting respiratory activity. Further in the text we refer to the complex values that appear in horizontal spectrum at the micro-Doppler rate of breathing and at corresponding propagation time as to 'main tone respiration signature'  $\underline{R}$ .



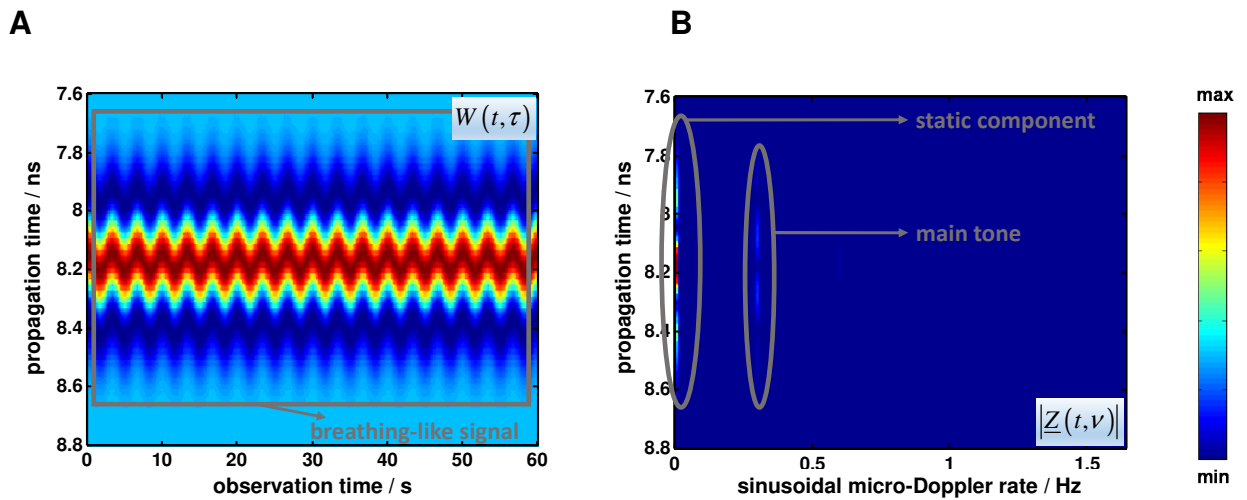


Figure 3.4: Simulated radargram of a breathing person and its amplitude spectrum without removing stationary component. Breathing amplitude: 3 cm, breathing rate: 0.3 Hz.

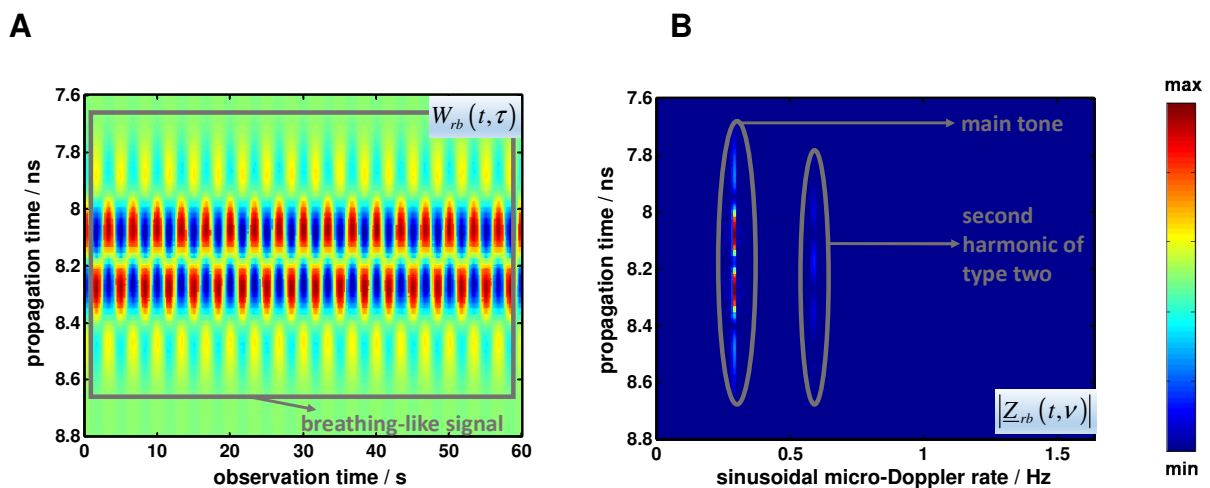


Figure 3.5: Simulated radargram of a breathing person and its amplitude spectrum after removing stationary component. Breathing amplitude: 3 cm, breathing rate: 0.3 Hz.

Second-type harmonic in figure 3.5 behaves as it was predicted in our theoretical considerations. It appears at 0.6 Hz. In propagation time its maximums (corresponding to extremums of initial pulse) appear together with minimums of main-tone signature and vice versa. No harmonics of higher order are detectable.

### 3.2 Respiratory motion in the measured data

Let us now consider measured radargram that contains respiratory motion. At this stage we need to decide which signal domain ensures better detectability of useful signal. For

this purpose figure 3.6 three representations of breathing signature in measured radar data are shown for through-wall scenario.

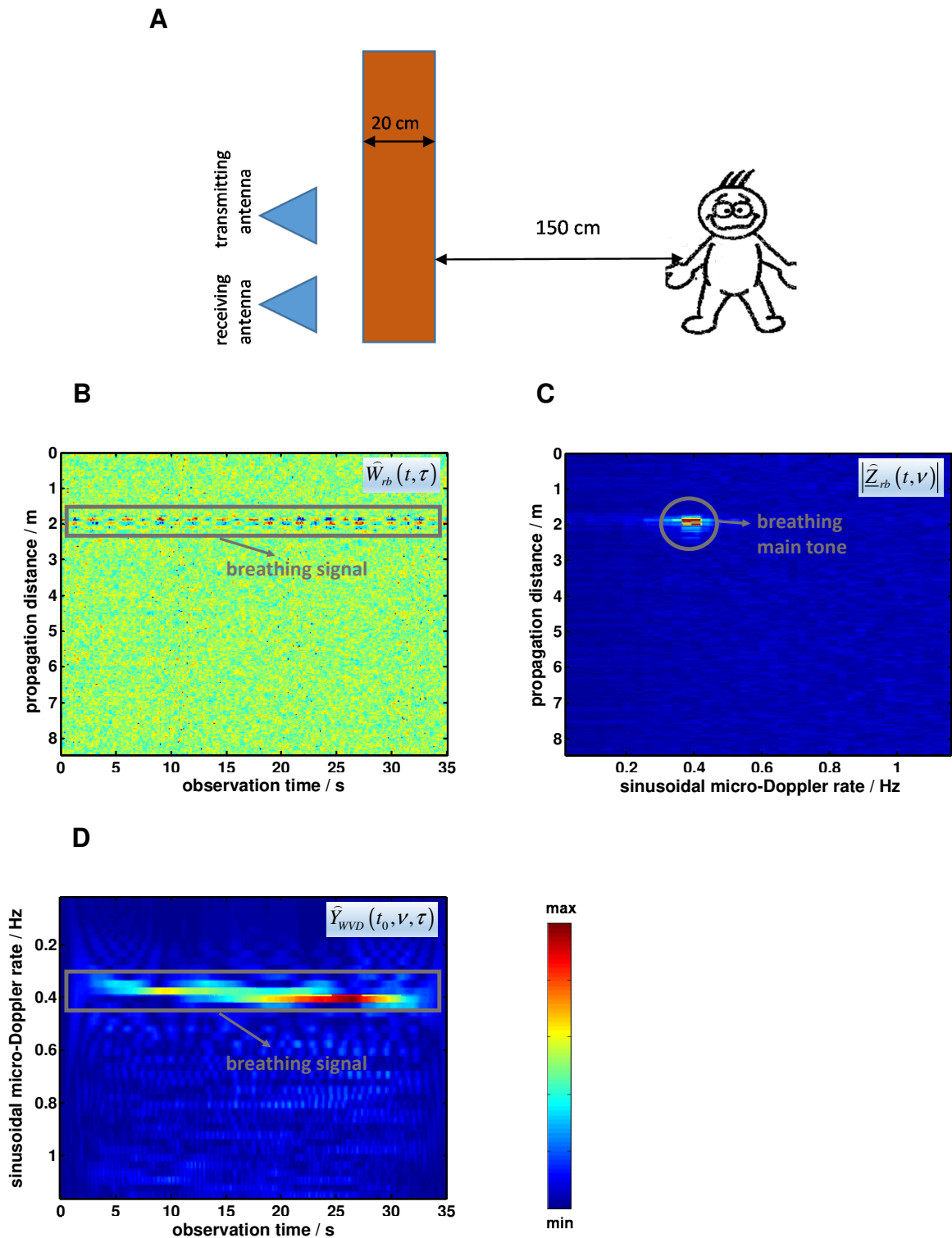


Figure 3.6: Person, breathing behind a wall: scenario description (A), radargram with background subtraction (B), radargram with FFT in slow-time direction (C) and the slice of Wigner-Ville distribution in slow-time direction at  $t_0$  (D).

Based on this figure we can make following observations:

- Time-domain representation (figure 3.6, B) is the closest to what was originally measured. Similar to the simulated data from figures 3.4 and 3.5 we can see in it that respiration is shown in the radar data as a very specific (almost periodical ‘horizontally’) variation at a certain distance from antennas (spread in distance ‘vertically’ over some interval). The main visual difference in comparison with the figures from the previous paragraph is certainly the presence of considerable noise (ratio  $\beta$  between maximal signal pixel and maximal noise pixel in figure 3.6, B is about 1.1). Under low SNR, which is typical for our task, this  $(t, \tau)$  signal representation is not the best since energy of useful signal is spread over observation time period.
- After Fourier-transforming the radargram ‘horizontally’ (figure 3.6, C) we can see that the data we have almost all breathing-related energy collected into one bright spot (as it was mentioned in many papers, for example [29], [1], [9]). This, in turn, means good contrast between signal and noise pixels in the images (in figure 3.6, C  $\beta$  is approximately 10). In this work such representation  $(t, \nu)$  serves as an input for further breathing enhancement.
- In time-frequency domain respiratory response can be analysed for example by means of Wigner-Ville distribution(WVD) of the horizontal lines of the radargram, which allows us to observe subtlest features of respiratory motion:

$$Y_{WVD}(t, \nu, \tau) = \int_{-\infty}^{+\infty} W\left(t, \tau + \frac{\zeta}{2}\right) W^*\left(t, \tau - \frac{\zeta}{2}\right) e^{-2\pi i \nu \zeta} d\zeta \quad (3.14)$$

When looking at a slice of Wigner-Ville distribution of breathing response taken at fixed instant  $t_0$  (figure 3.6, C) we can see that breathing is not stationary: magnitude, as well as frequency, was slightly changed during the measurement. Probably this happened because person under test started to breathe a bit differently.

Thus, when speaking about respiratory motion in radar response we should speak about quasi-stationary signals rather than stationary. Obviously, this leads to the idea of using various time-frequency methods to characterize respiratory motion. This approach is described in literature, for example in [19] and [17]. In general, time-frequency analysis is a very promising tool for the monitoring of respiratory and/or cardiac activity.

However, when considering application to search&rescue we mainly concentrated on the scenarios with low SNR, limiting ourselves to the problem of enhancing and detecting quasi-periodical motion and then localizing its source, without frequency tracking. In our example from figure 3.6 we can see that  $\beta$  in case of using Wigner-Ville distribution was somewhat lower than in horizontal Fourier spectrum (approximately 5 against 10). However, in order to demonstrate persistency of this effect, more noise was added into dataset described in figure 3.6. Wigner-Ville distribution and horizontal Fourier spectrum of such dataset are shown in figure 3.7.

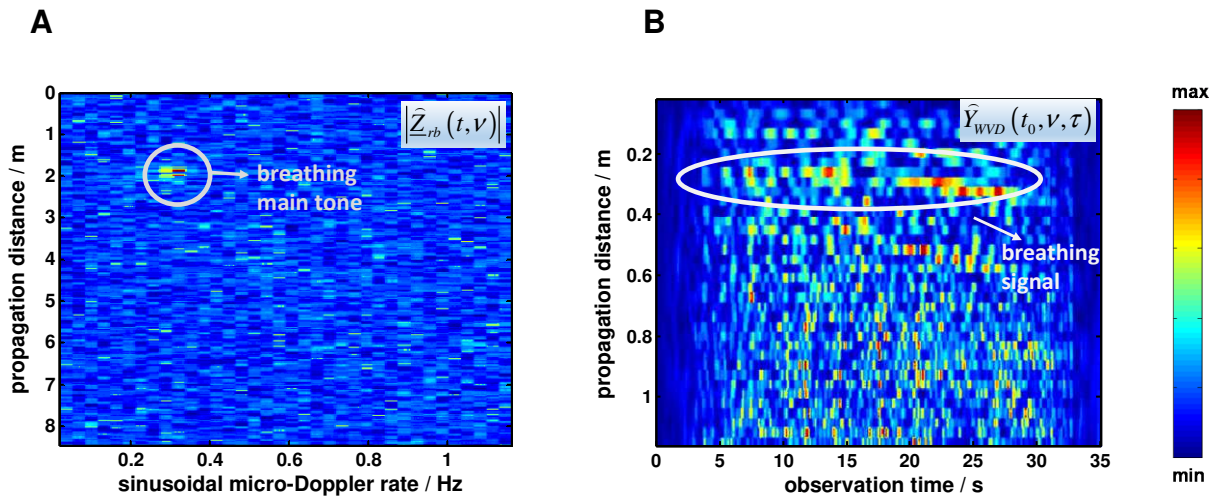


Figure 3.7: Person, breathing behind a wall, data with noise added: radargram with FFT in slow-time direction and Wigner-Ville distribution in slow-time direction. The same data without additional noise is shown in figure 3.6

We can see that in horizontal spectrum respiratory motion produces maximum of the image ( $\beta \approx 2$ ) while in time-frequency representation we cannot detect useful signal  $\beta \approx 1$ . Instantaneous amplitude of respiration in rescue scenarios is typically minor in comparison with noise and it is not well detected directly in time-frequency representation while it is visible in horizontal spectrum due to proper data accumulation in longer measurement. Besides, processing 3D image produced via WVD is cumbersome (hardly possible while remaining close to real time while relatively fast decision is needed in our application).

However, the fluctuation of breathing rate will limit the performance of a simple “horizontal” FFT over long time windows. In this work we accounted though to a certain extent for small changes in breathing rate by using Welch-like method controlling the size of our frequency cell where breathing is expected to be found (see chapter 3.3).

### ***3.3 Spectral estimation methods and detection of periodical motion.***

As it was discussed above, in order to estimate periodical motion it makes sense to transform discrete (and affected by noise) measured radargram  $\widehat{\mathbf{W}}(l\Delta t, m\Delta \tau)$  into sinusoidal micro-Doppler rate domain  $\widehat{\mathbf{Z}}(l\Delta t, k\Delta \nu)$ . This allows us to operate over the signal in the domain, where breathing is localized most compactly due to its periodicity.

The problem of calculating this spectrum, however, does not yield unambiguous solution in our case. According to Wiener-Khinchin theorem unambiguous solution exists when infinite amount of data is available (that is, when data represents a known function) and it is given by Fourier transform (equation 3.13). Otherwise, for the instances when only finite amount of data is available, one should choose an algorithm from the multiple parametric and non-parametric methods to calculate the spectral estimate of given time series, FFT being only one of them.

The majority of literature on breathing detection under low SNR [14], [20], etc. considers straightforward FFT as the only spectral method for breathing detection without any reference to its analogues. However, given numerous methods of calculating PSD the question about suitability of various spectral estimates regarding breathing detection had to be raised. In literature, this issue is touched in [27], where example of processing breathing-containing radar data with MUSIC is given.

How it is pointed out at [18] the problem of estimating multicomponent spectra as a whole from (typically) severely limited dataset treated via unconventional spectral methods is pretty much different from our task of detecting a single sine and estimating its parameters. In the most of problems properties of the spectrum as a whole are of interest. Unlike in the classic spectrum estimation problems our main interest is the enhancement of single periodical in comparison with noise, not estimating the noise statistical properties. In order to underline this difference in the problems under solution, let us consider an example.

Two particular cases of how periodical is not detected in noise while in average spectral estimate is better than when periodical is detected are given in figure 3.8.

We can see that noise level is estimated better with Yule-Walker method: power spectral density of white noise is theoretically constant (in infinite observations) and in case of using Yule-Walker method it really varies much less than after using FFT (that is, in figure 3.8, A we see more flat curve outside the signal region than in figure 3.8, B). However, due to this effect detecting single sine becomes problematic when noise is increased. It can be observed if we compare figure 3.8, C and figure 3.8, B that after FFT maximum of the spectrum is still produced at the breathing rate (0.3 Hz) while in

Yule-Walker spectrum noise peak is maximal. This happens because ‘flattening’ of the spectrum with Yule-Walker method ‘flattens’ sharp signal peak (and, in turn, signal peak influences the noise estimate). Thus, SNR is reduced.

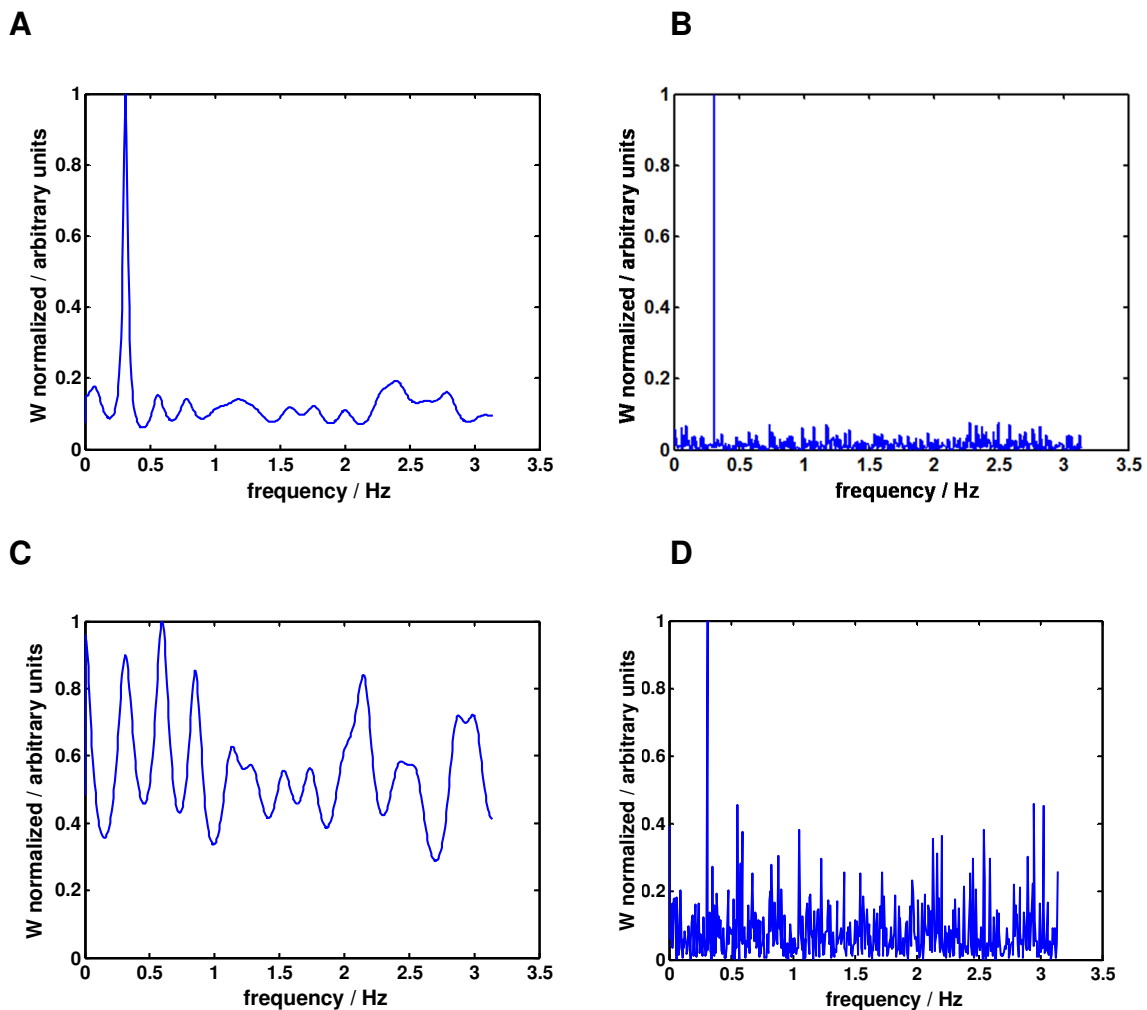


Figure 3.8: Yule-Walker spectrum (A and C) and FFT<sup>2</sup> spectral estimate (B and D) of single sine in AWGN. Results shown on top and on bottom are computed with identical datasets correspondingly.

Let us now formulate numerical problem of detecting respiratory motion in the radargram. When only one propagation time bin  $t_0 = l_0 \Delta t$  is considered our problem is reduced to a search for a small number of periodicals (most probably one) with unknown phase  $\varphi_1$  and amplitude  $D_0$  in Gaussian noise. From the viewpoint of detection theory we are looking for solution of the following problem with two hypothesis for every

slow-time frequency  $\nu = \frac{\omega}{2\pi}$ :

$$\begin{aligned}
H_0 : \widehat{\mathbf{W}}(l_0\Delta t, m\Delta\tau) &= \mathbf{n}(l_0\Delta t, m\Delta\tau), 0 \leq m \leq M-1 \\
H_1 : \widehat{\mathbf{W}}(l_0\Delta t, m\Delta\tau) &= D_0 \cos(\omega m\Delta\tau + \varphi_1) + \mathbf{n}(l_0\Delta t, m\Delta\tau), 0 \leq m \leq M-1
\end{aligned} \tag{3.15}$$

where  $\Delta\tau$  is slow-time sampling interval;  $m$  is observation time sampling index,  $\mathbf{n}(l_0\Delta t, m\Delta\tau)$  is AWGN. The amplitude  $D_0$  and phase  $\varphi_1$  are assumed to be realizations of uniformly distributed random variables remaining constant during measurement time  $M\Delta\tau$ . Hypothesis  $H_0$  means no presence of respiratory motion at  $l_0\Delta t$ ; hypothesis  $H_1$  means the opposite.

Optimal solution of the problem 3.15 is known. It is shown in figure 3.9: we need to apply two correlation receivers of original signal with sine/cosine of the same frequency and make decisions based on these values (how it is proven in [3]). Estimate of the signal amplitude is calculated according to:

$$|\widehat{\mathbf{Z}}| = \sqrt{\widehat{\mathbf{Z}}_c^2 + \widehat{\mathbf{Z}}_s^2} \tag{3.16}$$

where  $\widehat{\mathbf{Z}}_c$  and  $\widehat{\mathbf{Z}}_s$  are the outputs of correlation receivers.

We can see that calculations of  $\widehat{\mathbf{Z}}_c$  and  $\widehat{\mathbf{Z}}_s$  according to algorithm from figure 3.9 can be accomplished by means of FFT (and this gives us mathematical answer about why FFT is more efficient in application to breathing detection than other spectral-estimating techniques):

$$\widehat{\mathbf{Z}}(l_0\Delta t, k\Delta\nu) = \widehat{\mathbf{Z}}_c(l_0\Delta t, k\Delta\nu) + i\widehat{\mathbf{Z}}_s(l_0\Delta t, k\Delta\nu) = \sum_{m=0}^{M-1} \widehat{\mathbf{W}}(l_0\Delta t, m\Delta\tau) \underline{e^{-2\pi i k m / M}} \tag{3.17}$$

Breathing person can be located at any frequency  $m\Delta\nu$  within the specified interval with equal probability. The value from (3.16) is sufficient statistics for detection (for solving the problem given in (3.15)). This is true, however (with the precision of discretization step of horizontal frequency  $\Delta\nu$ ), only as long as we do not take into account deviations of real signal from sine with unknown phase (these deviations take form of harmonics and non-stationarities), and as long as we do not consider breathing person as a range-spread target. These issues are addressed further in this chapter. Another inevitable limitation on calculation according to expression 3.17 is that our dataset is finite both due to the observation time and sampling interval limitations. However, here these effects (they are called spectral leakage) are alleviated by the fact that both limitations are not as severe as in many other applications since with M-sequence radar we are able to collect at least hundred of IRFs per respiratory period and several hundreds of periods in total (within the 20 minutes interval)

Besides, optimal maximum likelihood estimate of the sine initial phase is also calculated from input signal correlations with sine/cosine as

$$\varphi_1 = \tan^{-1} \left( \frac{\widehat{\mathbf{Z}}_c}{\widehat{\mathbf{Z}}_s} \right) \quad (3.18)$$

This is an important result for detecting breathing person as a range-spread target, since there is a special relation between breathing phases from different propagation-time instants (this issue is addressed further in this work).

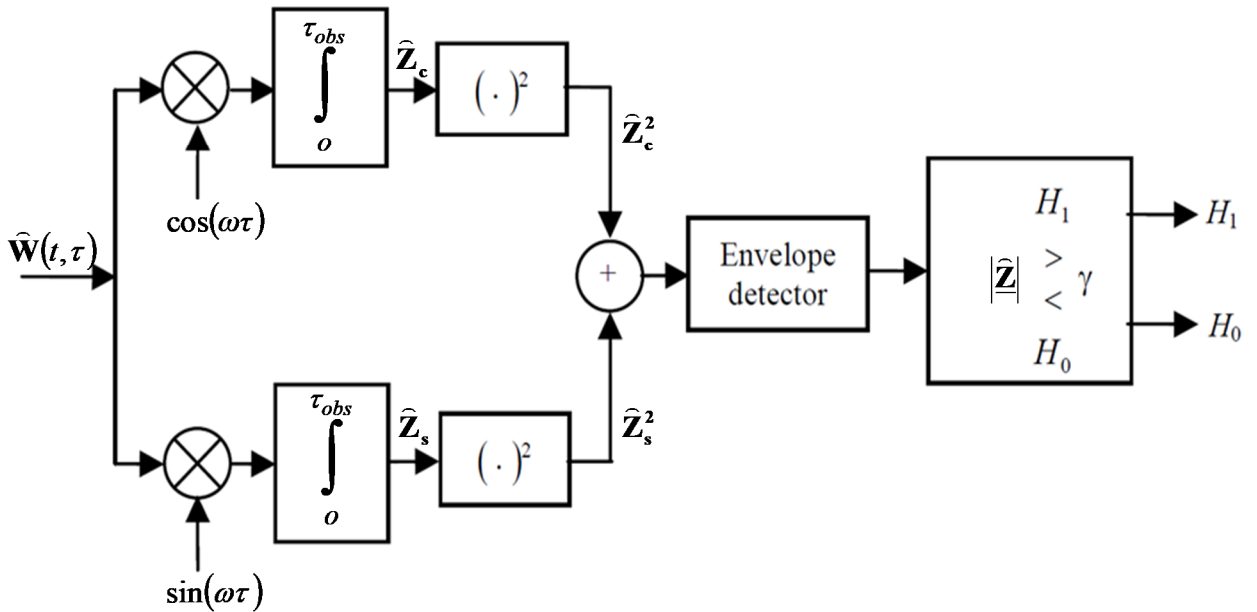


Figure 3.9: Optimal detection scheme for sinusoid in additive white Gaussian noise how it is given in [3]

We can estimate how much does FFT improve SNR depending on the number of available slow-time samples  $M$  in the following way. After FFT according to expression 3.17 our squared mean signal value is given by power spectral density (PSD) at the respiration sinusoidal micro- Doppler rate:

$$E_s = M^2 D_0^2 . \quad (3.19)$$

In order to keep the actual units, multiplication by  $\frac{\Delta\tau}{M}$  is often used in (3.19). However, since we only need the value in 3.19 to calculate SNR, such normalization does not have any influence on final results. Further in this work we refer to the ‘squared’ units of  $\widehat{\mathbf{Z}}(l_0\Delta t, m\Delta\nu)$  as to energy values as it is common in signal theory.

Noise variance we get the same way as in expression 3.19:



$$E_n = M\sigma^2 \quad (3.20)$$

Accordingly, SNR is given by:

$$SNR_{FFT} = \frac{E_s}{E_n} = \frac{MD_0^2}{\sigma^2} \quad (3.21)$$

Thus, in ideal case FFT helps to increase SNR in energy units proportional to the number of collected IRFs.

Based on the arguments given in this chapter, we use observation-time FFT of the pre-processed radargram as a basic tool and as an input for most of the further data processing methods.

### 3.3.1 Welch method in application to breathing detection

As it was discussed in chapter 3.2, breathing is in general non-stationary. Its frequency (and other parameters) can change over time. All these changes are subjective and only very limited amount of information about them (as seen by the radar) can be derived. First, increasing observation time increases the change probability, since we can safely suppose that probability of any change is equal at any moment. Second, minor changes become better visible after FFT with the time going for the following reason: according to

$$\Delta\nu = \frac{\nu_s}{2M} \quad (3.22)$$

the more observation time samples with the fixed horizontal sampling rate  $\nu_s$  we have the higher the micro-Doppler rate resolution  $\Delta\nu$  of the system.

According to equation 3.22, breathing becomes inevitably spread over several neighbouring  $\nu$  samples in case its rate was not constant during observation interval. Since useful signal energy is no longer concentrated within one micro-Doppler rate sample ('bright point'), FFT is no longer an optimal breathing-enhancing processing. However, any can 'limit' FFT resolution so that breathing is most probably confined within one sinusoidal micro-Doppler rate bin and have noise variance reduction with collecting new data. For this purpose well-known Welch method with fifty percent segments overlapping can be used. When applied to radargram classical Welch algorithm can be described in the following way:

1. Each horizontal line of the radargram  $\widehat{W}(l_0\Delta t, m\Delta\tau)$  is divided into the number of overlapping segments of length  $M$ . Over each  $p$ -th segment Discrete Fourier transform is subsequently performed:

$$\widehat{\underline{Z}}_p(l_0\Delta t, k\Delta\nu) = \frac{1}{M \sum_{m=0}^{M-1} w_m} \sum_{m=pM\eta}^{pM\eta+M-1} w_m \widehat{\underline{W}}(l_0\Delta t, m\Delta\tau) e^{-2\pi i m k / M} \quad (3.23)$$

Here  $\eta = 1 - x$  where  $x$  is the overlapping ratio.

2. The set of FFTs (as the power spectrums) is averaged over  $p$  in order to calculate PSD estimate

$$\widehat{\underline{Z}}_w(l_0\Delta t, k\Delta\nu) = \frac{1}{P} \sum_{p=0}^{P-1} |\widehat{\underline{Z}}_p(l_0\Delta t, k\Delta\nu)|^2 \quad (3.24)$$

Windowing with  $w_m$  is used in equation 3.23 in order to reduce the effect of sidelobes and consequent displacement of spectral components at the price of insignificantly reducing the resolution. In our case we do not expect in our data signal components stronger than breathing signature that could cause such sidelobe effect and thus rectangular window is to be used (even though other window types might be used if spectral leakage is considered important).

It should be always kept in mind that how it was shown earlier in this chapter in the case of ideal periodic motion optimal (in a certain sense) solution is given by Fourier transform, not by Welch method. That is, ideally the length of one segment in Welch method should correspond to the maximal observation time when breathing rate was not changed. No statistics is available about possible duration of this interval. However, reference observation time duration for one radargram processed via FFT to be found in literature is one minute (or even slightly below like in [6]) which implies absence of significant deviations during this time and good concentration within horizontal bin. Of course, if more statistics about how conscious and unconscious people breathe is available method parameters could be improved.

In this work Welch-style processing have proven to be helpful from the practical viewpoint in many scenarios both due to its detecting capabilities and because it is a very convenient method for implementing it in online (Welch method allows updating measurement results after new data segment is collected to get somewhat better estimate). Let us give some examples.

One example when breathing is not detected via full-length horizontal FFT is given in figure 3.10, A. It seems that respiratory signal energy was almost equally split between several points in micro-Doppler rate and as a result noise peaks are higher than signal ones ( $\beta$  in this image is less than one). Welch method, however, collected all breathing-related signal energy into one bright spot (see figure 3.10, B). As a result we can see that SNR was significantly increased ( $\beta$  is about two).

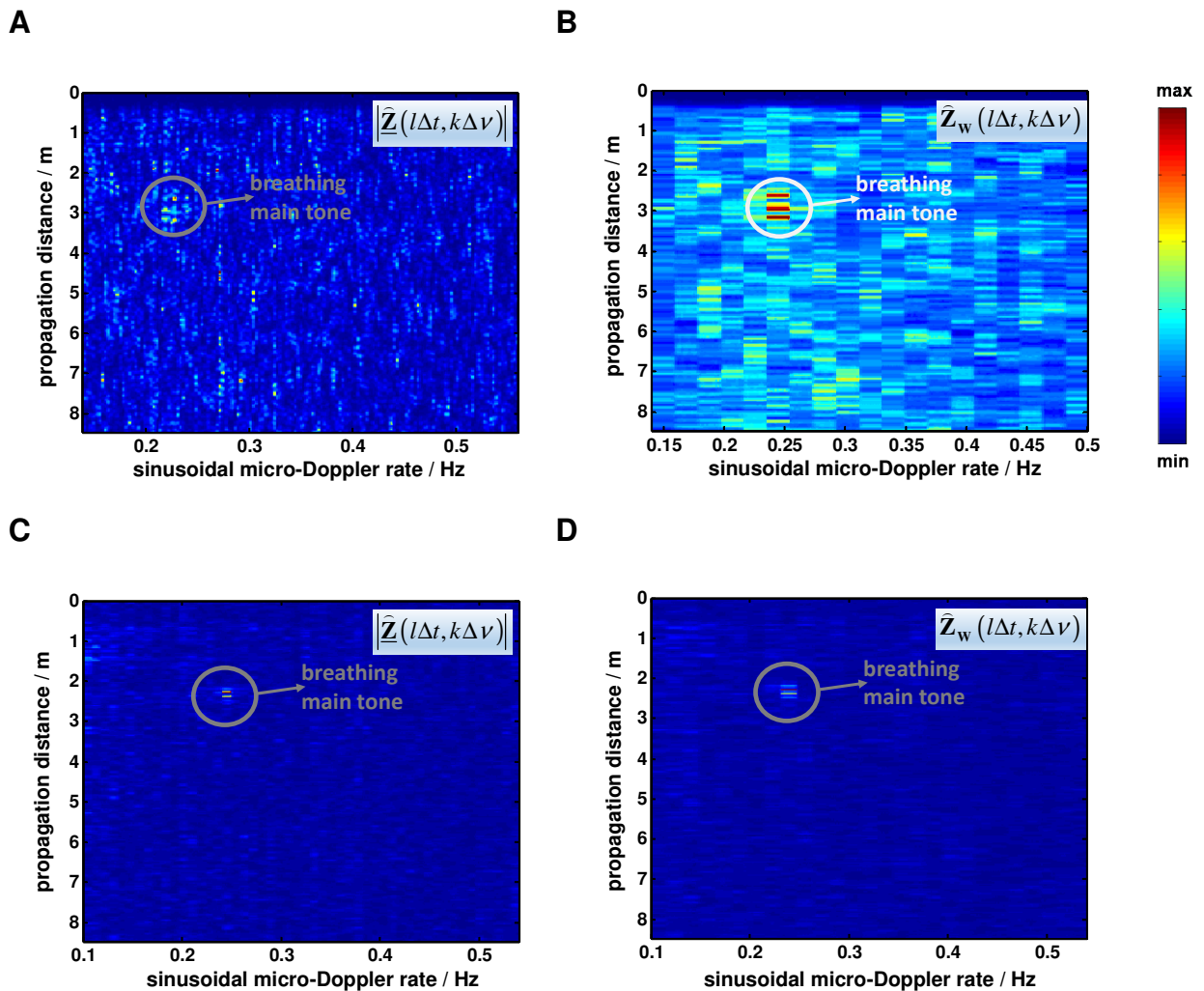


Figure 3.10: Person breathing more than one meter beneath concrete rubble as seen after FFT (A, C) and Welch method (B, D).

More often, however, after horizontal FFT there is a bin much brighter than others are. This situation is shown in figure 3.10 C and D: respiration was well detected by both methods with approximately the same SNR ( $\beta$  is about five)

Importantly, in first case data collection time was five minutes and in the second one it is about two minutes. This is probably one of the reasons why respiratory motion in the spectrum was more spread horizontally in the first case, as it was to be expected according to discussion above.

Of course, examples where breathing remained stable for two-three minutes can also be found and in this case full-length FFT performs better than Welch method due to FFT 'optimality'. If decision about the presence of person is to be made by operator, I would recommend having both results and looking for clear maximum in one of them in case it is not found in both images simultaneously. More generally, Welch method with different segment length might be considered.

In any case, overall efficiency of Welch algorithm depends on the efficiency of horizontal FFT of every segment. Thus, denoising algorithms that are derived further for being used with FFT and judgements about their efficiency are valid in case Welch method is applied.

Our main motivation for using Welch method is explained above. However, in addition we should list other useful features of this algorithm allow choosing it and not some other PSD-estimating technique:

- 1) Overlapping of data segments helps to reduce the variance over PSD estimate.
- 2) Statistical properties of Welch estimate are (along with some other methods) the best reached via classical, FFT-based data processing.
- 3) As any other classical FFT-based PSD estimate, Welch method keeps the linear relation between the height of signal peaks and the power of signal components. This is not true for many PSD-estimating methods. One example is shown in figure 3.11.

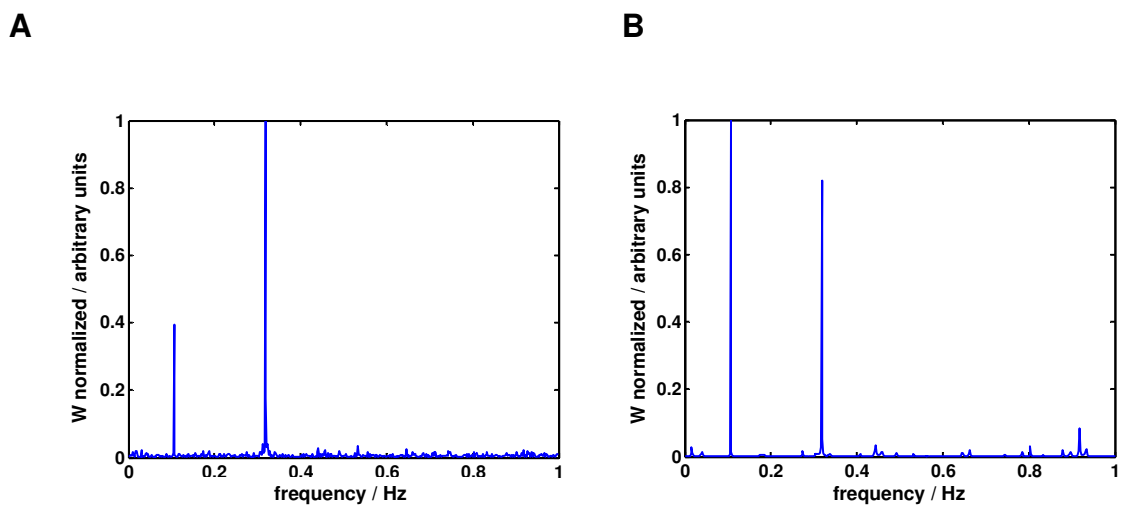


Figure 3.11: Spectrum of noisy dataset containing two periodicals, calculated with FFT (A) and MUSIC (B).

- 4) Dataset used to calculate PSD estimates shown in figure 3.11 was generated according to equation:

$$\widehat{W}(l_0 \Delta t, m \Delta \tau) = 0.4 \cos(0.1 * 2\pi m \Delta \tau) + \cos(0.35 * 2\pi m \Delta \tau) + n(m \Delta \tau) \quad (3.25)$$

We can see that both periodicals are well visible independently of the method of calculating them. However, in this particular case MUSIC ascribed larger amplitude to the periodical with lower frequency, which contradicts to simulation scenario. This property (proportionality between actual signal power and its estimate) is especially important in our case, since this relation is needed at the stage of SNR enhancement due to breathing person being a range-spread target further in this work.

- 5) In general, unlike Welch method, most of the advanced spectral-estimating techniques aim at increasing the resolution of PSD estimate at the price of insignificantly reducing the robustness of data processing method and worsening its statistical properties. However, robustness is more important in our case than frequency resolution: we control the frequency resolution of the spectral estimate by choosing the segment length in Welch method.

### **3.3.2 Bispectrum slice method**

Higher-order spectral analysis (HOSA) is widely used in signal processing due to its abilities to reducing white Gaussian noise and wide possibilities to handle harmonics arising during the measurement. Besides, it allows extraction of amplitude and phase information about periodicals while phase information is inevitably lost in second-order statistics.

As we have seen above, FFT allows extraction of amplitude and phase information of respiratory signature. However, the issues of treating first and second type harmonics in the presence of noise were not addressed yet.

In figure 3.12 measured harmonic-containing Fourier-transformed radargram with one breathing person is shown. Strong peak signals the presence of a person respiratory activity with a rate of about 0.4 Hz. More interesting is that there is also somewhat weaker peak at about 0.8 Hz, strictly two times the frequency of main signal component (first type harmonic). That is, particularly in this scenario we expect that processing described below can bring somewhat better result rather than FFT in terms of SNR and, most importantly, detection rate. As for the blurring of main peak in such a short dataset, I should note that in general data collected with standing people is much less stable that that with sitting or lying persons, due to occasional unwanted motion in the first case.

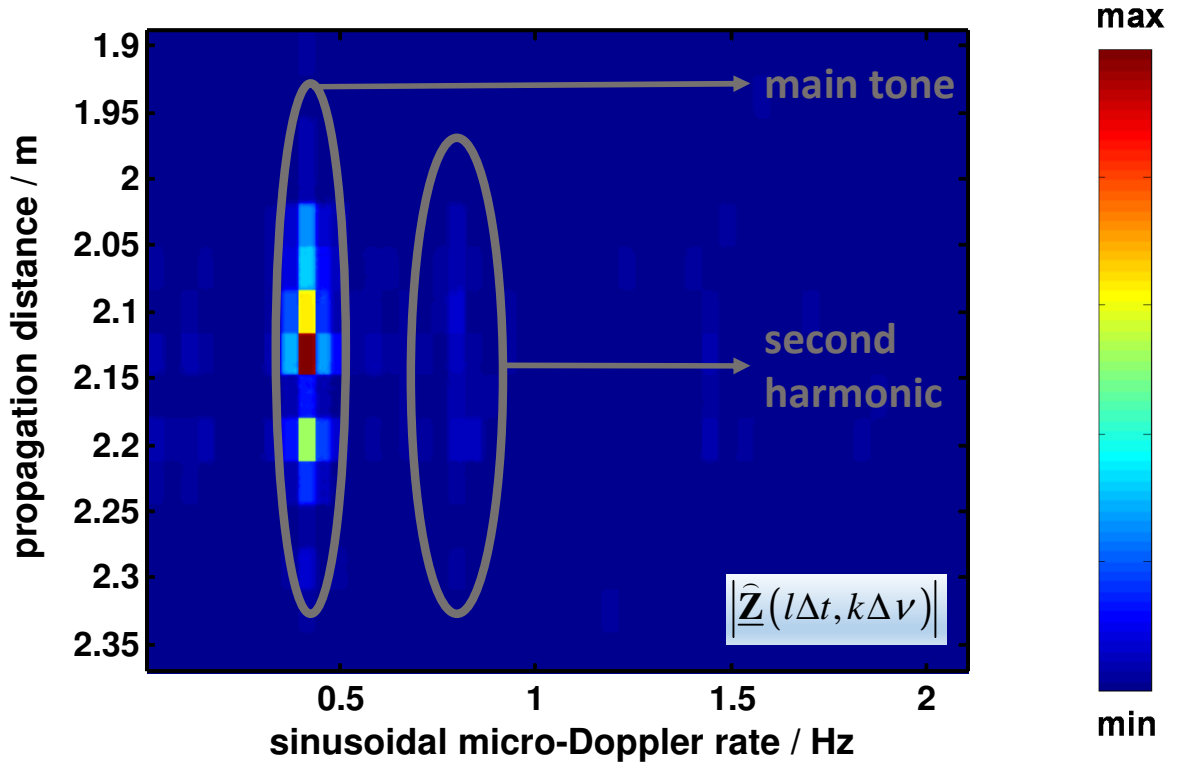


Figure 3.12. Standing person breathing. Brick wall was in between antenna and person. Data collection time is about 30 seconds.

In [10] a study on detecting weak periodicals in real (measured) noise by means of different HOSA techniques is given. For this work we have chosen bispectrum slice method as the one relying on the presence of second harmonic in order to check whether HOSA brings an improvement in comparison to FFT in detecting harmonic-containing respiratory motion. Importantly, according to [10] this technique will not work properly on pure sine without harmonics. The reason follows straight from the definition of this method given below.

Bispectrum is roughly estimated from Fourier transform spectrum of original data as:

$$\mathbf{G}(v_x, v_y) = \mathbf{FFT}(v_x) \mathbf{FFT}(v_y) \mathbf{FFT}^*(v_x + v_y) \quad (3.26)$$

That is, if we expect second harmonic of breathing to be strong, we can use the slice  $\hat{\mathbf{Z}}_B$  of bispectrum given below in equation 3.27 as a horizontal spectral estimate which can be subsequently used for further processing. For the case  $v_x = v_y = k\Delta\nu$  we can define:

$$\hat{\mathbf{Z}}_B(l_0\Delta t, k\Delta\nu) = \hat{\mathbf{Z}}(l_0\Delta t, k\Delta\nu) \hat{\mathbf{Z}}(l_0\Delta t, k\Delta\nu) \hat{\mathbf{Z}}^*(l_0\Delta t, 2k\Delta\nu) \quad (3.27)$$

Here  $\hat{\underline{z}}$  is determined via horizontal FFT. We can immediately note one disadvantage of breathing detection based on equation 3.27. The problem is that when we are looking for breathing-related harmonics inside the sinusoidal micro-Doppler rate interval  $\nu_{\min} \leq k\Delta\nu \leq \nu_{\max}$  in case of using 3.27 we have to use frequencies from outside this range, up to  $2\nu_{\max}$ . By doing this we introduce additional noise into our data. That is we can expect that harmonic distortion has to be pretty strong in order to compensate this effect in terms of SNR.

### ***3.4 Breathing detection based on the properties of main tone respiration signature***

As it was shown in chapter 3.2, breathing signature is slightly spread in propagation time  $t$  (and, consequently, in distance). The reason is that the varying pulse associated with human chest has a length  $u_w = Q\Delta t$  of  $Q > 1$  samples, as any UWB signal representing reflection from a physical object. This phenomenon and how it can be used to denoise the radargram is discussed below.

#### **3.4.1 FIR filtering in range direction**

Frequency bandwidth of the measured IRF is typically wider than operational bandwidth of antenna system. At the same time unlike noise useful signal can only be found at the frequencies where antennas work. Accordingly, obvious step for increasing SNR is denoising by FIR (Finite Impulse Response) filtering in vertical direction. Therefore, measured radargram after removing from it stationary background  $\hat{\mathbf{W}}_{\text{rb}}(l\Delta t, m\Delta\tau)$  is convolved with a filter function  $\mathbf{g}_f$  to get the filtered radargram  $\hat{\mathbf{W}}_f$ :

$$\hat{\mathbf{W}}_f(l\Delta t, m\Delta\tau) = \sum_{p=0}^L \mathbf{g}_f(p) \hat{\mathbf{W}}_{\text{rb}}((l-p)\Delta t, m\Delta\tau) \quad (3.28)$$

Note, that in 3.28 we do not yet take into account other aspects that could put stricter actual bandwidth limitations on main tone respiration signature (propagation through more than one meter of rubble, potentially moist, with properties that are not completely known *a priori*). Typical influence of these factors, however, consists of shifting the respiration signature in radar data towards the lower frequencies, since propagation loss of building material decreases with frequency. The same is true when we speak

about moisture influence. One measurement example, demonstrating this phenomenon is given in figure 3.13:

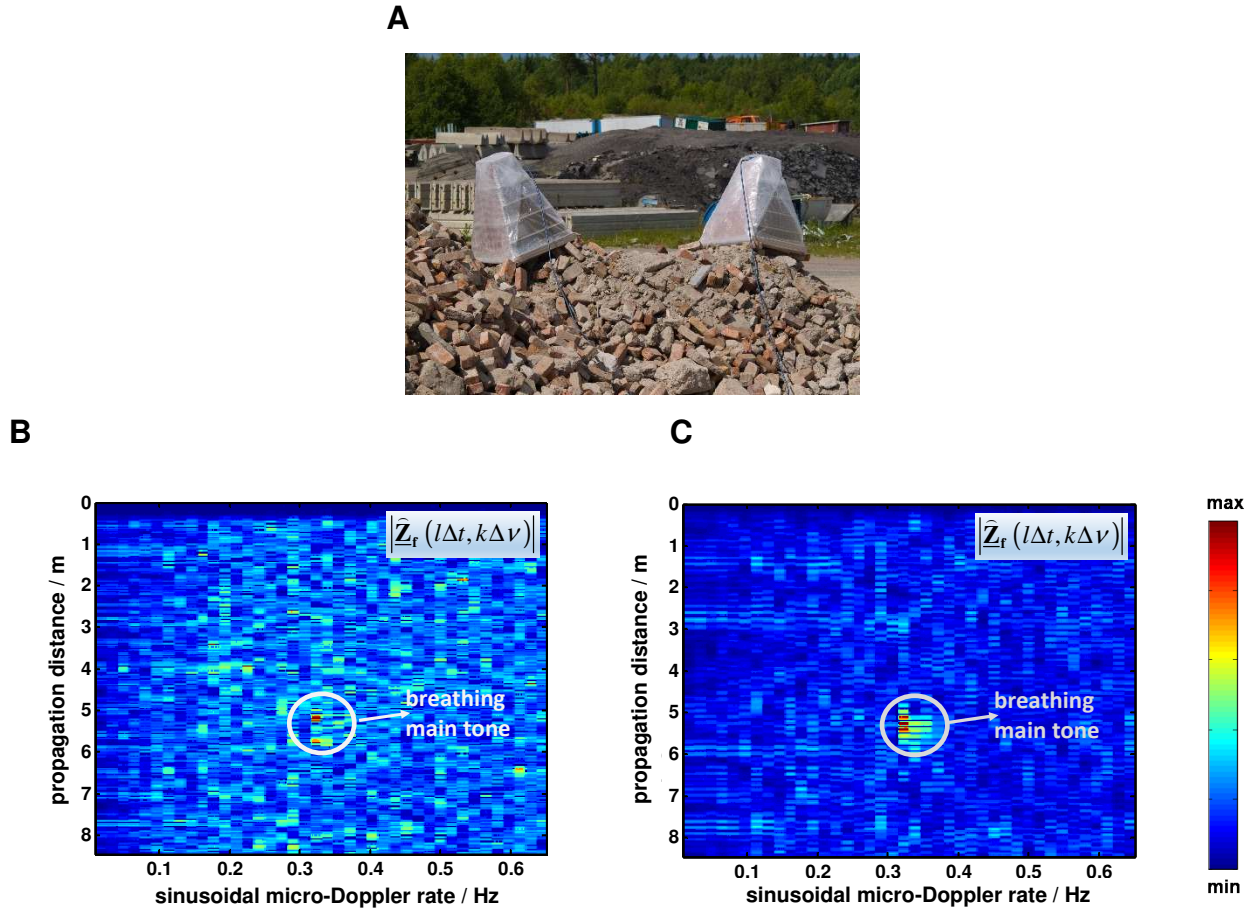


Figure 3.13: Person, breathing beneath the heap of bricks inside the pipe, made of reinforced concrete. Data is filtered with upper cut-off frequency of 300 MHz (B) and 700 MHz (C).

### 3.4.2 Statement of the problem of respiratory motion enhancement due to respiratory signature being range-spread

In filtered horizontal spectrum of the radargram  $\hat{\mathbf{Z}}_r(l\Delta t, k\Delta \nu)$  maximization of detection probability is considered with respect to the following problem:

$$\begin{aligned}
 H_0 : \hat{\mathbf{Z}}_r((l+q)\Delta t, k\Delta \nu) &= \mathbf{n}((l+q)\Delta t), -\frac{Q}{2} \leq q \leq \frac{Q}{2} \\
 H_1 : \hat{\mathbf{Z}}_r((l+q)\Delta t, k\Delta \nu) &= \mathbf{R}(q\Delta t) + \mathbf{n}((l+q)\Delta t), -\frac{Q}{2} \leq q \leq \frac{Q}{2}
 \end{aligned} \tag{3.29}$$

Here  $H_1$  and  $H_0$  are hypothesis of main tone respiration signature  $\mathbf{R}(q\Delta t)$  being accordingly either present or absent in the measured data. Symbols used in (3.29) are clarified in figure 3.14:  $Q\Delta t$  is the length of the respiration signature, its values being



considered at all possible instants  $q\Delta t$ . The problem (3.29) has to be solved at all propagation time instances  $t \leq t_{\max}$  (and accordingly  $0 \leq l < L$ ) inside radar unambiguous range (unless another limit is given by specific measurement scenario) and all sinusoidal micro-Doppler rates  $\nu \leq \nu_{\max}$  ( $0 \leq k < K$ ) which interval represents all possible breathing rates of different people.

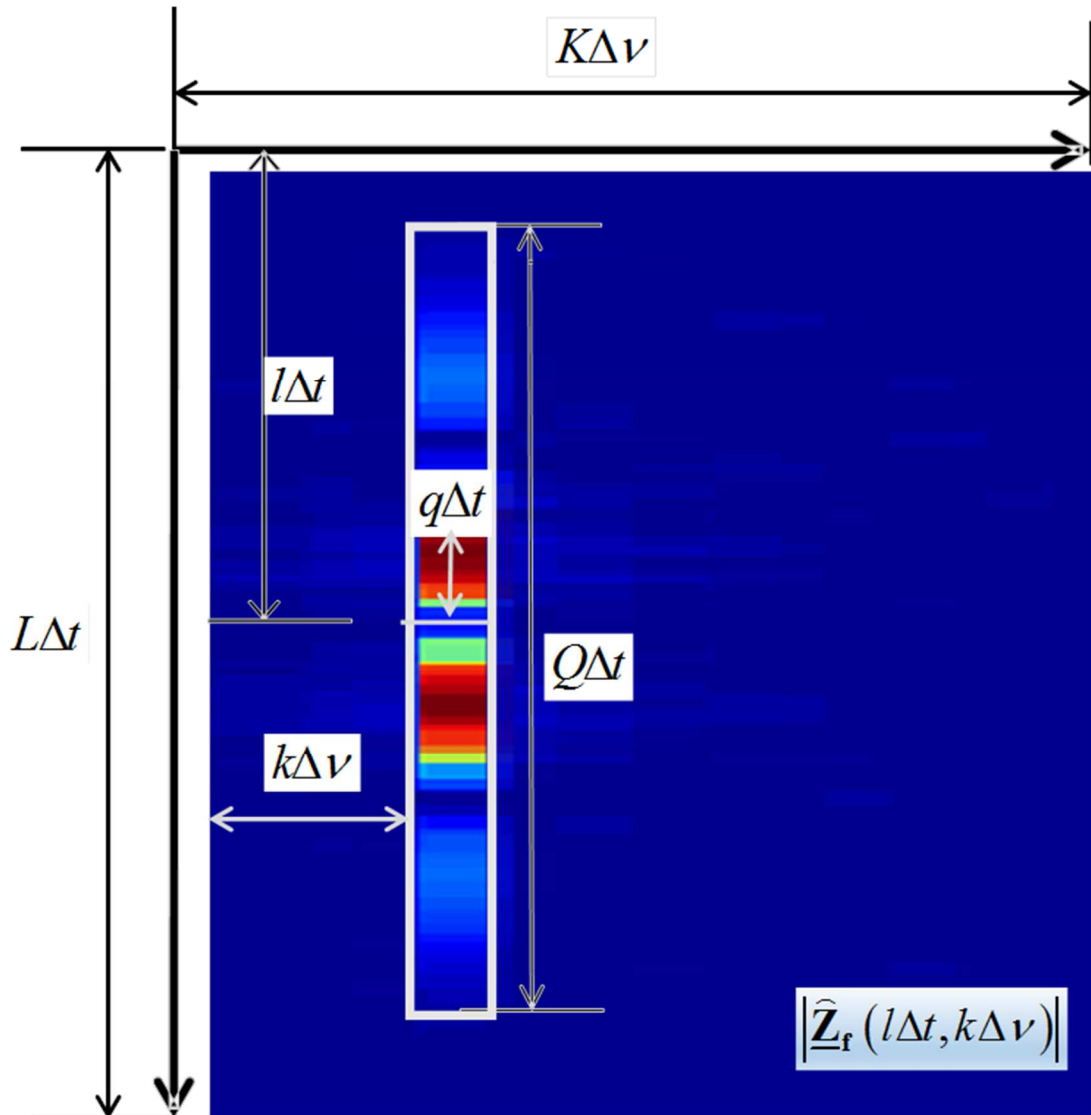


Figure 3.14: Blockwise processing of radar data for breathing enhancement

### 3.4.3 Optimal detection by means of correlation detector as a boundary for SNR improvement. Correlation processing with measured reference signature.

If respiratory motion was single-tone and main tone respiration signature was known, we could use  $\underline{\mathbf{R}}$  and apply an optimal processing based on correlation detection (CD):

$$\widehat{\mathbf{Z}}_{CD}(l\Delta t, k\Delta \nu) = \frac{1}{Q} \left| \sum_{q=-Q/2}^{q=Q/2} \widehat{\mathbf{Z}}_t((l+q)\Delta t, k\Delta \nu) \mathbf{R}^*(q\Delta t) \right| \quad (3.30)$$

Taking the absolute value in this equation means that we do not rely on the knowledge of breathing initial phase (since there is no chance to get this knowledge in practice). Besides, knowledge of main-tone amplitude  $D_0$  is not important. That is, substituting  $\mathbf{R}$  with  $D_0 e^{i\phi} \mathbf{R}$  would produce identical results in terms of SNR.

We can define the SNR after using CD processing as following:

$$SNR_{CD} = \frac{\frac{1}{Q} \left| \sum_{q=-Q/2}^{q=Q/2} \mathbf{R}(q\Delta t) \mathbf{R}^*(q\Delta t) \right|}{\sigma^2} = \frac{E_t}{\sigma^2} \quad (3.31)$$

Here  $E_t$  is the total energy of breathing signal in  $\mathbf{R}$ .  $SNR_{CD}$  calculated according to (3.31) does not depend on whether preliminary FIR filtering from chapter 3.4.1 was used or not. This is true since we suppose that FIR filter attenuates only those frequencies that contain only noise. However, when using CD processing after filtering and not instead of it one should take care of filtering  $\mathbf{R}$  with the same FIR filter as measured data.

In order to evaluate the efficiency of CD, let us first estimate SNR in case our data processing consisted only of FIR filtering and maximum search:

$$SNR_m = \frac{\mathbf{R}(q_m \Delta t) \mathbf{R}^*(q_m \Delta t)}{\sigma^2} \frac{B}{B_r} = \frac{E_m}{\sigma^2} \frac{B}{B_r} \quad (3.32)$$

Here  $SNR_m$  and  $E_m$  are SNR and signal energy that appear at an instant  $q_m \Delta t$  when breathing signal is maximal and when we are likely to detect it in case no CD processing is applied. In (3.32) we have taken into account that  $SNR_m$  is increased by FIR filtering ( $B$  and  $B_r$  are complete frequency band and frequency band retained after filtering out high-frequency noise).

Potential improvement of using the CD processing can be described by the following coefficient:

$$K_{CD/\max} = \frac{SNR_{CD}}{SNR_m} = \frac{E_t}{E_m} \frac{B_r}{B} = \frac{QE_{av}}{E_m} \frac{B_r}{B} \quad (3.33)$$

Here  $E_{av}$  is the average value of signal energy within one fast-time instant of main tone respiration signature. To get an impression about how big is  $K_{CD/\max}$ , we have to make some suggestions about how main tone respiration signature looks like. Let us consider  $\mathbf{R}$  being sinc-shaped pulse (this corresponds to using M-sequence radar since autocorrelation function of M-sequence after applying anti-aliasing filter is sinc). In what

follows, parameters are chosen close to what was observed in measured data. If the power of the waveform has sinc-squared shape  $E = A^2 \text{sinc}^2\left(\frac{u}{k}\right)$  and the main lobe covers  $[-\pi, \pi]$ , we can numerically estimate  $E_r$  within main lobe being 9.03 when  $E_m = 1$ . Further, if we suppose filtering out half of the signal energy due to the absence of useful signal at higher frequencies,  $\frac{\Delta F_r}{\Delta F} = \frac{1}{2}$ , according to 3.33 we get:

$$K_{CD/\max} = \frac{9.03}{2} \approx 4.5 \quad (3.34)$$

That is, typical value of potential increase due to CD processing is in the order of 6.5 dB in energy (which is equivalent to penetrating several centimeters of typical building material). Switching to different pulse shape is unlikely to change this estimate much (e.g. by an order) Value defined by equation 3.33 to a certain extent can be considered as a limit for breathing-detecting processing in range direction when the only information available includes completely: breathing behavior at the main rate, antenna frequency bandwidth and rubble attenuation. In practice we do not have all of this information or in the best case we have it in the form of estimates which can deviate a bit from reality and data processing methods described later in this chapter perform somewhat worse than the limit.

In order to directly apply CD data processing to measured data one needs to acquire R estimate first. It needs to be collected by means of the same hardware as during survival search later and measured through significant (close to the limit of detection, more than one meter) layer of rubble material found in disaster area.

Of course there are multiple factors hampering reference matching (difference in chest sizes, rubble structure and heterogeneity, difference in breathing magnitudes). One of these factors, pulse change due to the propagation through different layer of rubble in comparison with reference is considered below. However, exact matching between reference and actual main tone respiration signature is not necessary for improving detection rate (although with ideal reference there is more of improvement). Moreover, even if our reference waveform will be completely different from that of a breathing person (like taking noise replica instead of a reference) that would statistically mean rather no improvement than cancelling the detection.

In order to illustrate how respiration signature is changed by propagation through typical rubble material transmission measurement with 30 cm- thick concrete wall between

antennas was carried out by means of M-sequence radar unit described in chapter 6. Measurement scenario is depicted in figure 3.15 A and B.

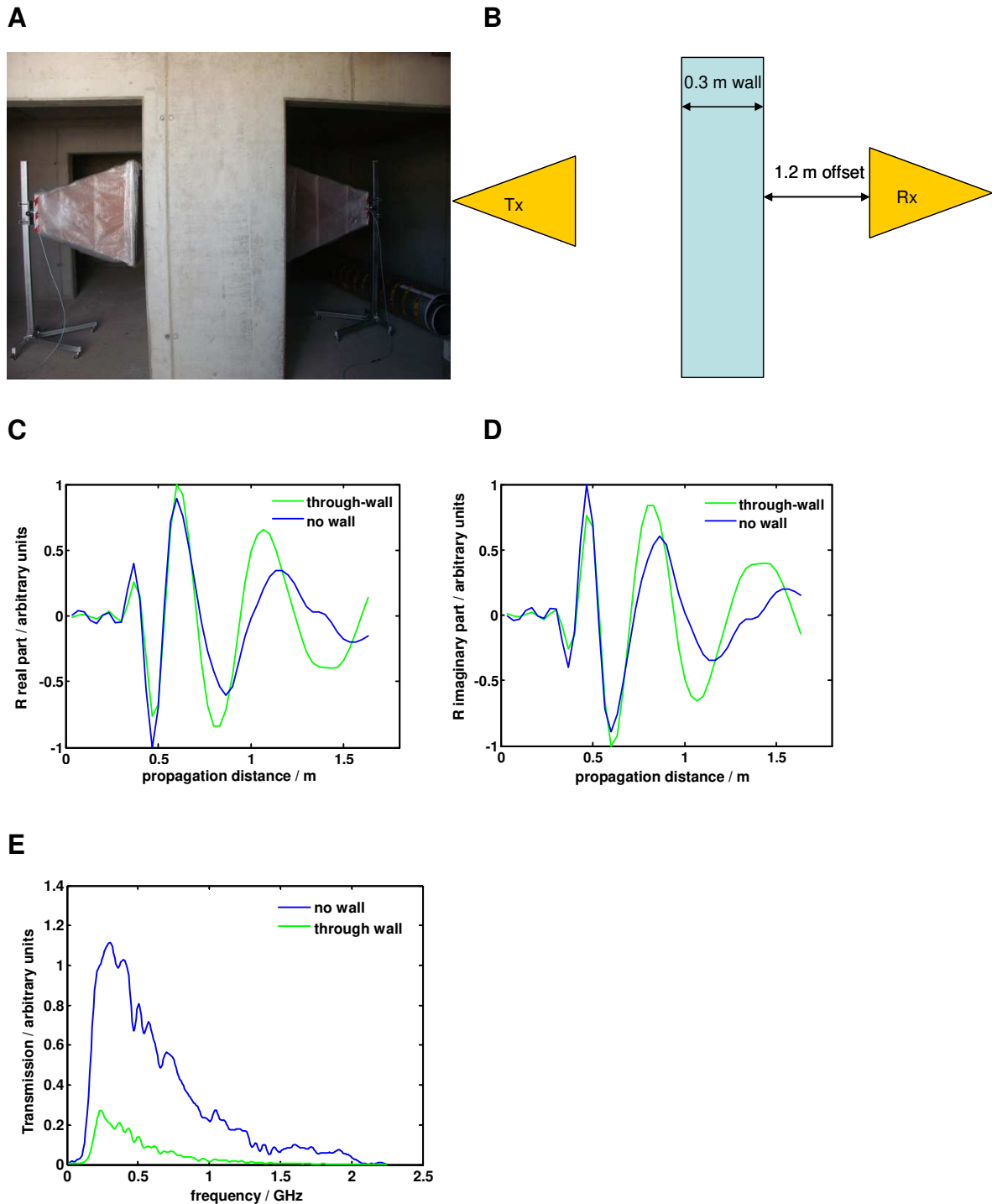


Figure 3.15: Transmission measurements through concrete wall: scenario description (A, B) and results (C, D and E)

Additionally transmission was measured without a wall between antennas. After that both measured waveforms  $X_{1,2}(l\Delta t)$  were modulated with harmonic variation  $d_{br}$  in order to imitate respiratory activity:

$$\mathbf{W}_{1,2}(l\Delta t, m\Delta \tau) = \mathbf{X}_{1,2} \left( l\Delta t - 2 \frac{d_{br}(m\Delta \tau)}{c} \right), \quad (3.35)$$

$$d_{br}(\tau) = d_0 \sin(2\pi\nu_0\tau) \quad (3.36)$$

Here  $d_0$  was set to 0.5 cm (which corresponds to 1 cm between human chest at the opposite stages of breathing),  $\nu_0 = 0.3$  Hz

By means of FFT in observation time  $\mathbf{R}_{1,2}$  are computed from  $\mathbf{W}_{1,2}$  and shown in figure 3.15 C and D along with the spectrum of ‘through-wall’ and ‘no wall’ transmission (figure 3.15 E). Difference between two respiration signatures allows judging how much real breathing measurement might vary in comparison with reference taken with the same person 15 cm deeper beneath concrete rubble (here two times difference with wall thickness arises due to the propagation of electromagnetic waves through rubble two ways when looking for a buried victim).

Following conclusions can be drawn. We see in figure 3.15 E in the spectrum that radar signal is significantly attenuated due to the wall presence. However, at the same time two main tone respiration signatures normalized on maximum are not much different in the region where breathing variation is the most significant. Accordingly, this observation suggests good result for CD processing with reference in the investigated case. They differ somewhat more in the late time (effect might be mainly caused by antenna-wall reflection appearing in the measured data).

Of course, more tests would be needed before bringing this method into search and rescue on the solid basis. First results with estimating  $\mathbf{R}$  from the radargram with one breathing person and applying reference for detecting different person are described later in this chapter.

#### 3.4.4 Energy detector (incoherent summation)

Probably the easiest data processing method that can be used for denosing in range direction is incoherent summation (IS):

$$\hat{\mathbf{Z}}_{IS}(l\Delta t, k\Delta \nu) = \frac{1}{Q} \left| \sum_{q=-Q/2}^{q=Q/2} \mathbf{w}(q\Delta t) \hat{\mathbf{Z}}_t((l+q)\Delta t, k\Delta \nu) \hat{\mathbf{Z}}_t^*((l+q)\Delta t, k\Delta \nu) \right| \quad (3.37)$$

Like in many other applications windowing is used in (3.37). We can choose the windowing function  $\mathbf{w}(q\Delta t)$  that seems to suit breathing-containing measured data. Ideally, this function reflects how much breathing is weaker on the sides of the window

in comparison with the center and gives smaller weight to the samples with smaller SNR (thus, paragon  $w(q\Delta t)$  equals  $\underline{\mathbf{R}}(q\Delta t)\underline{\mathbf{R}}^*(q\Delta t)$ ). Since while looking for respiratory motion we check all possible propagation time values, in case breathing is present we will inevitably enhance it when its maximum is in the center of the window.

In figure 3.16 main tone respiration signature, measured with radar through brick wall and its envelope are shown. While CD processing described above requires the complete knowledge of this signature (except for the phase shift and amplitude multiple), ideal windowing function for energy detector is the envelope of main tone respiration signature (again, except for arbitrary amplitude multiple). No any more information is required by incoherent summation. This means however somewhat lower performance of incoherent summation in comparison with correlation detector.

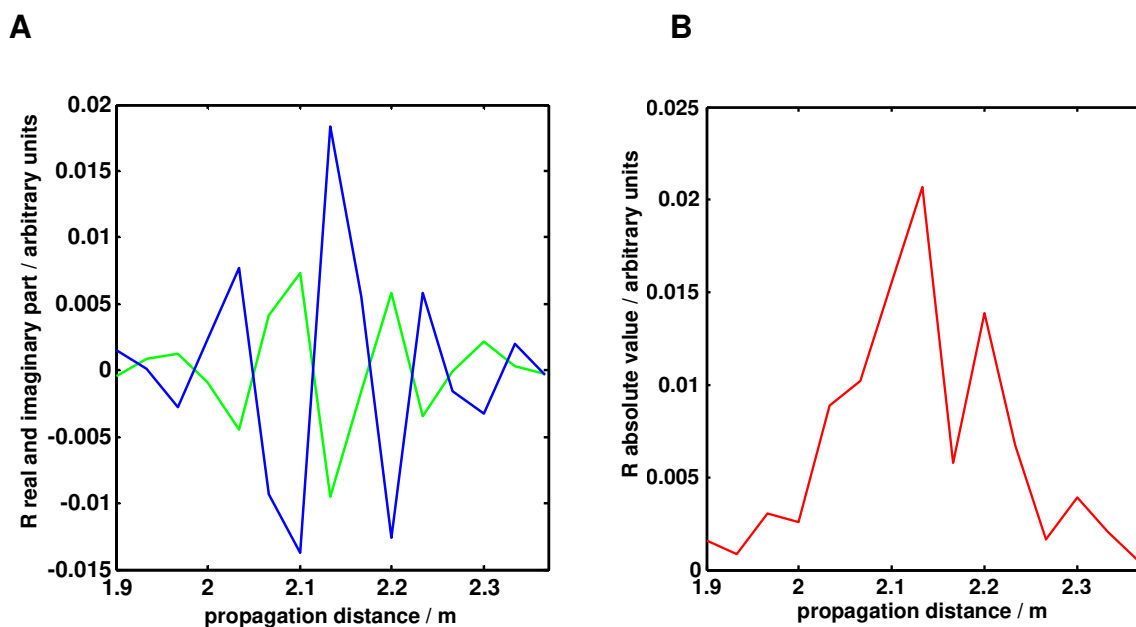


Figure 3.16: Noised main tone respiration signature (A) and its envelope (B).

One obvious disadvantage of energy detection that had to be addressed is that it ignores coherence, existing between the breathing-related periodicals. One way of utilizing this information (without elevating the level of knowledge required in comparison with incoherent summation) is considered in the next part.

### 3.4.5 Breathing signature enhancement via slow-time cross-correlation functions

We can see in figure 3.17 that phases of the breathing-related periodical are not distributed randomly: there are two types of them, maximums of one type correspond to

the minimums of another (that is, phase shift by  $\pi$  between different types and 0 inside one type). This effect appears because breathing signature arises as a periodic oscillation of the signal having two distinct types of edges: the rising and the falling one. Periodicals from the same edge type are in phase, periodicals from different edge types are in counterphase.

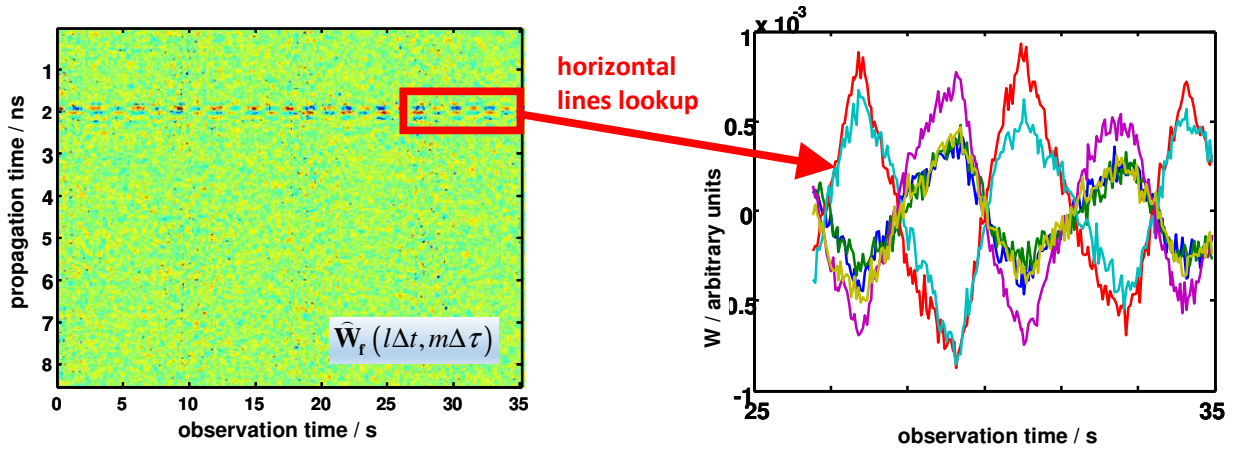


Figure 3.17: Person, breathing behind a wall. Radargram and several of its horizontal lines from the area where person is present.

Let us now consider main tone respiration signature at two arbitrarily chosen instants,  $q\Delta t$  and  $\tilde{q}\Delta t$ :  $\underline{\mathbf{R}}(q\Delta t) = |\underline{\mathbf{R}}(q\Delta t)| \exp(i\varphi_1)$  and  $\underline{\mathbf{R}}(\tilde{q}\Delta t) = |\underline{\mathbf{R}}(\tilde{q}\Delta t)| \exp(i\tilde{\varphi}_1)$ . Given what we told above about phase shift between different periodicals  $\Delta\varphi_1 = \varphi_1 - \tilde{\varphi}_1$  we can state that:

$$\underline{\mathbf{R}}(q\Delta t) \underline{\mathbf{R}}^*(\tilde{q}\Delta t) = |\underline{\mathbf{R}}(q\Delta t)| |\underline{\mathbf{R}}^*(\tilde{q}\Delta t)| e^{i\Delta\varphi} = \begin{cases} |\underline{\mathbf{R}}(q\Delta t)| |\underline{\mathbf{R}}^*(\tilde{q}\Delta t)|, \Delta\varphi = 0 \\ -|\underline{\mathbf{R}}(q\Delta t)| |\underline{\mathbf{R}}^*(\tilde{q}\Delta t)|, \Delta\varphi = \pi \end{cases} \quad (3.38)$$

That is, unlike in situation with pure noise (that generates random phase shifts), products  $\underline{\mathbf{R}}(q\Delta t) \underline{\mathbf{R}}^*(\tilde{q}\Delta t)$  yield real-valued numbers when dealing with breathing-containing radar data, which allows us to enhance respiration signature by applying subsequently following calculations inside every block of data in input horizontal spectrum  $\hat{\underline{\mathbf{Z}}}_r$ :

1. Calculating real parts of products  $\hat{\underline{\mathbf{Z}}}_r((l+q)\Delta t, k\Delta\nu) \hat{\underline{\mathbf{Z}}}_r^*((l+\tilde{q})\Delta t, k\Delta\nu)$  for all possible  $q$  and  $\tilde{q}$  within the window of length  $Q\Delta t$ . These products represent slow-time cross-correlation functions in sinusoidal micro-Doppler rate domain,

and thus we called the denoising method based on them cross-correlation (CC) method

2. Averaging second powers of these terms (according to [22] second power yields somewhat better results).

These steps can be summarized in the following expression:

$$\widehat{\mathbf{Z}}_{CC}(l\Delta t, k\Delta \nu) = \frac{1}{Q^2} \sum_{q=-Q/2}^{q=Q/2} \sum_{\tilde{q}=-Q/2}^{\tilde{q}=Q/2} \left| \Re \left( \mathbf{w}(q\Delta t) \widehat{\mathbf{Z}}_f((l+q)\Delta t, k\Delta \nu) \mathbf{w}(\tilde{q}\Delta t) \widehat{\mathbf{Z}}_f^*((l+\tilde{q})\Delta t, k\Delta \nu) \right) \right| \quad (3.39)$$

Here  $\mathbf{w}(q\Delta t)$  is a windowing function with the same meaning as in case of incoherent summation.

Let us compare performance of CC and IS methods. In order to do this we first determine SNR of  $\widehat{\mathbf{Z}}_{CC}$  and  $\widehat{\mathbf{Z}}_{IS}$  estimates (in energy units). For both convenience and brevity we consider only two fast-time instants  $(l+q_1)\Delta t$  and  $(l+q_2)\Delta t$ ,  $|q_1 - q_2| < Q$ .

This can be interpreted as scrutinizing only one of the terms averaged in 3.39 or, alternatively, as studying the properties of complete respiration signature consisted of two points (two-point pulse). We do not consider windowing (rectangular window is taken) at the first stage. Even though, as it was shown above, windowing is usually needed, non-windowed case is also important for comparison due to the fact that ideal windowing function is never known (that is, in practice we always deal with a mix of windowed and non-windowed case)

SNR yielded by CC method after calculating according to 3.39 is given by:

$$SNR_{CC}^2 = \frac{z_1^4 + z_2^4 + 2(z_1 z_2)^2}{\mathbb{E} \left\{ \left( \underline{n}_1 \underline{n}_1^* \right)^2 + \left( \underline{n}_2 \underline{n}_2^* \right)^2 + 2 \left| \Re e^2 \left( \underline{n}_1 \underline{n}_2^* \right) \right| \right\}} \quad (3.40)$$

Here in order to shorten the equations we use notation  $z_1 = |\mathbf{R}(q_1\Delta t)|$ ,  $z_2 = |\mathbf{R}(q_2\Delta t)|$ ,  $\underline{n}_1 = \underline{n}((l+q_1)\Delta t, k\Delta \nu)$ ,  $\underline{n}_2 = \underline{n}((l+q_2)\Delta t, k\Delta \nu)$ . SNR of incoherent summation method is directly calculated from 3.37 (numerator and denominator before averaging had to be squared for dimensionality reasons in order to make proper comparison with value in 3.40):

$$SNR_{IS}^2 = \frac{(z_1^2 + z_2^2)^2}{\mathbb{E} \left\{ \left( \underline{n}_1 \underline{n}_1^* + \underline{n}_2 \underline{n}_2^* \right)^2 \right\}} \quad (3.41)$$



Let us check how SNR of both methods depends on the ratio  $k_r = \frac{z_2^2}{z_1^2}$ . Supposing  $z_1 \geq z_2$  (and accordingly  $0 \leq k_r \leq 1$ ) we can consider all possible ratios between  $z_1$  and  $z_2$  that we can encounter in measured data. After introducing  $k_r$ , 3.41 and 3.40 become:

$$SNR_{IS}^2 = z_1^4 \frac{(1+k_r)^2}{E\left\{\left(\underline{n}_1 \underline{n}_1^* + \underline{n}_2 \underline{n}_2^*\right)^2\right\}} \quad (3.42)$$

$$SNR_{CC}^2 = z_1^4 \frac{1+k_r^2+2k_r}{E\left\{\left(\underline{n}_1 \underline{n}_1^*\right)^2 + \left(\underline{n}_2 \underline{n}_2^*\right)^2 + 2\left|\text{Re}^2\left(\underline{n}_1 \underline{n}_2^*\right)\right|\right\}} \quad (3.43)$$

In order to compare the SNR performance of CC and energy method following value is to be calculated as the functions of  $k_r$ :

$$K_{CC/IS} = \frac{SNR_{CC}}{SNR_{IS}} \quad (3.44)$$

$K_{CC/IS}$  that we get by means of simple simulation according to 3.42 and 3.43 is plotted in figure 3.18. We can conclude that:

1. As it was expected, cross-correlation method outperforms incoherent summation for all possible  $k_r$  values. This happens due to the cancellation of part of the noise contribution in denominator in (3.43) in comparison with (3.42) while the amount of useful signal is not reduced (note that numerators in (3.42) and (3.43) are the same).
2. Improvement due to applying (3.39) in non-windowed case does not depend on  $k_r$  and that is, the same amount of improvement appears independently of the shape of main tone signature (given that two-point pulse is considered).
3. The amount of improvement is not particularly high. As it was shown above, complete knowledge of main tone respiration signature yields typically dozens of percent of the magnitude SNR gain (over using no signal enhancement due to the breathing signature being range-spread). However, improvement seen in figure 3.18 is reached due to utilizing very limited amount of a priori information. Using more information means applying windowing.

Now let us consider performance of cross-correlation processing and incoherent summation with respect to windowing. Since purpose of the windowing is to make data samples with stronger signal components more relevant, windowing function is in the best case connected with main tone respiration signature. That is, the natural choice

would for both considered methods would be using the envelope of respiration signature:

$$\mathbf{w}(q\Delta t) = |\underline{\mathbf{R}}(q\Delta t)|^2 \quad (3.45)$$

If all the same calculations (3.40—3.44) are carried out with windowing results are following:

$$SNR_{IS}^2 = z_1^4 \frac{(1+k_r^2)^2}{E\left\{\left(\underline{n}_1 \underline{n}_1^* + k_r \underline{n}_2 \underline{n}_2^*\right)^2\right\}} \quad (3.46)$$

$$SNR_{CC}^2 = z_1^4 \frac{1+k_r^4 + |2k_r^2|}{E\left\{\left(\underline{n}_1 \underline{n}_1^*\right)^2 + k_r^2 \left(\underline{n}_2 \underline{n}_2^*\right)^2 + 2|k_r \operatorname{Re}^2\left(\underline{n}_1 \underline{n}_2^*\right)\right\}} \quad (3.47)$$

Let us first consider how much the performance of cross-correlation method is improved in comparison with non-coherent summation when both methods use windowing according to (3.45).

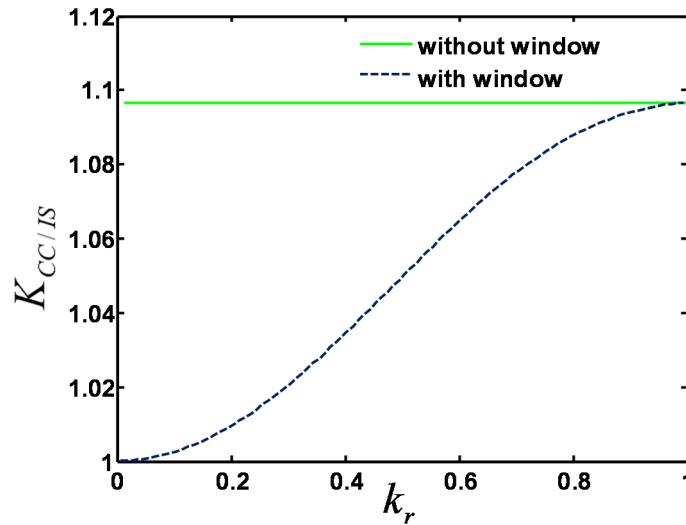


Figure 3.18: SNR of CC method with and without windowing in comparison with incoherent summation with windowing.

Like in the non-windowed case,  $K_{CC/IS}$  shown in figure 3.18 is calculated according to (3.44). Again we can see that CC method outperforms incoherent summation, but unlike in windowed case the amount of this improvement depends on  $k_r$ . This effect is easily explained by the notion that in  $k_r = 0$  case when breathing information is only present within one point of two-point pulse cross-terms used in CC method go to zero and they cannot add anything useful. Actually, it is evident from (3.46) and (3.47) that

$SNR_{IS} = SNR_{CC}$  in case  $k_r = 0$ . On another hand, the less difference between signal energy between the pulse bins the more the significance of cross-terms.

In the end we should consider the total SNR improvement brought both by windowing and utilizing coherence of respiration signature in comparison with ‘non-windowed’ energy detection alongside with considering the windowing effect on  $SNR_{IS}$ . Corresponding figure is 3.19. In addition to concluding that CC method outperforms incoherent summation (which was already shown above) we can mention pretty significant improvement of both CC and incoherent summation performance due to using windowing (when we say significant—we keep in mind the ‘limitng’ considerations from 3.4.3).

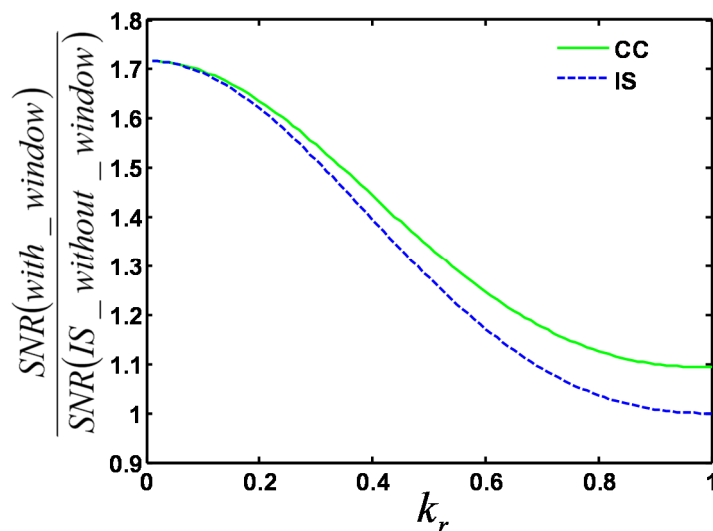


Figure 3.19: SNR improvement due to windowing.

Besides, we see that efficiency of using windowing from (3.45) decreases with growing  $k_r$ . This is easily explained via considering ‘edge’  $k_r$  values:

1.  $k_r = 0$ : In this case windowing means denoising, weighting purely noise component with zero. Maximal improvement in comparison with no weighting is reached because without windowing we add pure noise to our signal unlike in all other cases
2.  $k_r = 1$ : In this case windowing according to (3.45) means the same data processing as in ‘nonwindowed’ case, since we apply rectangular window. Thus, for incoherent summation there is no difference in SNR due to windowing while for CC some improvement is reached.

### 3.5 Welch method modification

Unlike incoherent summation from 3.4.4 cross-correlation data processing from 3.4.5 and correlation detector from 3.4.3 cannot be applied in one data processing cycle with classical Welch method. The reason is that output of the Welch method is power spectral density (PSD) and thus, phase information is lost. However, since Welch method is based on calculating complex-valued FFTs of data segments it can be easily modified in order to include cross-correlation data processing or correlation detector. Adjusted algorithm is given below.

1. Each filtered radargram  $\widehat{\mathbf{W}}_f(l\Delta t, m\Delta \tau)$  is divided in horizontal direction into a number of overlapping segments of length  $M$ . Over each  $p$ -th segment Discrete Fourier transform is subsequently performed:

$$\underline{\widehat{\mathbf{Z}}}_p(l\Delta t, k\Delta \nu) = \frac{1}{M \sum_{m=0}^{M-1} w_i} \sum_{m=pM\eta}^{pM\eta+M-1} w_m \widehat{\mathbf{W}}(l\Delta t, m\Delta \tau) e^{-2\pi i m k l / M} \quad (3.48)$$

2. Unlike in classical Welch method we get real-valued data from  $\underline{\widehat{\mathbf{Z}}}_p(\mathbf{t}_0, k\Delta \nu)$  by using one of the adjusting functions for SNR improvement from this chapter  $f_{ad}$  (correlation detector, incoherent summation, cross-correlation data processing):

$$\widehat{\mathbf{Z}}_p^{\text{ad}}(l\Delta t, p\Delta \nu) = f_{ad}(\underline{\widehat{\mathbf{Z}}}_p(l\Delta t, k\Delta \nu)) \quad (3.49)$$

3. The set of FFTs (as the power spectrums) is averaged over  $p$  in order to calculate modified Welch spectral estimate:

$$\widehat{\mathbf{Z}}_{\text{MW}}(l\Delta t, k\Delta \nu) = \frac{1}{P} \sum_{p=0}^{P-1} |\widehat{\mathbf{Z}}_p^{\text{ad}}(l\Delta t, k\Delta \nu)|^2 \quad (3.50)$$

### 3.6 SVD-based breathing detection in the clutter-free case (reference method)

Before we proceed to the thesis part where data processing methods described above are tested via simulation and measurements, let me briefly introduce the technique for respiratory signal enhancement that was suggested in [35]. In this work algorithm from [35] is used as a reference tool.

Key operation of reference method is singular value decomposition (SVD). SVD reveals the orthogonal basis of vectors (principal components, PCs) with a specific property, that projection of original observations on the first principal component contains the

largest variance possible (first vector is chosen in such a way, that the variance in the projection is maximal).

We perform SVD of complex horizontal spectrum of the filtered radargram as following:

$$\hat{\mathbf{Z}}_f = \mathbf{U}\mathbf{S}\mathbf{V}^* = \sum_{i=1}^M \mathbf{u}_i S_{i,i} \mathbf{v}_i^* \quad (3.51),$$

where  $\mathbf{V} = [\mathbf{v}_1, \mathbf{v}_2, \dots, \mathbf{v}_M]$  and  $\mathbf{U} = [\mathbf{u}_1, \mathbf{u}_2, \dots, \mathbf{u}_M]$ . SVD calculates  $M$  uncorrelated sequences, PCs  $S_{i,i} \mathbf{v}_i$ .  $\mathbf{S}$  is a diagonal matrix of singular values, and its elements  $S_{i,i}$  decrease for larger  $i$ . Both PCs  $S_{i,i} \mathbf{v}_i$  and eigenvectors  $\mathbf{u}_i$  often have simple graphical interpretation, depending on the nature of input data. For instance, in ground penetrating radar first PCs often represent surface clutter component, and first  $\mathbf{u}_i$  show how ground return changes with the position of measurement ([36]).

With respect to our problem application of SVD is thoroughly considered in [20], [35] and by the author of this thesis in [30], focus of all works being on clutter removal. However, in addition in [35] ability of SVD to increase the SNR in the clutter-free case is mentioned and demonstrated.

According to reference method from [35], in our search for breathing signature after calculating SVD according to 3.51 we consider singular matrices  $|S_{j,j} \mathbf{u}_j \mathbf{v}_j^*|$  for different  $j$  values, ( $j \leq J$ ) where  $J$  is determined experimentally. Theoretically, due to uncorrelatedness of respiratory motion with noise and clutter, one of these matrices (with number  $j = \gamma$ ) is dominated by respiration signature, other matrix elements being minor. Therefore, we can put down an expression for horizontal spectrum estimate after noise and all sorts of clutter are removed from the measured data by means of SVD:

$$\mathbf{Z}_{\text{SVD}} = |S_{\gamma,\gamma} \mathbf{u}_\gamma \mathbf{v}_\gamma^*| \quad (3.52)$$

In case of SNR being high enough we could safely make  $J$  equal two, but since we are interested in low-SNR scenario, here we present results for  $J = 4$ .

### 3.7 Evaluation from modeling

In this part we investigate by means of modeling how much methods (including reference method) described in this chapter improve the probability of detecting a victim in comparison with horizontal FFT-squared of a radargram.

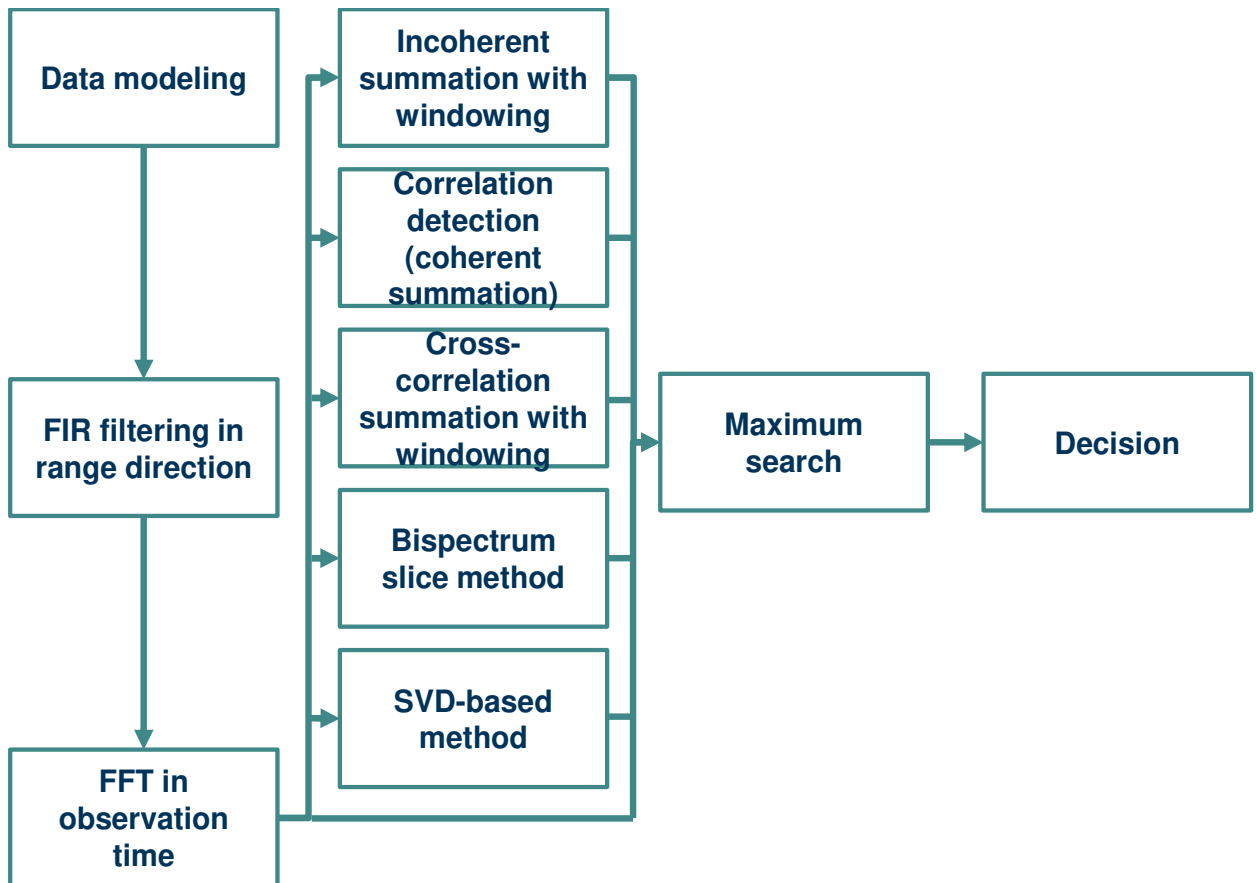


Figure 3.20: Chart, describing how simulated data is processed

First we generate a radargram that contains respiration-like motion. One of the scenarios is an exception: instead of simulating breathing we use measured data. Then we add AWGN (noise level is varied, in total number of experiments with identical noise level we denote as  $N_e$ ) and perform data processing. Data processing steps are summarized in figure 3.20. We perform FIR filtering in the range direction and cancel part of high-frequency noise (this step simulates matching of the radargram frequency bandwidth to the frequency bandwidth of antennas and it is described in chapter 3.4.1). After that horizontal FFT is carried out and one by one signal enhancement techniques described in this chapter are applied.

We consider that breathing person was detected if maximum of the image appeared at fast-time instant where person have been and at corresponding sinusoidal micro-Doppler rate (this is a simplistic approach, however, since we only need to know relative performance of the methods, it can be used). For each method we calculate the number of detections  $N_d$  and calculate the detection probability as a measure of efficiency for every method:

$$P = \frac{N_d}{N_e} \quad (3.53)$$

This measure of efficiency is suitable for evaluating the performance of different techniques under low-SNR conditions [10].

### 3.7.1 Test scenarios

Three test scenarios were implemented. Two of them are based on the simulated radargram and in the third one contains measured radar data with respiratory motion. In particular, our test included:

- **Scenario 1.** Chest shift  $\mathbf{d}$  was simulated as a single-tone motion:

$$\mathbf{d}(m\Delta\tau) = d_{i1} \sin(2\pi\nu_{i1}m\Delta\tau) \quad (3.54)$$

Particular values of single-tone respiration amplitude  $\mathbf{d}_{i1}$  and rate  $\nu_{i1}$  (as well as other simulation parameters) are given in table 3.1.

- **Scenario 2.** Since according to some sources breathing signal is not always a pure sine, in addition to **scenario 1** we consider respiratory motion containing first-type harmonic with amplitude  $\mathbf{d}_{i2}$  and rate  $\nu_{i2}$ :

$$\mathbf{d}(m\Delta\tau) = d_{i1} \sin(2\pi\nu_{i1}m\Delta\tau) + d_{i2} \sin(2\pi\nu_{i2}m\Delta\tau) \quad (3.55)$$

Further breathing-like motion in the radargram was simulated as a shift of the pulse  $\mathbf{W}_s(l\Delta t)$  according to equations 3.54 and 3.55 with AWGN  $\mathbf{n}(l\Delta t, m\Delta\tau)$  added:

$$\widehat{\mathbf{W}}(l\Delta t, m\Delta\tau) = \mathbf{W}_s\left(l\Delta t - 2\frac{r_0 - \mathbf{d}(m\Delta\tau)}{c}\right) + \mathbf{n}(l\Delta t, m\Delta\tau), \quad (3.56)$$

$\mathbf{W}_s(l\Delta t)$  was a third order derivative of Gaussian wavelet with pulse width  $t_p$  (shown in figure 3.21):

$$f_G(t) = \exp\left(\frac{9t^2}{2t_p^2}\right), \quad (3.57)$$

$$W_s(t) = f_G^{(3)}(t)$$

Wavelet shape was an arbitrary choice.

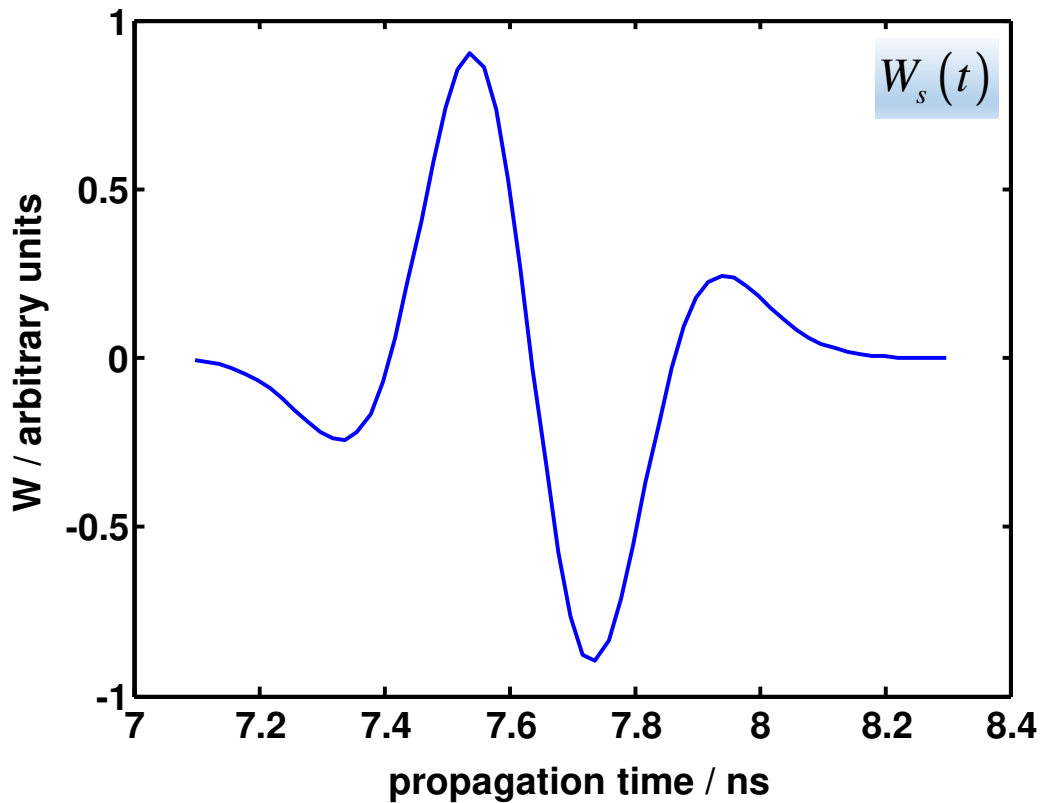


Figure 3.21: Signal pulse used in the test scenarios.

For **scenario 1** resulting radargram and its spectrum are shown in figure 3.22 A and B. Except for the main term, we observe second type harmonic as it was predicted in chapter 3.1. In contrast, in the radargram spectrum generated as **scenario 2** (figure 3.22, C and D) we see main signal tone, first type harmonic (unlike second type harmonic it peaks at the same fast time instants as the main tone) and interfering terms at higher frequencies (how it was implied by expression 3.8).



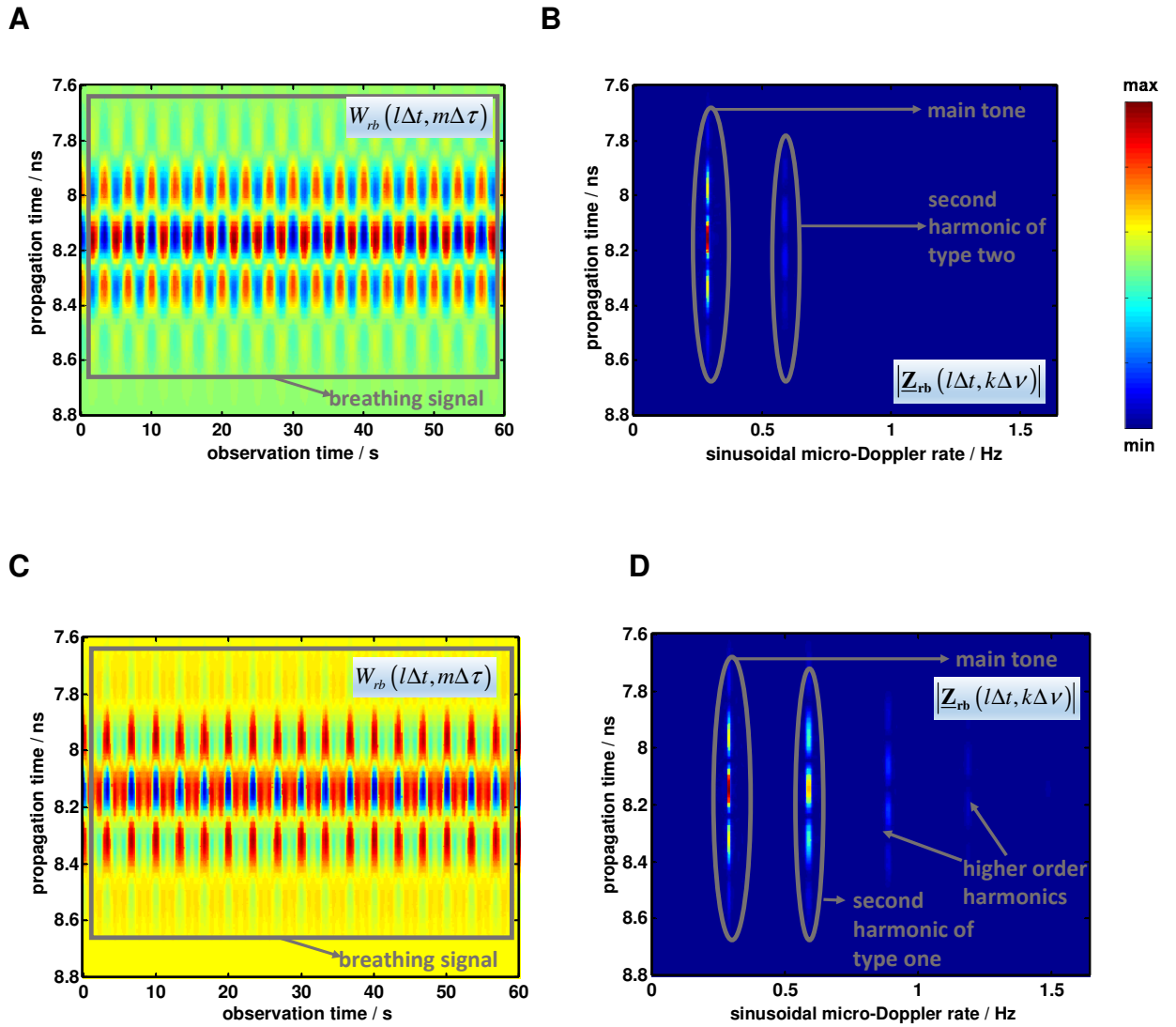


Figure 3.22: Simulated radargram and its horizontal spectrum before adding noise and after subtracting stationary signal. **Scenario 1:** A and B; **scenario 2:** C and D.

- Scenario 3.** Here instead of simulating respiratory motion, we used radar data acquired during measurement campaign with person under test (PUT) being 1.3 meters beneath reinforced concrete (figure 3.23, A). Besides, we used second dataset with respiratory motion as a reference (figure 3.23, B and C). Reference was used as a second input of correlation detector (that is, as an ideal main tone respiration signature) and it was collected with another PUT and slightly different antenna position. Such approach allows us to bring correlation detector closer to practical application. In other aspects testing procedure remained the same as with simulated datasets: AWGN of different levels was added into radargram (even though some amount of noise was already acquired during the measurement).

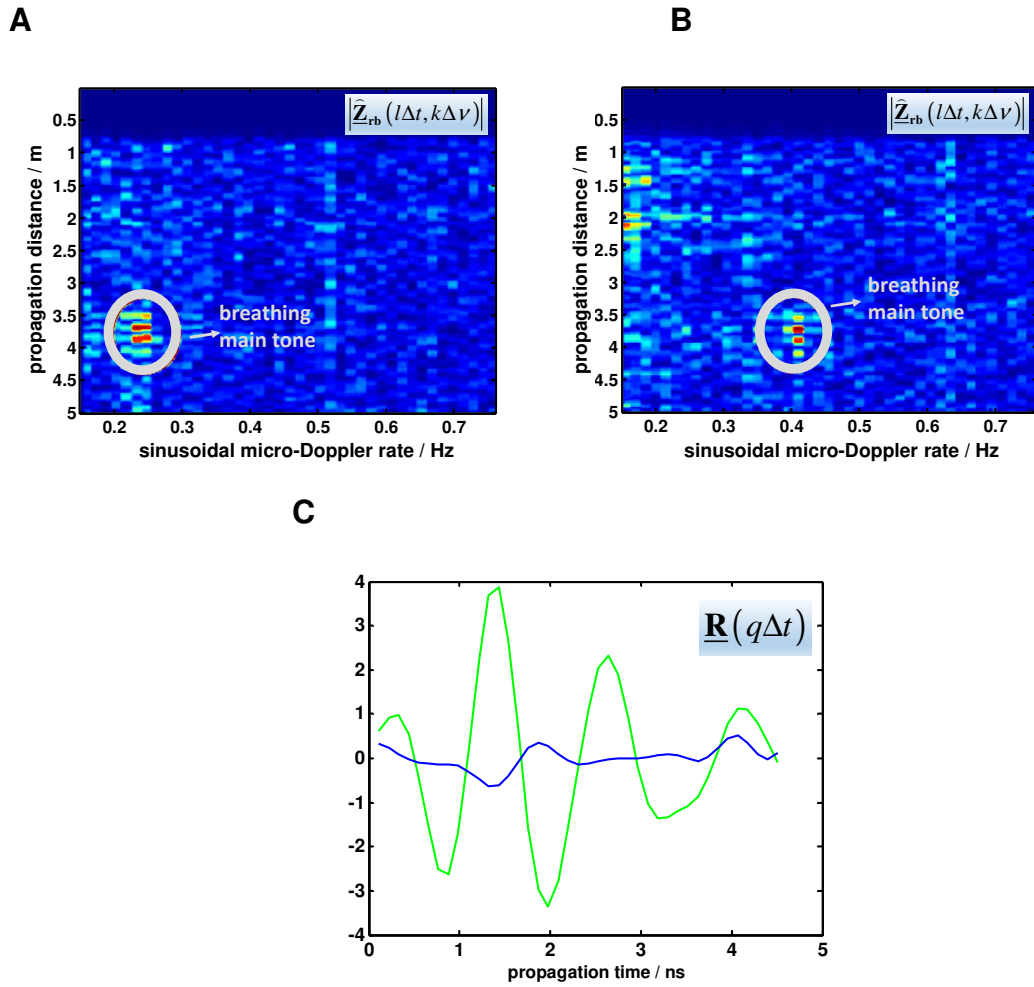


Figure 3.23: Measured datasets used for evaluation of algorithms in **scenario 3**: detection dataset (A), reference dataset (B), reference main tone respiration signature (C, real part as a green curve and imaginary part as a blue one)

Name	Notation	Value
Pulse length	$t_p$	1 ns
Breathing rate	$\nu_{r1}$	0.3 Hz
Rate of 'artificial' harmonic	$\nu_{r1} = 2\nu_{r1}$	0.6 Hz
Breathing magnitude	$d_{r1}$	0.5 cm
Magnitude of 'artificial' harmonic	$d_{r2} = \frac{d_{r1}}{\sqrt{2}}$	$\approx 0.35$ cm
Number of experiments for every noise level	$N_e$	1000
Data acquisition time		1 minute

Table 3.1: Parameters of simulations for the evaluation of algorithms

### 3.7.2 Simulation: results and discussion

Simulation results for **scenarios 1, 2** and **3** are shown in figures 3.24, 3.25 and 3.26 respectively.

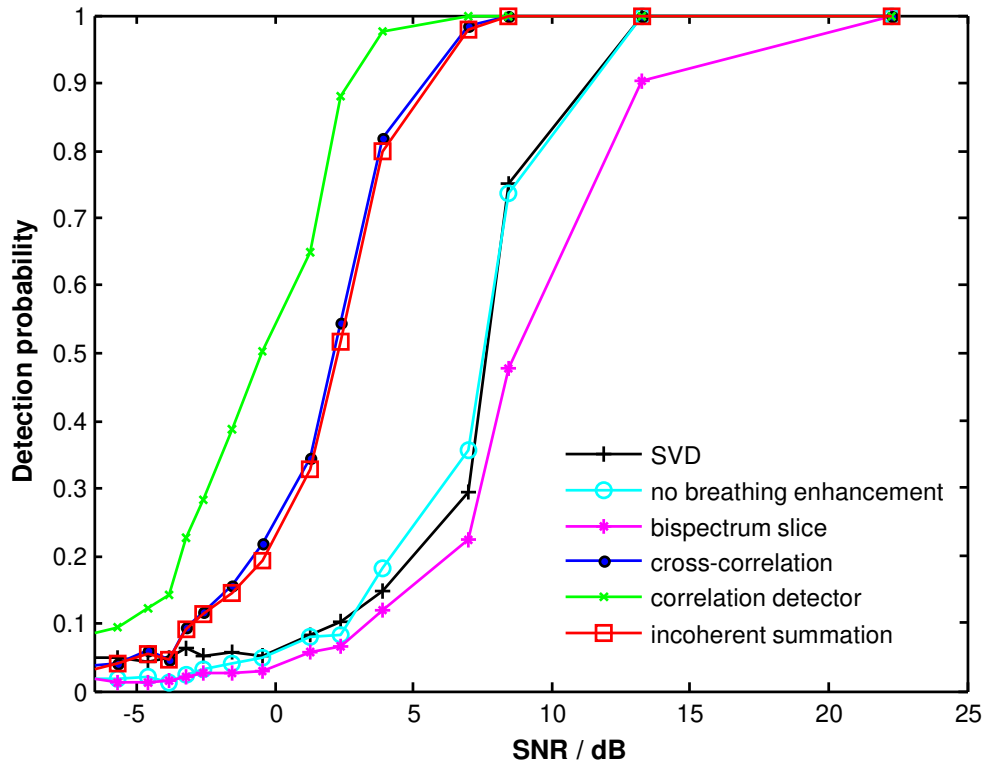


Figure 3.24: Efficiency of different algorithms: **scenario 1**

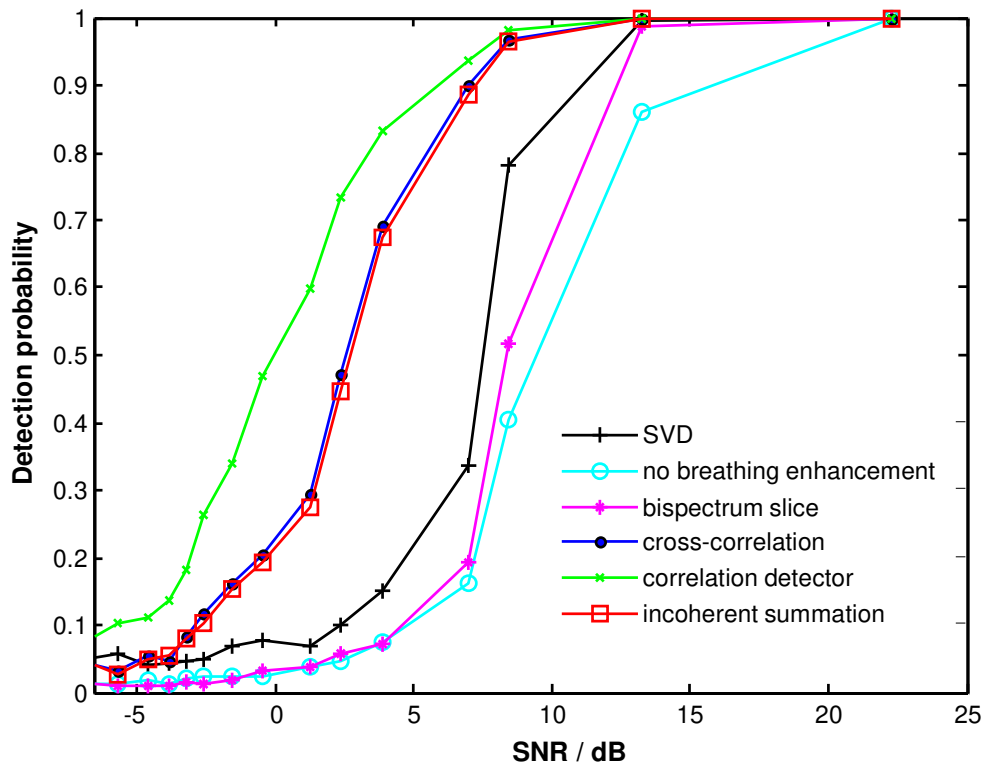


Figure 3.25: Efficiency of different algorithms: **scenario 2**

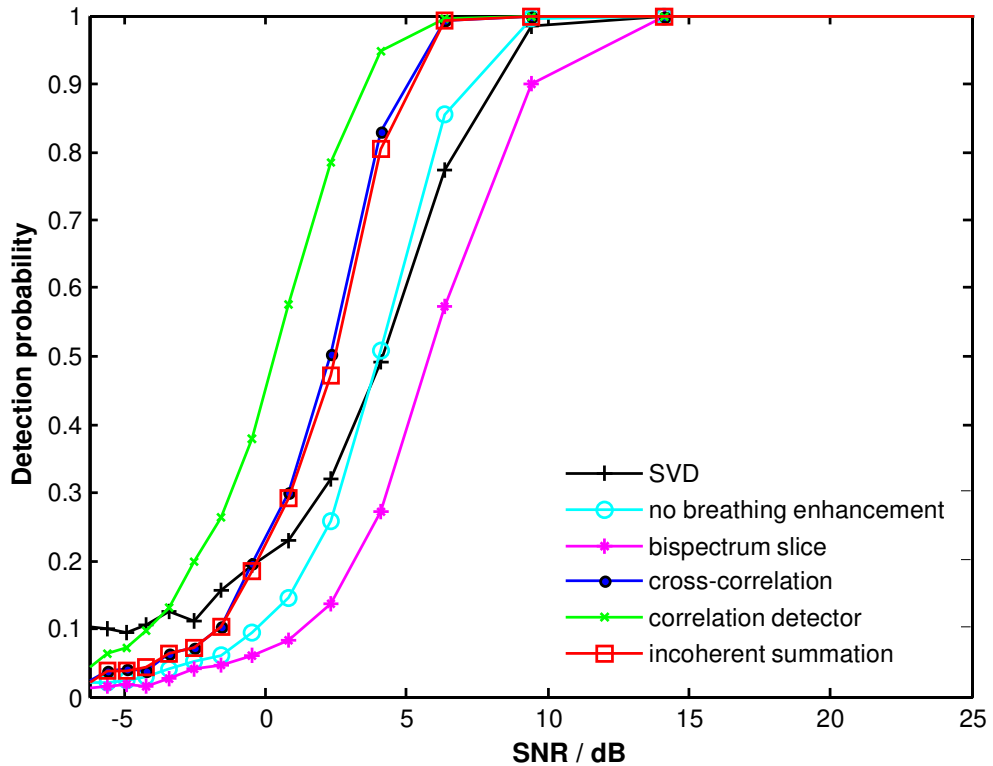


Figure 3.26: Efficiency of different algorithms: **scenario 3**

The main conclusions that may be drawn from these figures are following:

1. As it was expected, results produced by different methods in terms of the number of detections understood as in (3.53) lay in between 'no breathing enhancement' in range direction and 'correlation detector', performance difference between the best and the worst methods being 5-10 dB which corresponds to our estimate in 3.4.3. There is one exception, though: in case of weak harmonics (**scenarios 1 and 3**) bispectrum slice method performs worse than if nothing is done for denoising except for Fourier transform. This might be easily explained: in case of harmonic-free radargram using bispectrum slice method means adding noise from higher sinusoidal micro-Doppler rates into horizontal spectral estimate. Second-type harmonic appeared to be too weak to overcome this effect.
2. However, as it is to be expected, efficiency of bispectrum slice method grows when more harmonics are present in the radargram (**scenario 2**). At the same time efficiency of SVD-based denoising grows as well. Explanation is simple: since SVD performs decomposition of different signal parts based on their uncorrelatedness, adding the harmonic (which is correlated with main tone) increases the total signal energy of breathing-containing principal component. Therefore, rises the probability of separating it from noise. This effect is

demonstrated in figure 3.27: both main-tone signature and its first type harmonic are ascribed to one PC and we see both in figure 3.27, B. At the same time, SVD did not exhibit significant gain in case of ‘single sine’ scenario even though second-type harmonic was present in the radargram. It appears that due to the difference in signature shapes between main respiratory peak and second type harmonic, SVD splits them into different components. As a result, we do not see second type harmonic in main-tone singular matrix (figure 3.27, A). In addition, it should be noted that efficiency of SVD grows when the maximal range for searching the survivors is decreased. Besides, using SVD-based method instead of bispectrum slice has one more advantage: SVD benefits from any target motion correlated with breathing while bispectrum slice relies on second harmonic only.

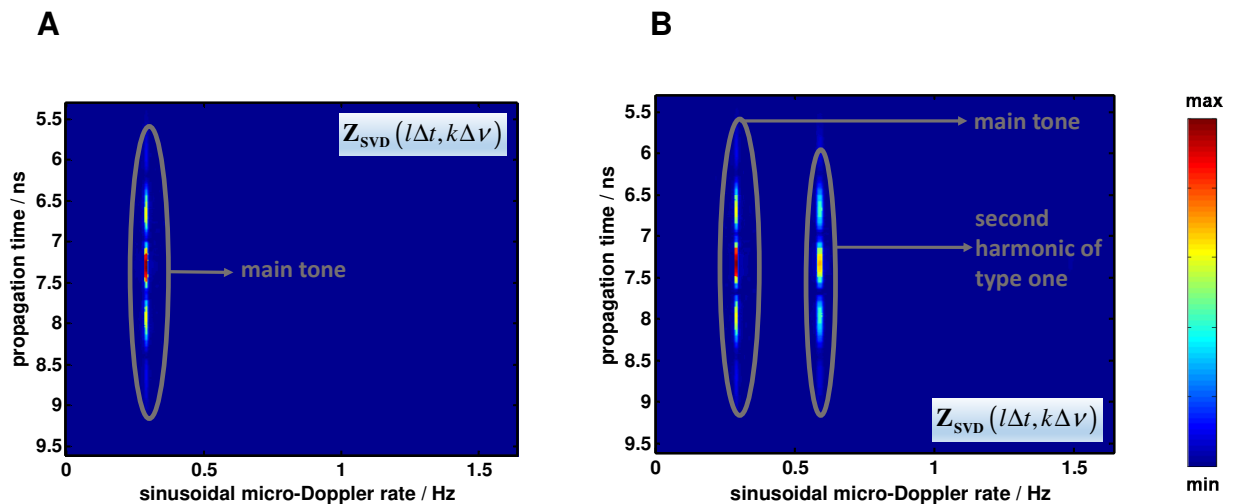


Figure 3.27: First singular matrix of two modelled datasets in the noise-free case: **scenario 1** (A) and **scenario 2** (B)

3. We see both in figure 3.24 and figure 3.25 that (as it was supposed) using ideal windowing function brings significant improvement to incoherent summation and cross-correlation detection (approximately half of the difference between ‘no breathing enhancement’ and optimal data processing with complete knowledge of main tone respiration signature). Besides, simulation results confirm our prediction that cross-correlation data processing slightly outperforms energy detection when using the same windowing function due to utilizing information about coherence of respiratory motion in the radargram.

4. In addition, we can say that for **scenario 3** performance of cross-correlation detector decreased in comparison with the case when we take as a reference ideal main tone respiration signature. However, it still produced the best result among other methods.

### ***3.8 Breathing detection through the heap of rubble, online measurement results***

Statistical evaluation of different data processing methods is given above. In this part we supplement this evaluation with practical online measurement results that were achieved during extensive measurement campaign at the facility of Swedish Rescue Services Agency (SRSA). Most of the measurements were carried out on the pile of diverse rubble (mainly composed of reinforced concrete, figure 3.28). Measurement scenario for tests with one person under test (PUT) is sketched in figure 3.29.

**A**



**B**



Figure 3.28: Detection area

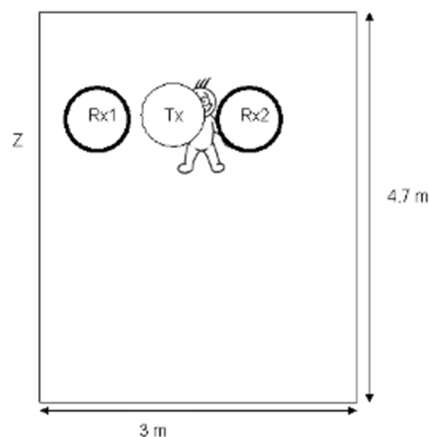


Figure 3.29 Scenario for establishing penetration capabilities of the radar, view from above

Detection methods described in this work are online and they were implemented inside GUI, operating the radar device. Explanation of GUI is shown in figure 3.30. Respiratory activity is detected as a bright point on the image in the left part of the screen which shows horizontal spectrum of the radargram  $\hat{\mathbf{Z}}_w(l\Delta t, k\Delta\nu)$ .

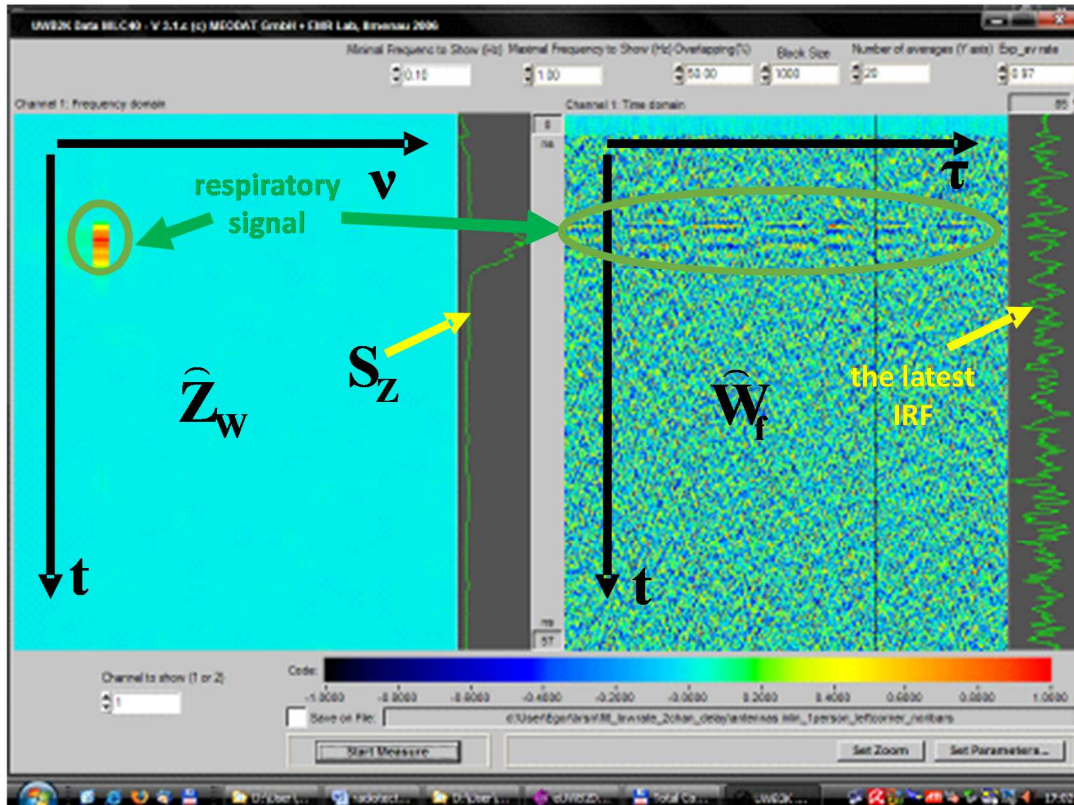


Figure 3.30: One person detected through 1.2—1.3 meters of rubble

Second image on the right part of the screen contains preprocessed radargram  $\hat{\mathbf{W}}_f(l\Delta t, m\Delta\tau)$  itself and it can be used for detecting stronger irregular motion (in figure 3.30 for example, breathing was strong enough to produce periodical pattern on the right side of the screen). In addition, there are two one-dimensional plots. First one shows  $\hat{\mathbf{S}}_z(l\Delta t)$  is  $\hat{\mathbf{Z}}_w(l\Delta t, k\Delta\nu)$  after horizontal summation: This plot can be helpful in the cases when respiratory motion was split among several cells in horizontal direction or when detecting weak non-periodical motion. The second plot shows the last measured IRF in preprocessed radargram.

During measurement campaign thickness of rubble was increased from 1.2--1.3 (results are in figures 3.30 and 3.31) up to 1.6—1.7 meters, which depth (as it can be seen in figure 3.32) produced result on the limit of our detecting capabilities. Detection through 1.2—1.3 meters is evident (although as it could be observed that some positions and people produce better result than others).

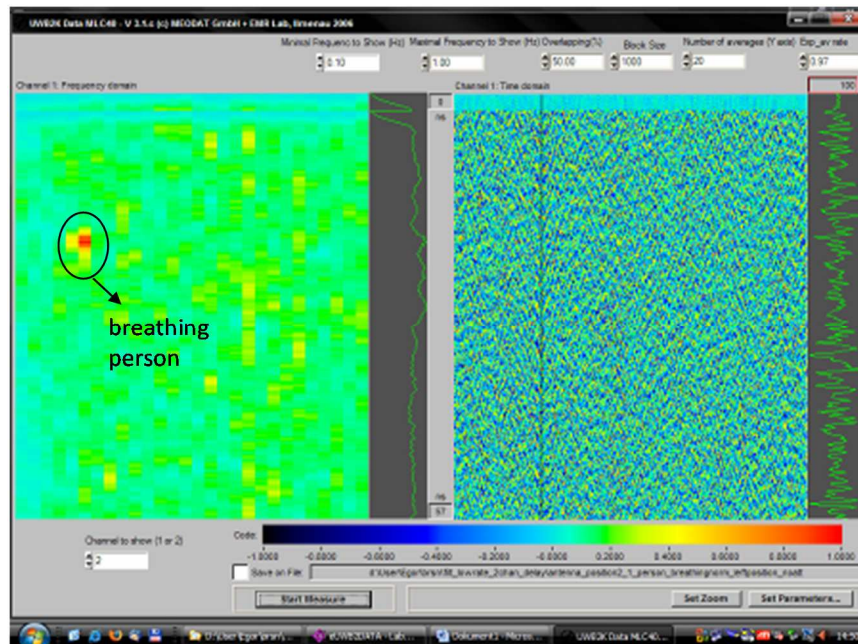


Figure 3.31: One person detected through 1.2—1.3 meters of rubble

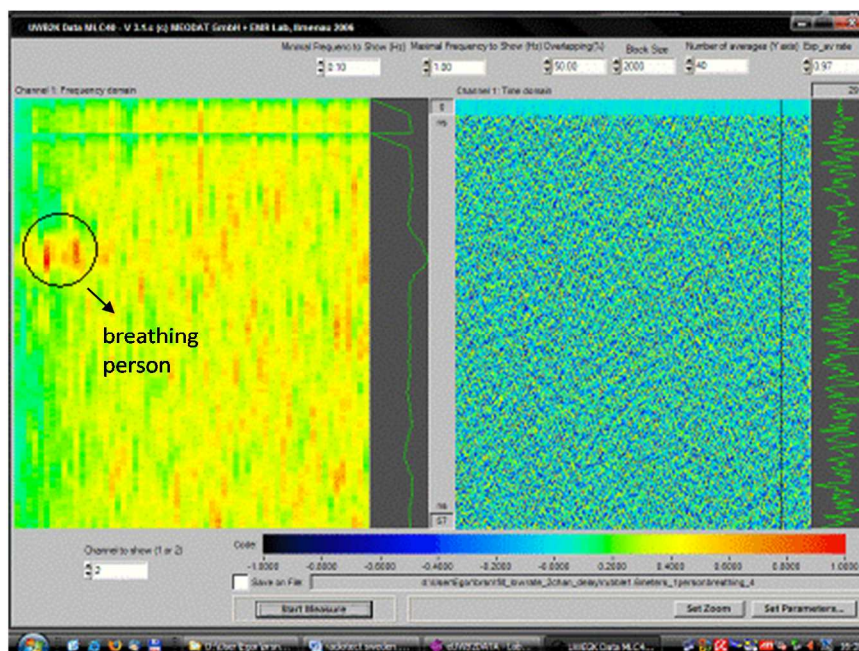


Figure 3.32: One person detected through 1.6—1.7 meters of rubble



Besides, successful tests with multiple persons (up to three) were carried out. Corresponding measurement scenarios are sketched in figure 3.33 while results are presented in figures 3.34 and 3.35. Motion of each person was observed as a distinct bright spot on the left part of the measurement GUI.

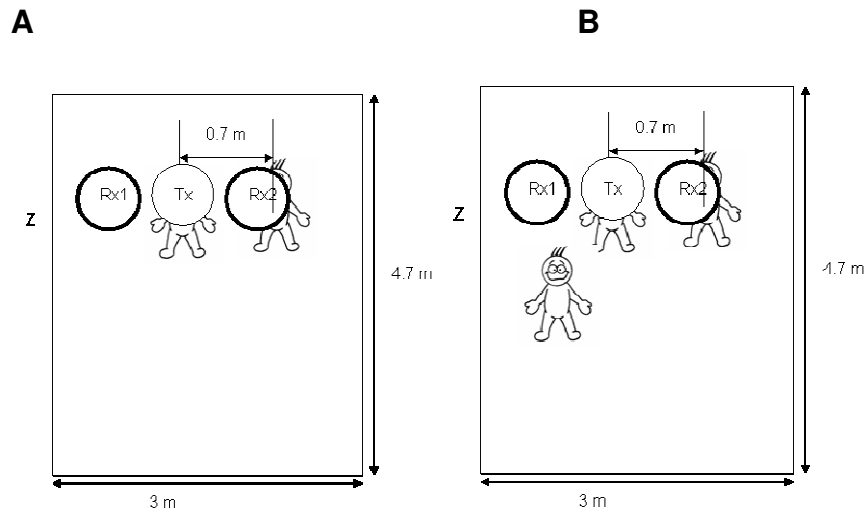


Figure 3.33: Detection of multiple people through rubble pile, view from above. A: two breathing people (measurement result is in figure 3.34). B: Person who is not strictly below antennas is moving strongly with his hands, two other persons breathe only

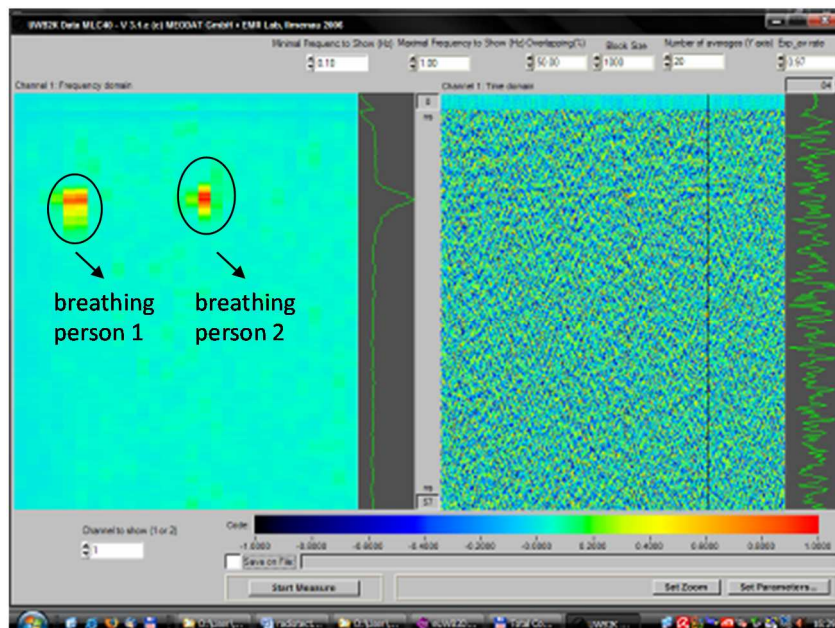


Figure 3.34: Detection of two breathing people through 1.2–1.3 meters of rubble, description is shown in figure 3.33 A

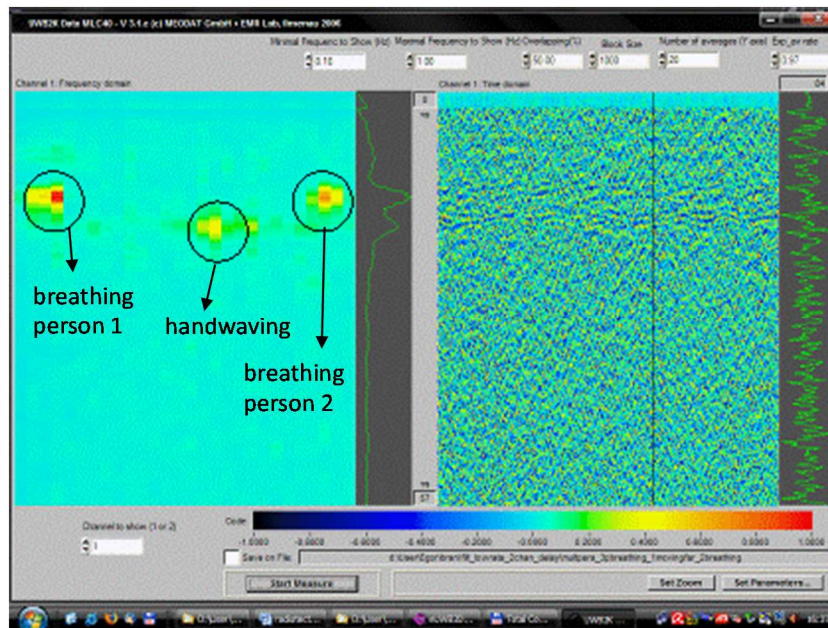


Figure 3.35: Detection of three breathing people through 1.2—1.3 meters of rubble. Description is shown in figure 3.33, B.

## 4 Clutter

Clutter is a sum of reflections from unwanted objects that are present in the radargram. Potential clutter sources (objects within antenna beam) are diverse (some of them are shown in figure 4.1). Some of these objects are not moving and we speak about their contribution as about stationary clutter. In contrast, non-stationary clutter is caused by moving objects. It makes sense to consider removal of these two distinct clutter types separately and this way it is done in this chapter.

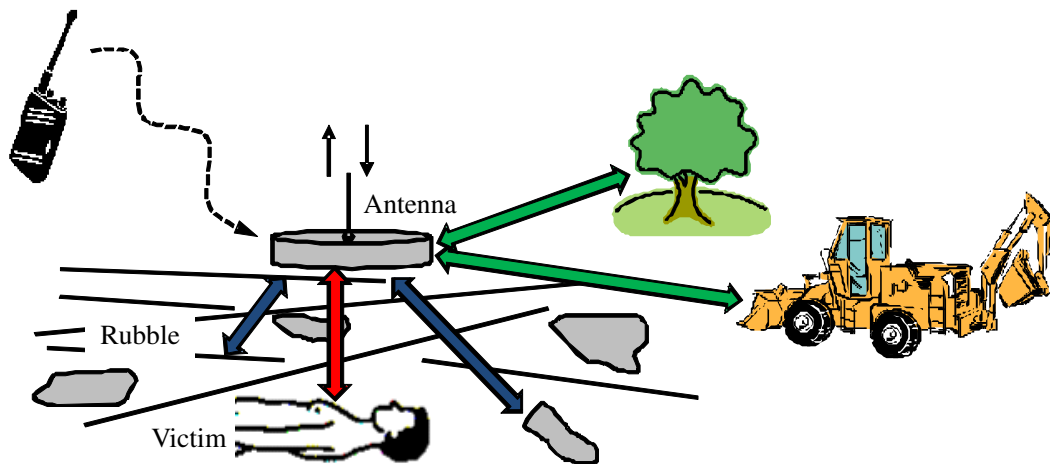


Figure 4.1: Clutter sources at measurement place

### 4.1 Stationary clutter

There is no way to avoid stationary clutter, since we do not perform victim detection in the open space and, moreover, rubble (which is necessarily present in our measurement scenario) is a source of stationary clutter.

As we discussed it in example in chapter 2, when jitter is negligible, stationary background can be estimated as a horizontal average of the radargram  $\widehat{\mathbf{W}}(l\Delta t, m\Delta \tau)$ . In case our aim is to detect respiratory motion this simple technique performs satisfactory: it really removes the static scenery while noise and target motion are preserved. However, it is convenient to adapt stationary clutter estimate  $\widehat{\mathbf{W}}_{\text{st}}(l\Delta t, m\Delta \tau)$  to slow changes, like radar drift. For this purpose, one can estimate background via horizontal exponential averaging:

$$\begin{aligned}\widehat{\mathbf{W}}_{\text{st}}(l\Delta t, 0) &:= \widehat{\mathbf{W}}(l\Delta t, 0) \\ \widehat{\mathbf{W}}_{\text{st}}(l\Delta t, m\Delta \tau) &= \alpha \widehat{\mathbf{W}}(l\Delta t, m\Delta \tau) + (1-\alpha) \widehat{\mathbf{W}}_{\text{st}}(l\Delta t, (m-1)\Delta \tau)\end{aligned}\quad (4.1)$$

Averaging parameter  $\alpha$  is chosen in way that only ‘very slow’ signal components with sinusoidal micro-Doppler rate below low limit (like 0.02 Hz) are considered clutter.

### 4.2 Non-Stationary clutter

Most of the authors (as well as this work up to this point) consider UWB breathing detection in the absence of interfering motion, which is easy to ensure under laboratory conditions. However, in real rescue scenarios moving objects are likely to be present.

The presence of moving objects within radar beam represents much bigger problem than stationary clutter. Therefore, all remaining part of this chapter is devoted to this problem.

Typical non-stationary clutter sources (see figure 4.1) include:

- People and trucks passing by. It may be hard to guarantee that the area is free from them under conditions of real rescue operation
- Wavering trees or metallic ribars that are the part of collapsed building. Detecting and removing them might cause significant time and effort
- Cell phones and walkie-talkies often used by rescue personnel as the sources of narrowband electromagnetic interference

Certainly, to a very considerable extent, non-stationary clutter has to be reduced by avoiding its sources at least within the first few meters around the antennas and by shielding the device, which is usually not very effective for low frequencies. Besides,

when clutter source is situated in the place where breathing person is unlikely to be found (for example, above the air-debris border) clutter response is weakened at the stage of localization (described in the next chapter).

Of course, when looking for survivors, antennas are directed downwards where sources of non-stationary clutter are unlikely to be found. Unfortunately, in practice antennas radiate at every angle. Even though backward antenna radiation is much weaker than the forward one, cluttering reflections from behind may produce stronger variations in the data than respiratory activity of survivors. This happens due to tremendous signal losses in the rubble layer between antennas and a victim.

Therefore, at the current stage non-stationary clutter cannot be completely excluded from the measured data. This is aggravated by the fact that even if clutter source is situated more than 10 meters away from antenna it is likely to appear in the radargram at the range typical for trapped people.

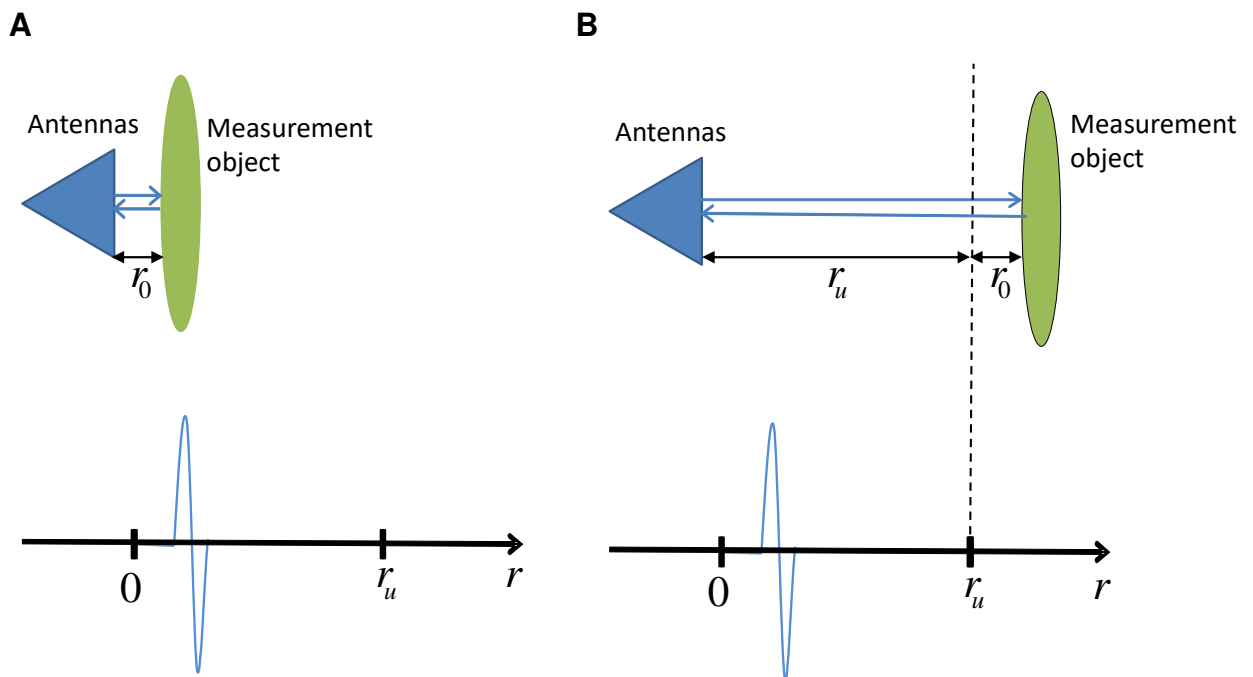


Figure 4.2: Radar target and its reflection inside(A) and outside (B) the unambiguity range

In order to explain the effect we need to remember that radar continuously emits the train of probing pulses (in our case— M-sequences) with period  $T_p$ . Accordingly, when distance to the certain object  $r$  satisfies the condition

$$r > cT_p \tag{4.2}$$

its reflection appears after the second probing pulse is already emitted and its time of arrival does not correspond to the physical distance between the object and antennas. Instead, it will look for us like object reflection appeared  $T_p$  nanoseconds earlier than it had to. This effect is illustrated in figure 4.2. Distance  $r_u = cT_p$  is called radar unambiguity range (since when all objects are situated closer than  $r_u$  their positions are unambiguously reflected in radargram). It is required in our task that potential victim is situated within radar unambiguity range in order to have correct information about his/her position and that is one of the reasons why radar device with considerable  $r_u$  of 17 meters was chosen. However, it might still be too shot to show cluttering objects at the correct distance.

That is, how it is shown in figure 4.2, clutter can appear in the vicinity of breathing person due to being away more than  $r_u$  and in this case neither removal of all moving objects a few meters around antennas nor applying localization algorithms will help. Hence, we also have to consider some means to suppress it algorithmically. In this chapter we discuss how reflection from the clutter source  $\mathbf{n}_{cl}(l\Delta t, m\Delta \tau)$  can be removed from the radargram  $\widehat{\mathbf{W}}(l\Delta t, m\Delta \tau)$  in presence of additive noise  $\mathbf{n}(l\Delta t, m\Delta \tau)$ :

$$\widehat{\mathbf{W}}(l\Delta t, m\Delta \tau) = \mathbf{W}(l\Delta t, m\Delta \tau) + \mathbf{n}_{cl}(l\Delta t, m\Delta \tau) + \mathbf{n}(l\Delta t, m\Delta \tau) \quad (4.3)$$

### 4.3 Simulated dataset to demonstrate algorithms that remove non-stationary clutter

In order to underline particular aspects of how different clutter-removing tools work we process example of a radargram generated according to expression 4.3. Respiratory signal in this dataset is simulated in the same way as it was done in chapter 3:

$$\mathbf{W}(l\Delta t, m\Delta \tau) = \mathbf{W}_s \left( l\Delta t - 2 \frac{r_0 - d(m\Delta \tau)}{c} \right) \quad (4.4)$$

$$d(m\Delta \tau) = d_{r1} \sin(2\pi v_{r1} m\Delta \tau) \quad (4.5)$$

As a clutter source object, moving forwardly with velocity  $s$  was used.

$$\mathbf{n}_{cl}(l\Delta t, m\Delta \tau) = \frac{A_{cl}}{\left( l\Delta t - 2 \frac{r_0 - sm\Delta \tau}{c} \right)^2} \mathbf{W}_s \left( l\Delta t - 2 \frac{r_0 - sm\Delta \tau}{c} \right) \quad (4.6)$$

Since clutter object changes its position up to considerable distance of five meters within measurement time we cannot ignore amplitude modulation from equation 2.9 in

the denominator of expression 4.6 how we do it in 4.4. Value  $A_{cl}$  is chosen so that clutter is much stronger than respiratory signal. Simulation parameters are summarized in table 4.1.

Test dataset generated according to expression 4.3, its signal and clutter components are shown in figure 4.3. Non-stationary clutter exceeds useful signal so much that the latter is almost invisible.

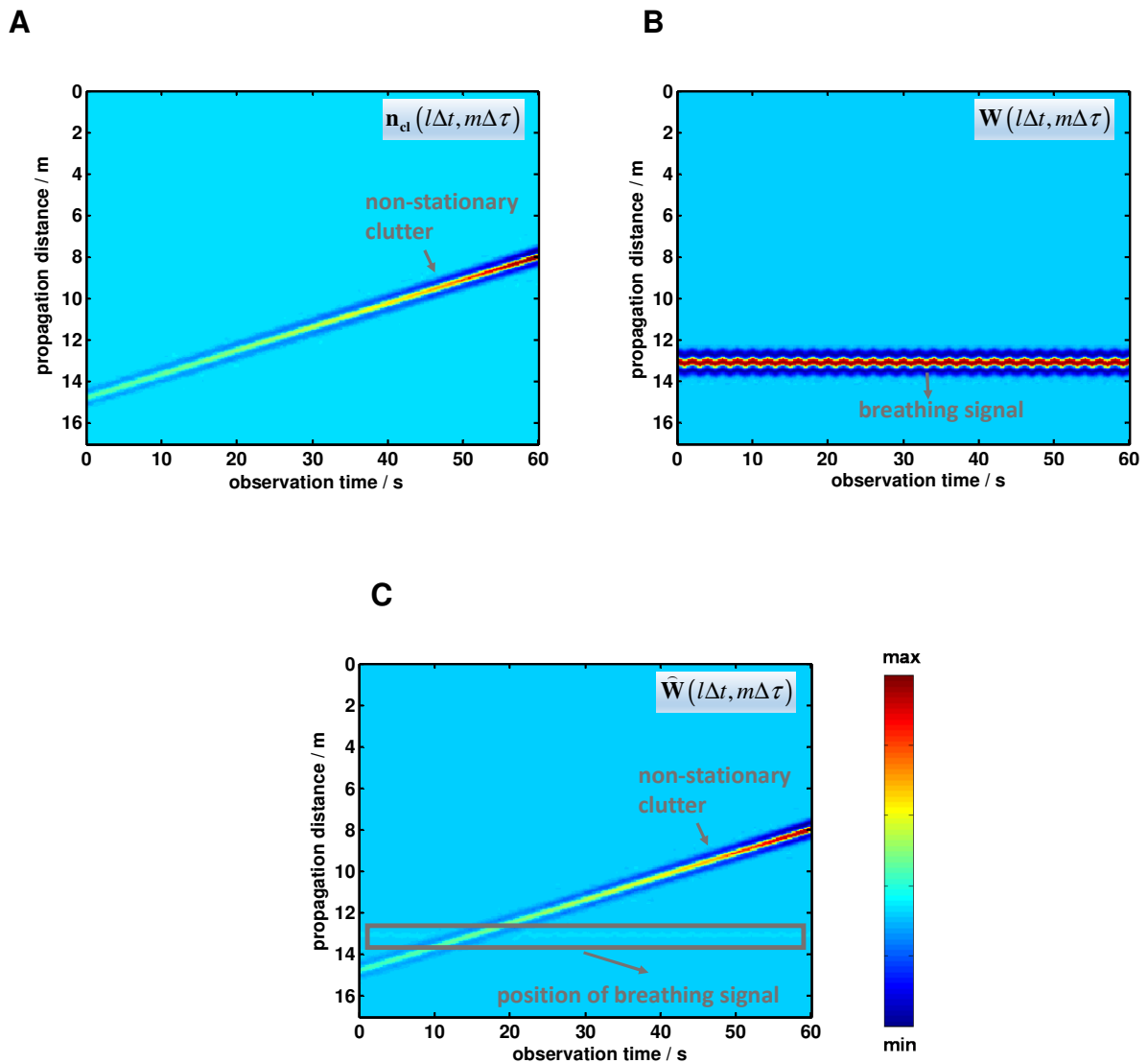


Figure 4.3: Simulated clutter (A), simulated respiratory signal (B) and their sum (C)

As a first data processing step we subtract our estimate of stationary clutter generated according to expression 4.1. First ten seconds of observation time are needed for filter in 4.1 to stabilize. Therefore, in what follows we skip this part of a radargram and our dataset becomes shorter.

Radargram after performing these steps is shown in figure 4.4, A. We cannot of course detect respiratory motion with our eyes in such signal representation. However, even after performing horizontal FFT (figure 4.4 B, C) it is only possible find respiration signature (marked) if we know where to look for it. Breathing does not produce the brightest spot on the image. Even in figure 4.4, C where highest clutter is zoomed out  $\beta$  is about 0.3 (that is, strongest clutter pixel is about three times brighter than the strongest signal pixel). Thus, we can state that without non-stationary clutter removal breathing is not detected in the synthesized dataset.

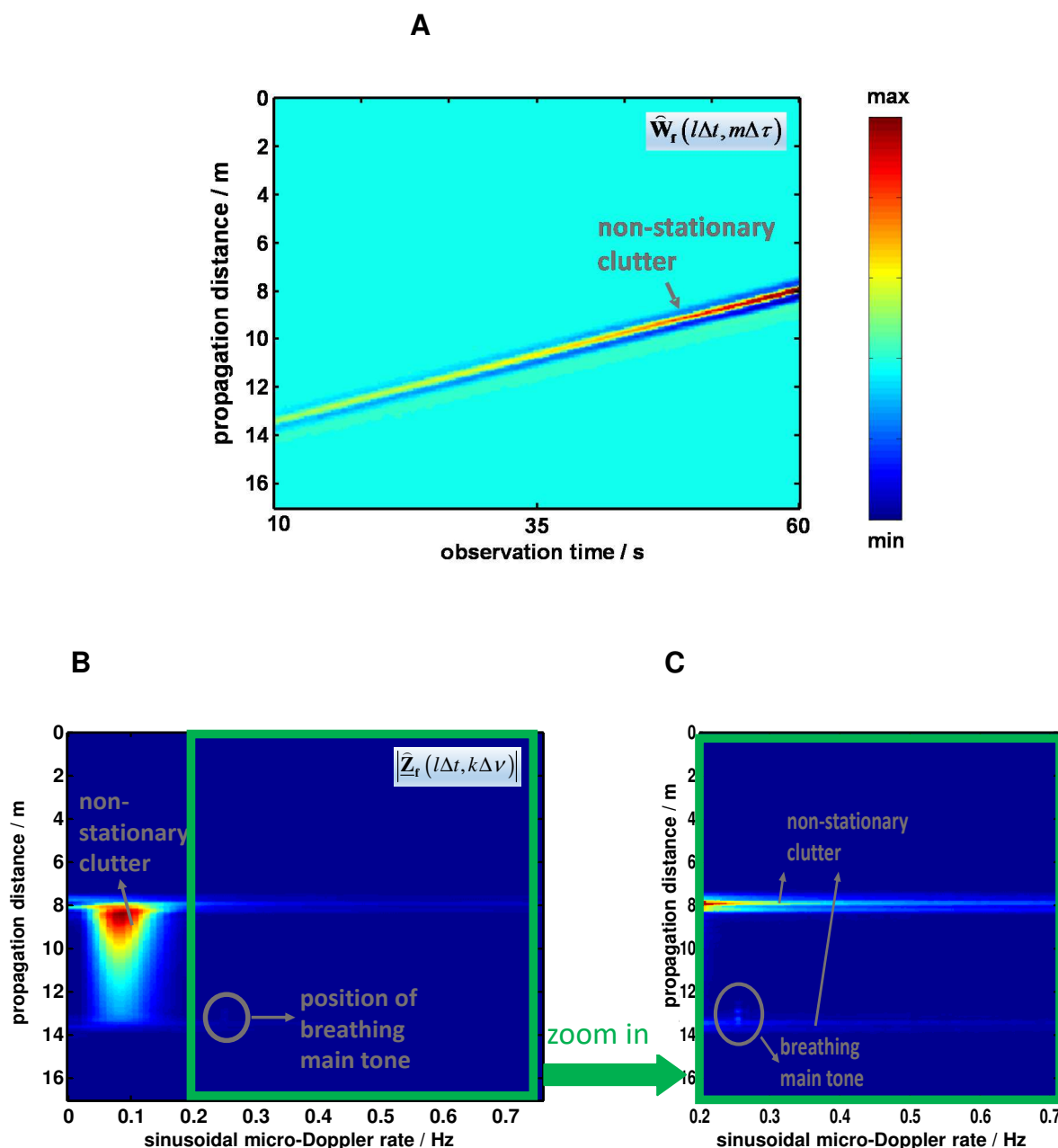


Figure 4.4: Simulated cluttered dataset after horizontal exponential filtering (A), its horizontal spectrum (B) and replica of the spectrum (C)



Name	Notation	Value
Pulse length	$t_p$	1 ns
Breathing rate	$\nu_{r1}$	0.25 Hz
Breathing magnitude	$d_{r1}$	1 cm
Velocity of 'clutter object'	$s$	5 meters/minute
Signal to clutter ratio (at $\tau = 0$ )	$\beta$	$\approx 0,07$
Data acquisition time		1 minute

Table 3.1: Parameters of simulations for the evaluation of algorithms

#### 4.4 SVD-based clutter removal

As we mentioned earlier, SVD is a powerful tool for removing non-stationary clutter. Idea behind it is that this technique allows to separate uncorrelated motion sources from one another and in the most cases respiratory motion will not correlate with clutter.

After performing SVD(here we perform it with horizontal spectrum, but the order of FFT and SVD can be changed without changing the result) we can suppose that if clutter was stronger than useful signal (typical situation, unfortunately) it can be estimated from  $M_c$  strongest principal components as following:

$$\mathbf{H}_{\text{SVD}} = \sum_{j=1}^{M_c} S_{j,j} \mathbf{u}_j \mathbf{v}_j^* \quad (4.7)$$

This method allows to get adequate clutter estimate in many practical scenarios (we give several examples in [30]).

Another approach that we consider as a reference method was already shortly described in this work in 3.6. Its high ability to find respiratory motion under severe clutter has also been demonstrated [35]. Method includes checking several (recommended value is  $J = 4$ ,  $j \leq J$ ) singular matrices and choosing one that contains signature of respiratory activity. In case there is respiratory motion in the radargram, one of these matrices (corresponding to  $j = \gamma$ ) looks like breathing signature while others are determined by noise and non-stationary clutter. Therefore, free of clutter signal estimate is given by:

$$\mathbf{Z}_{\text{SVD}} = \left| S_{\gamma,\gamma} \mathbf{u}_\gamma \mathbf{v}_\gamma^* \right|. \quad (4.8)$$

However, efficiency of SVD is scenario-dependent (which is not surprising given the huge diversity of potential clutter motion sources). Let us consider in details how does it treat our synthesized dataset. At first we do not confine ourselves to the breathing rates interval  $v_{\min} < v < v_{\max}$  before SVD is calculated.

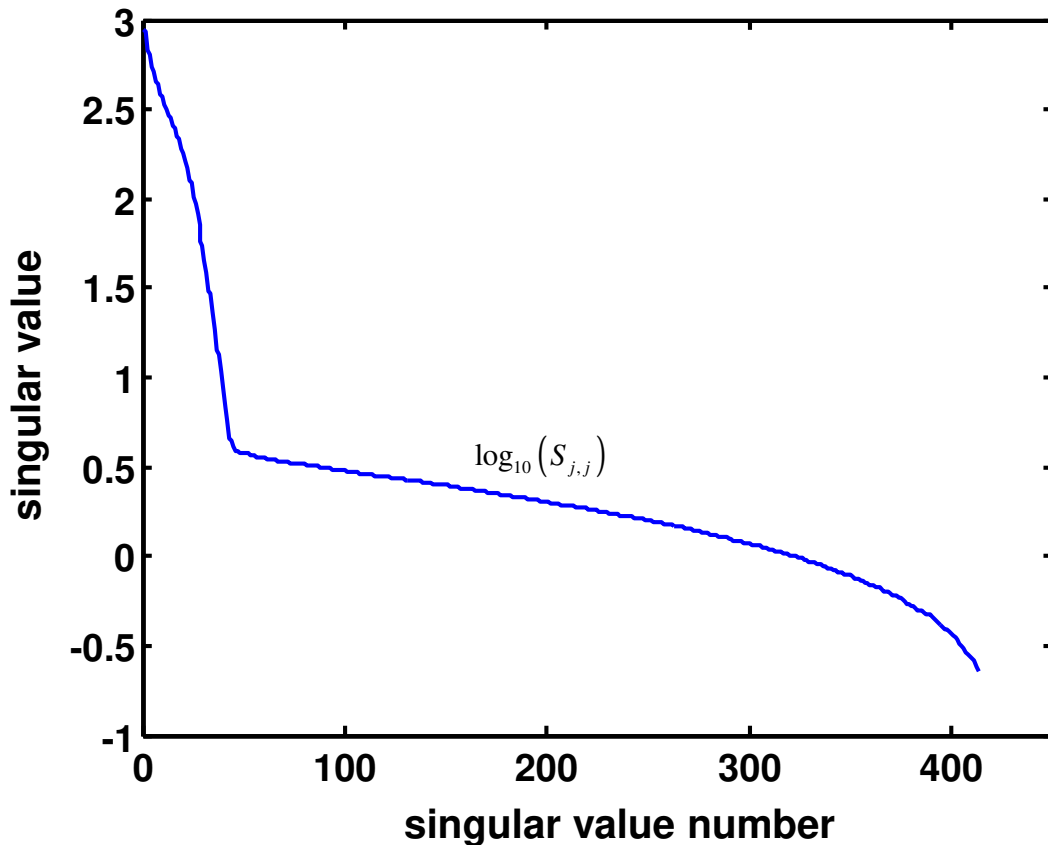


Figure 4.5: Singular values of the simulated cluttered dataset.

In figure 4.5 singular values versus their number are shown. The number of the singular values (and, accordingly, principal components) that explain deterministic motion can be estimated from this figure. To do this we should note that there are two completely different parts of the curve in figure 4.5. One corresponding to lower singular value numbers (up to  $M_d \approx 45$ ) represents strong deterministic components while singular values higher than  $M_d$  represent noise (noise PCs are not that different from one another in terms of energy and, accordingly, singular value)

Thus, we suppose that to find the breathing-related PC among a number of clutter components, anyone has to make search between 45 singular matrices determined by equation 4.8 ( $J = 45$ ), since we have no reason to be sure that breathing was strong enough to be confined to a smaller number of PCs.

Both SVD-based methods that deal with clutter (equations 4.7 and 4.8) are based on manipulations with singular matrices. Let us check how they look for our synthesized dataset. First four singular matrices are shown in figure 4.6, and, unfortunately, they do not contain breathing signal (which is to be found at 0.25 Hz at the distance of 13-14 meters) and reflect non-stationary clutter.

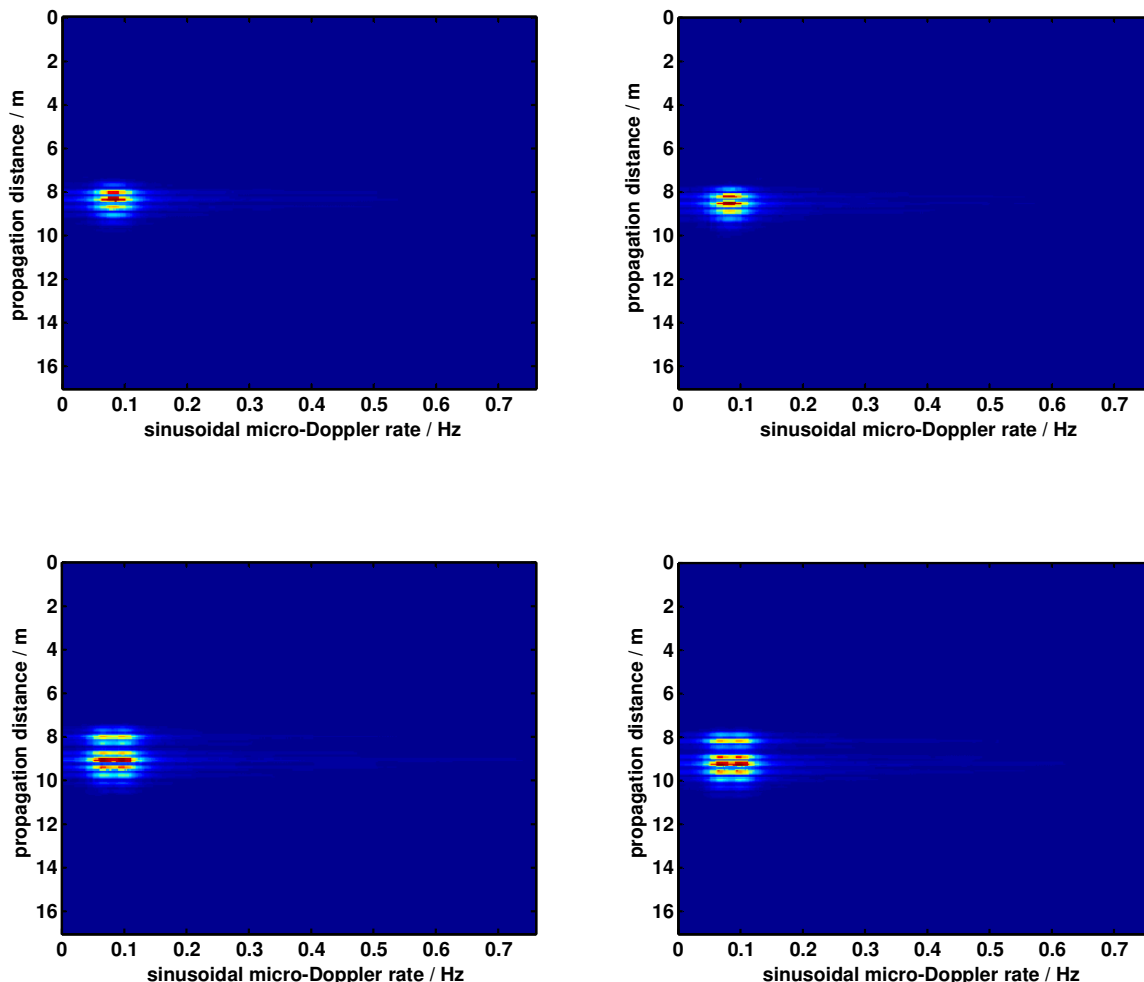


Figure 4.6: Singular matrices corresponding to four largest singular values of the simulated cluttered dataset ( $j=1,2,3,4$ ).

If for a certain cluttered scenarios  $J$  is much bigger than four ( $J=4$  is suggested in [35]), following danger is increased: one of the clutter-related singular matrices can contain bright spot within the range of breathing-related sinusoidal micro-Doppler rates, and the more singular matrices we have to consider the more this danger is for the natural reasons. One of the examples of clutter singular matrices that contain breathing-like signature is shown in figure 4.7.

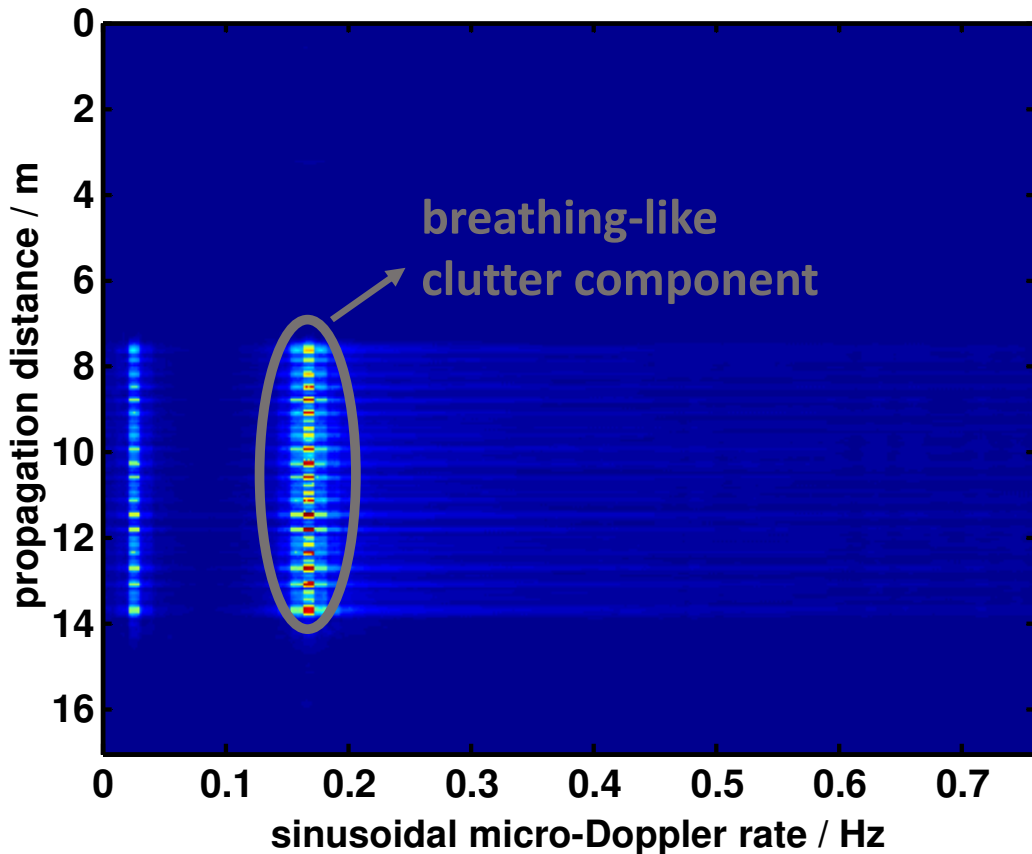


Figure 4.7: Singular matrix corresponding to part of clutter in simulated cluttered dataset ( $j=12$ ).

We see that bright spot horizontally is mainly localized at sinusoidal micro-Doppler rates about 0.18 Hz. This might cause false alarm. Of course, singular matrix in figure 4.7 lacks another important feature of breathing signature, which is spatial localization of the bright spot. This localization is missing here, however, just because our clutter sources during the data acquisition time moved for as much as 5 meters. This doesn't always happen in practice (for example, wavering trees and ribars are hardly likely to produce such motion magnitude).

Besides, the very fact that SVD splits the data into the set of uncorrelated sequences, does not automatically mean that the measure of 'uncorrelatedness' is high enough and breathing will always appear as a separate component, free from clutter parts. Actually, this might be the reason why we could not locate one particular breathing-containing singular matrix in the simulated dataset.

We could find singular matrix with breathing signature when SVD was performed over the horizontal spectrum of synthesized dataset when upper sinusoidal micro Doppler rate was limited with 1 Hz. Still, this singular matrix corresponds to 23<sup>rd</sup> singular value

(meaning that dozens of matrices are to be considered in order to find this component). Corresponding singular matrix is shown in figure 4.8:

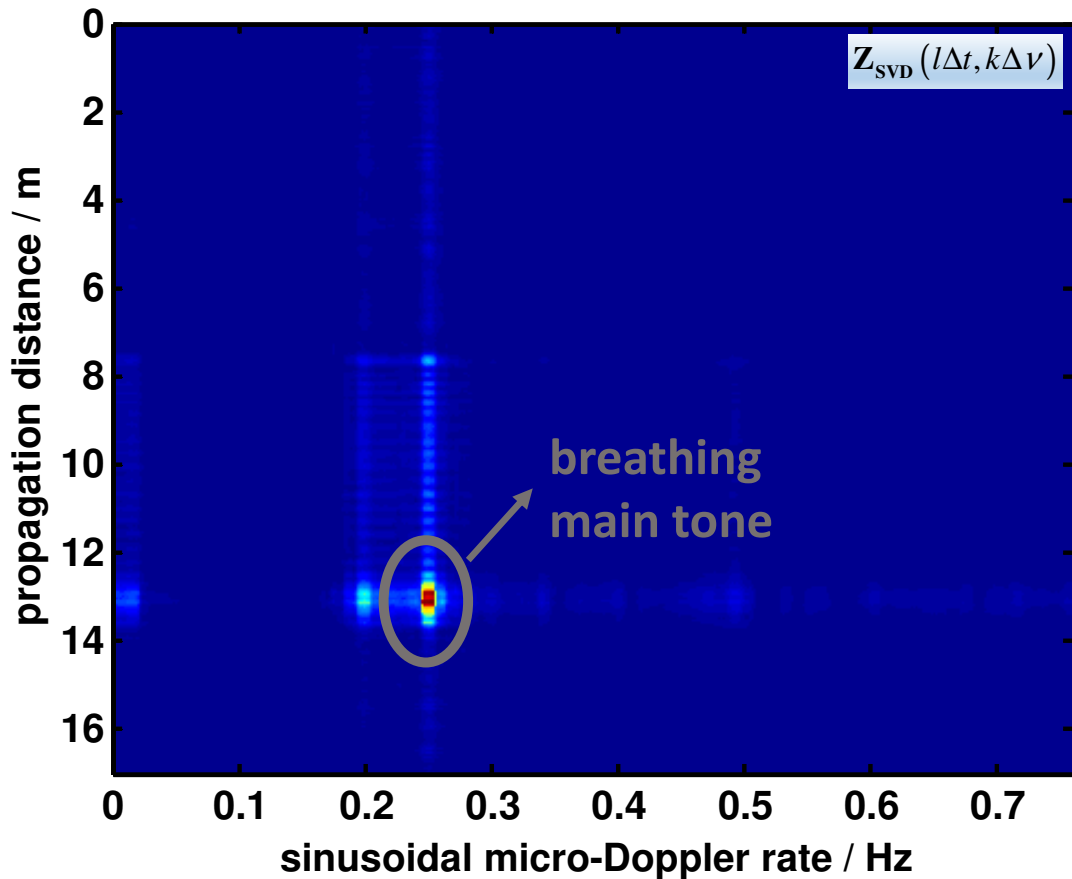


Figure 4.8: Singular matrix corresponding to respiratory signal in simulated cluttered dataset ( $j = 23$ ).

#### 4.5 Clutter localization from 'slow' variation

The only a priori assumption about clutter used by SVD is its uncorrelatedness with the breathing signature. In all other senses it performs blind separation of the respiratory signal from unwanted signal parts. The question arises, however, whether there are any properties of clutter that might serve as additional information to improve clutter-removing procedure.

There seems to be no reason for clutter to be localized within the same micro-Doppler rate window where we detect breathing signature. In practice, clutter signals often produce wide spectrum of distortion with significant slow (below 0.2 Hz) components at every  $\tau$  instant (this can be seen in figure 4.4, for example).

It is described in the beginning of this chapter (expression 4.1) how we create the estimate of stationary and ‘very slow’ (like drift of the electronic) clutter by means of simple exponential averaging filter. If we now apply the same type of filter to our radargram once again with higher than in 4.1 cut-off (for example  $\nu = 0.1$  Hz), we get matrix  $\mathbf{W}_{low}(l\Delta t, m\Delta \tau)$  that contains ‘slow’ part of non-stationary clutter alongside noise part. Breathing signature in  $\mathbf{W}_{low}(l\Delta t, m\Delta \tau)$  is attenuated by our filter.

Of course,  $\mathbf{W}_{low}(l\Delta t, m\Delta \tau)$  itself is not very useful as a clutter estimate since it is only a low-pass filtered version of  $\mathbf{W}_f(l\Delta t, m\Delta \tau)$  while clutter spreads up to much higher sinusoidal micro-Doppler rates than cut-off of the low-pass filter. However,  $\mathbf{W}_{low}(l\Delta t, m\Delta \tau)$  can be used as a clutter ‘map’. That is, by locating bright spots in  $\mathbf{W}_{low}(l\Delta t, m\Delta \tau)$  we can mark  $l\Delta t$  and  $m\Delta \tau$  instants when radargram  $\mathbf{W}_f(l\Delta t, m\Delta \tau)$  is cluttered. These ‘bright spots’ have to be brighter than noise, of course, and our criteria for classifying  $(l\Delta t, m\Delta \tau)$  as cluttered was:

$$|\mathbf{W}_{low}(l\Delta t, m\Delta \tau)| > 3\sigma_{low}, \quad (4.9)$$

Here  $\sigma_{low}$  is a noise standard deviation calculated after low-pass filtering. The easiest possible way to build a clutter removing procedure based on expression 4.9 is just to set all the pixels in  $\mathbf{W}_f(l\Delta t, m\Delta \tau)$  to zero when 4.9 is satisfied (as it is done in [30]).

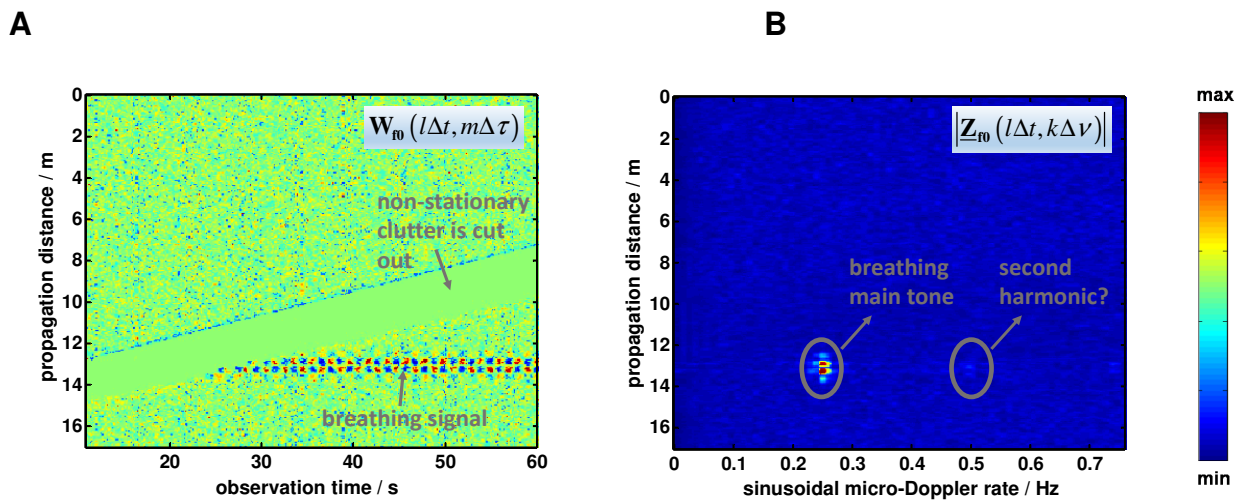


Figure 4.9: Clutter is cancelled due to using slow variation in simulated cluttered dataset: filtered radargram (A) and its horizontal spectrum (B)

This way we create radargram  $\mathbf{W}_{f_0}(l\Delta t, m\Delta\tau)$  where non-stationary clutter is cancelled. Results of such data processing with synthesized dataset are shown in figure 4.9. Clutter is removed and we see clear breathing signature ( $\beta \approx 5$ ). We even arguably see its second harmonic slightly above noise peaks. In figure 4.9, A we can also identify an area where clutter was set to zero. Unfortunately, part of the useful signal was 'cancelled' together with clutter at the  $(l\Delta t, m\Delta\tau)$  regions where breathing and clutter intersected. Such behaviour seems to be the main drawback of this simple algorithm. Even though in practical scenarios it has shown good results (how it is shown in [30]) this method cannot help much in situations when clutter and useful signal intersect. In the next thesis part we describe how this drawback can be alleviated. Method can be modified to detect clutter due to its high-rate (like above 1 Hz) components.

#### ***4.6 Clutter removal by means of SVD after localizing it in low-frequency variation***

As it was mentioned above, even though  $\mathbf{W}_{\text{low}}(l\Delta t, m\Delta\tau)$  is strongly correlated with clutter contaminating  $\mathbf{W}_r(l\Delta t, m\Delta\tau)$ , it is not really a valid clutter estimate since it does not include perturbations that intersect with respiration signature in  $\nu$ . However, this 'correlatedness' can be used to get more useful clutter estimate inside the following clutter-removing procedure (first published in [32]):

1.  $\underline{\mathbf{Z}}_{\text{low}}$ , horizontal spectrum of  $\mathbf{W}_{\text{low}}$  is calculated from the radargram
2. SVD of  $\underline{\mathbf{Z}}_{\text{low}}$  is performed. For that purpose, the observation time spectrum is written as a matrix, i.e.:

$$\underline{\mathbf{Z}}_{\text{low}}^T = \mathbf{U}\mathbf{S}\mathbf{V}^* \quad (4.10)$$

We decompose the transposed version of  $\underline{\mathbf{Z}}_{\text{low}}$  to work with PCs (principal components) that reflect the behaviour in observation time. Based on the distribution of the singular values in  $\mathbf{S}$ , we select the number  $M_d$  of reasonable PCs and we take the sub-matrix  $\mathbf{U}_M$  out of related to the strongest singular values. Here value  $M_d$  should (ideally) be equal to the number of components that explain deterministic signal in  $\underline{\mathbf{Z}}_{\text{low}}$ . Thus, method to determine this number in practice is to look for the steep jump in singular

values changing rate (for example, as we discussed, this jump is good visible in figure 4.5)

3. We “extrapolate” non-stationary clutter to the whole radargram horizontal spectrum  $\underline{Z}_f$  :

$$\underline{H}_{SVD2} = \underline{U}_M \underline{U}_M^* \underline{Z}_f \quad (4.11)$$

This procedure gives us clutter estimate  $\underline{H}_{SVD2}$  being the part of  $\underline{Z}_f$  ‘explained’ by clutter PCs derived from low-frequency horizontal spectrum  $\underline{Z}_{low}$

4. Finally, the radargram is cleaned from non-stationary clutter by subtraction:

$$\underline{Z}_{SVD2} = \underline{Z}_f - \underline{H}_{SVD2} \quad (4.12)$$

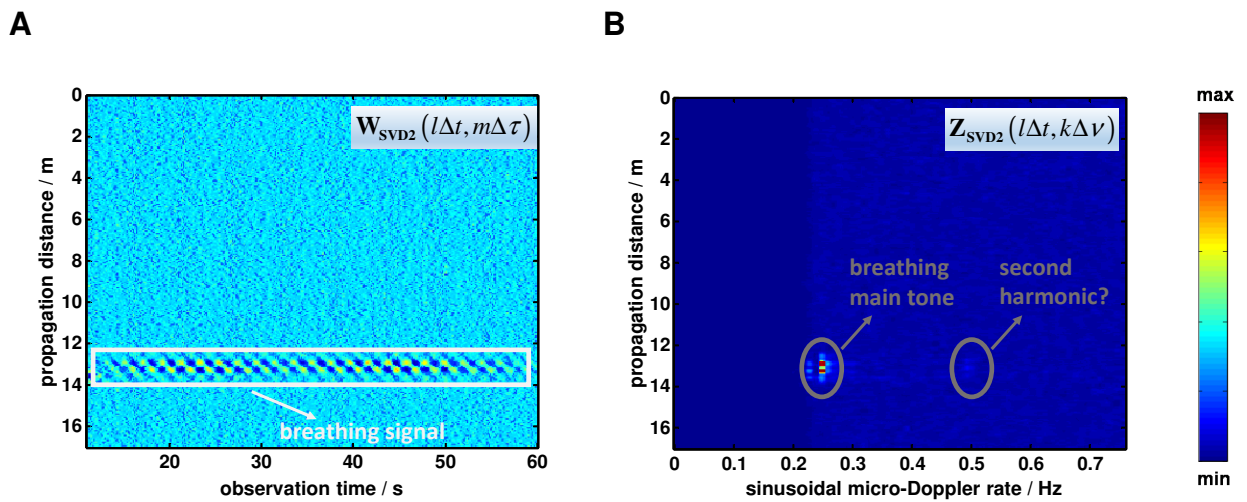


Figure 4.10: Clutter is cancelled in simulated cluttered dataset due to using low-frequency variation by means of SVD: radargram (A) and its horizontal spectrum (B).

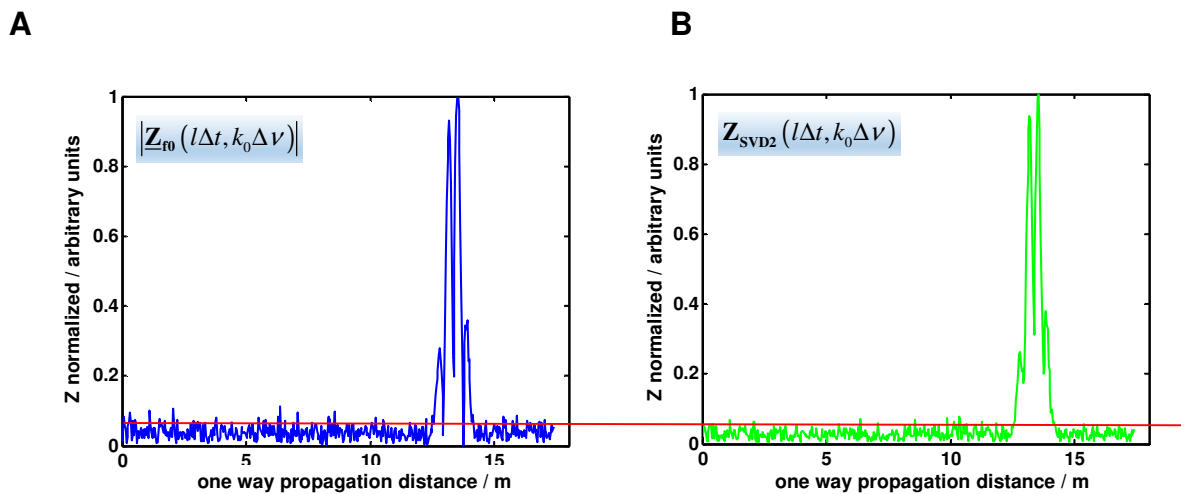


Figure 4.11: Vertical lines of horizontal spectrum at 0.25 Hz after clutter removal by setting radargram cluttered region to zero (A) and via SVD (B)



Results for removing the clutter via this method from our synthesized dataset are shown in figures 4.10 and 4.11. We see in figure 4.10, A that in comparison with decluttering like in chapter 4.5 (figure 4.9), using SVD as described above removed the clutter and at the same time it allowed to retain respiratory signal over its complete horizontal length. One of the consequences is that SNR in horizontal spectrum after using this method is a bit higher. This can be observed in figure 4.11 where resulting curves are shown for both methods and noise peaks for the method from chapter 4.6 are slightly lower than those for the method from chapter 4.5.

Some examples of how algorithm successfully performs clutter removal from measured data are given in figure 4.12.

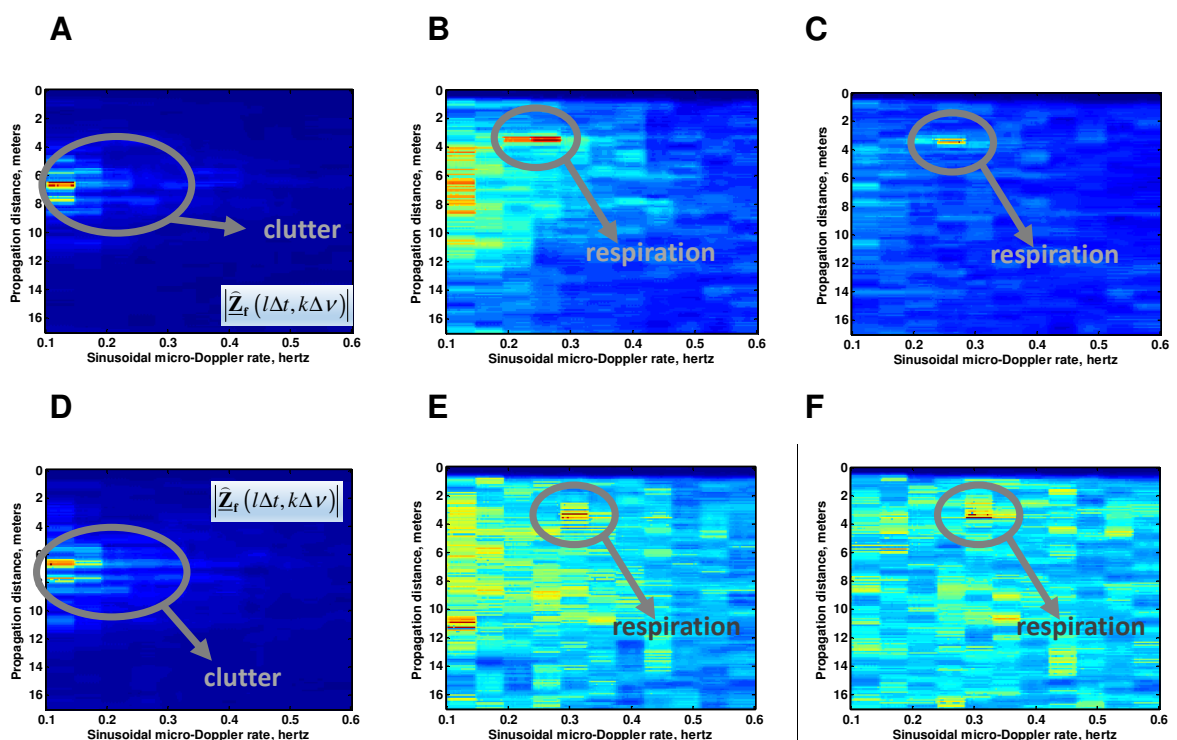


Figure 4.12: Non-stationary clutter removal for two different scenarios (A, B, C represent the first one; D, E, F,-- the second). A, D: original data after Fourier-Transform in observation time. B, E: clutter reduction by SVD. C, F: clutter reduction by estimating it in low-frequency variation.

## 5 Person localization by respiratory motion

Localization of breathing person is the final stage of processing radar data in search and rescue. This stage incorporates most of the added value of system in total, since while there are multiple methods for detecting trapped victims (search dogs is probably most successful one), finding out the position of person is much more difficult with present techniques.

### *5.1 Localization principle. Time of arrival and time difference of arrival estimates.*

With one transmitter (in figures transmitter is denoted as Tx), number of receiving antennas necessary to localize a person is three [30]. However, it is convenient to consider main aspects of the problem for 2d space, two receiving antennas (Rx1 and Rx2) as it is shown in figure 5.1 and then extend it to 3d and three receivers.

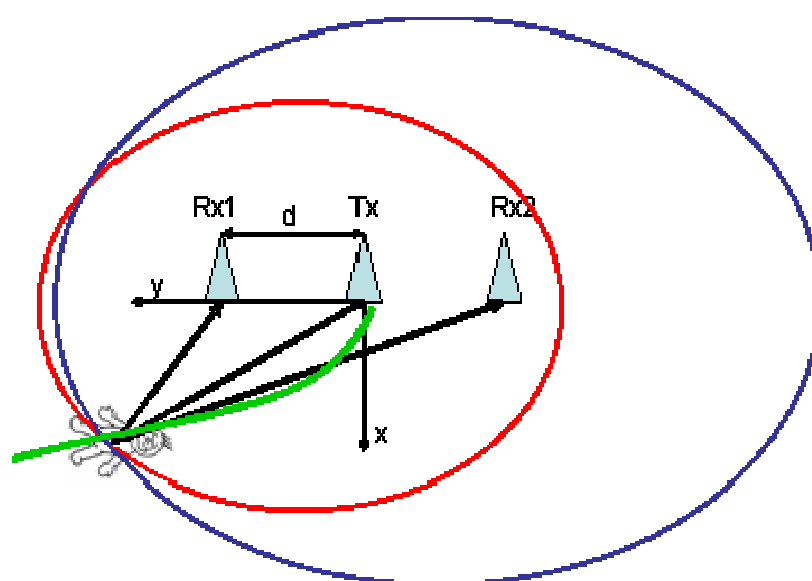


Figure 5.1: 2d localization with one transmitting (Tx) and two receiving antennas (Rx1 and RX2)

Antenna configuration shown in figure 5.1 reproduces antenna system of radar prototype created in RADIOTECT project and most of the data was collected with person right beneath the antennas.

In radargram electromagnetic waves reflected from different objects arrive at different instants in fast time, which instants are related to distance passed by the waves. In homogeneous media distance passed by electromagnetic waves between transmitter,  $i$ -th receiver and reflected from some object equals

$$r_i = \frac{ct}{\sqrt{\epsilon}} \quad (5.1)$$

We consider rubble as a homogeneous media, since no information about its internal structure is available. Although in our experiments on real rubble no significant effects of its heterogeneity spoiled localization results, it is likely to limit system performance for many scenarios.

For 2d scenario in figure 5.1 set of possible Cartesian coordinates  $(x, y)$  of reflecting object appearing in a radargram at distance  $r_i$  is given by following equations:

$$r_1 = \sqrt{x^2 + y^2} + \sqrt{(x-d)^2 + y^2} \quad (5.2)$$

$$r_2 = \sqrt{x^2 + y^2} + \sqrt{(x+d)^2 + y^2} \quad (5.3)$$

Each of equations 5.2 and 5.3 defines an ellipse with focal points at the positions of transmitter and one of the receiving antennas. When we find a point beneath antennas where two ellipses corresponding to one object cross, we estimate position of this object via calculating time of arrival (TOA) of electromagnetic waves.

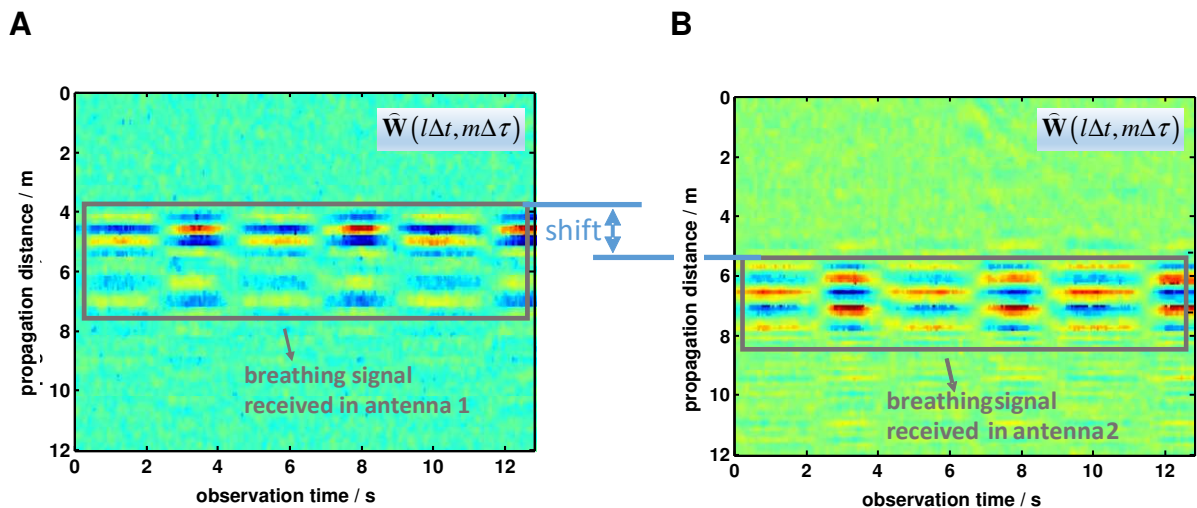


Figure 5.2: Breathing person as seen in radargram: signal received by first antenna (A) and by second antenna (B).

It can be seen in figure 5.2 that there is certain shift of breathing response in one channel relative to the second one in fast time. For each such shift there is a hyperbola in the space (shown green in figure 5.1), representing all possible points where reflecting object can be situated. This hyperbola is determined by equation 5.4:

$$r_{1,2} = r_1 - r_2 = \sqrt{(x+d)^2 + y^2} - \sqrt{(x-d)^2 + y^2} \quad (5.4)$$

Using 5.4 for localization means applying time-difference of arrival (TDOA) approach. For given antenna configuration it is possible to calculate position of the object by means of combined TOA/TDOA estimate (finding crossing of ellipse and hyperbola). Often using combined TOA/TDOA method yields less angular error in localization than pure TOA. This can be explained by the notion that at the crossing ellipse and hyperbola lines are almost orthogonal which makes target image less blurred. Example where this effect can be observed is shown in figure 5.3: object mark in TOA image is bigger and it bends around antennas much more than in TOA/TDOA image.

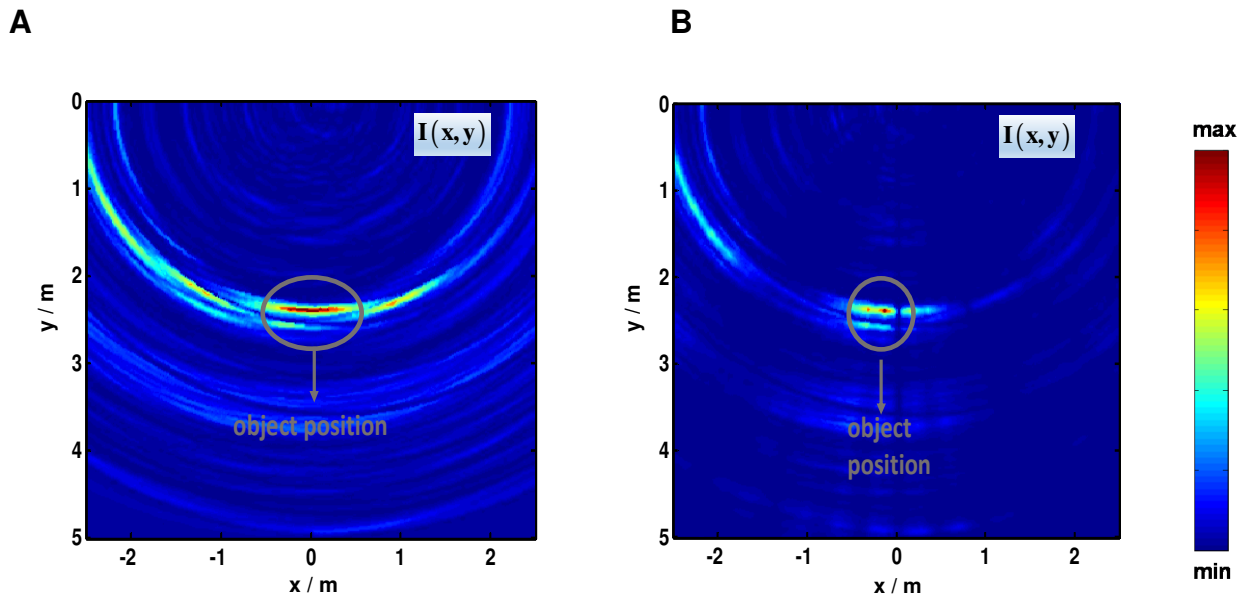


Figure 5.3: Person seen by radar localized via TOA method (A) and combined TOA/TDOA approach (B)

## 5.2 Localization algorithm

On the basis of localization view from previous subchapter, following algorithm was created and used:

1. Detecting breathing signature and its sinusoidal micro-Doppler rate ( $k_0 \Delta \nu$ ) in one of the horizontal spectrum estimates  $|\widehat{\underline{Z}}(l \Delta t, k_0 \Delta \nu)|$  (optionally, in horizontal

spectrum estimate after enhancing respiratory motion via one of the method from chapter 3).

2. For both receiving channels vectors  $\underline{\mathbf{Z}}(l\Delta t, k_0\Delta \nu)$  are calculated.
3. Equation 5.1 together with any of the equations (5.2—5.4) allow us to calculate ‘geometry’ matrices  $\Gamma_i(\mathbf{x}, \mathbf{y})$  that contain distances  $r_i$  travelled by electromagnetic waves for specific antenna pair corresponding to the breathing person being located at the specific point in space  $(\mathbf{x}, \mathbf{y})$ . Matrices contain all possible distances for TOA and TDOA estimates.
4. Interpolation of each  $\underline{\mathbf{Z}}(l\Delta t, k_0\Delta \nu)$  (for TOA) and their local average cross-correlations (for TDOA) onto appropriate 2d “geometry” matrix and addition (or, alternatively, multiplication) of the results to receive resulting image  $\mathbf{I}(\mathbf{x}, \mathbf{y})$  where respiratory motion is shown as a bright spot. Example of such images is given in figure 5.3.

For 3d localization and three receiving antennas almost identical approach was used with TOA estimates. The only modification is extension of “geometry” matrices to 3d.

Algorithm has following limitations:

- Heterogeneity of rubble can cause serious mistakes in some scenarios
- Imprecise value of  $\varepsilon$  for rubble material under real conditions can cause some error in localization.
- In the case of two or more victims if they are situated at almost identical distances to antennas ghost target can appear (this happens because ellipses related to different victims cross). However, all victims in this case will be shown.

### ***5.3 Measurement results***

Data collection for testing localization of victims was accomplished at the same measurement location as described in the final part of the chapter three.

Two types of localization were successfully applied to measured data:

1. 2d localization when person is situated in the same plane as three antennas with combined TOA/TDOA method (results are shown in figure 5.4) 3d localization of person with TOA when additional measurement after relocating antenna was carries out (figure 5.5).

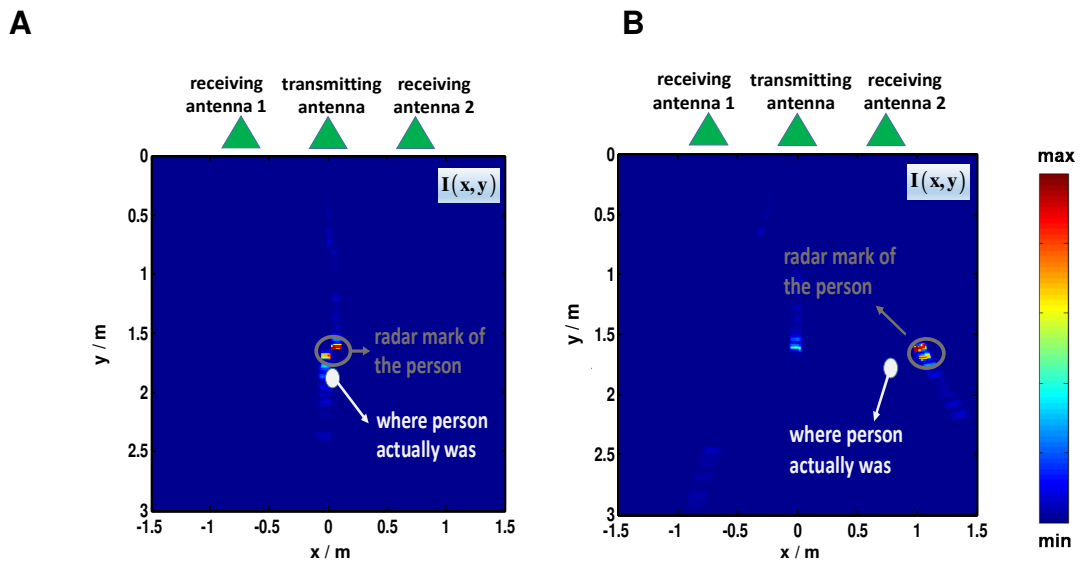


Figure 5.4: Detection and 2d localization of two persons breathing at different positions one after another.

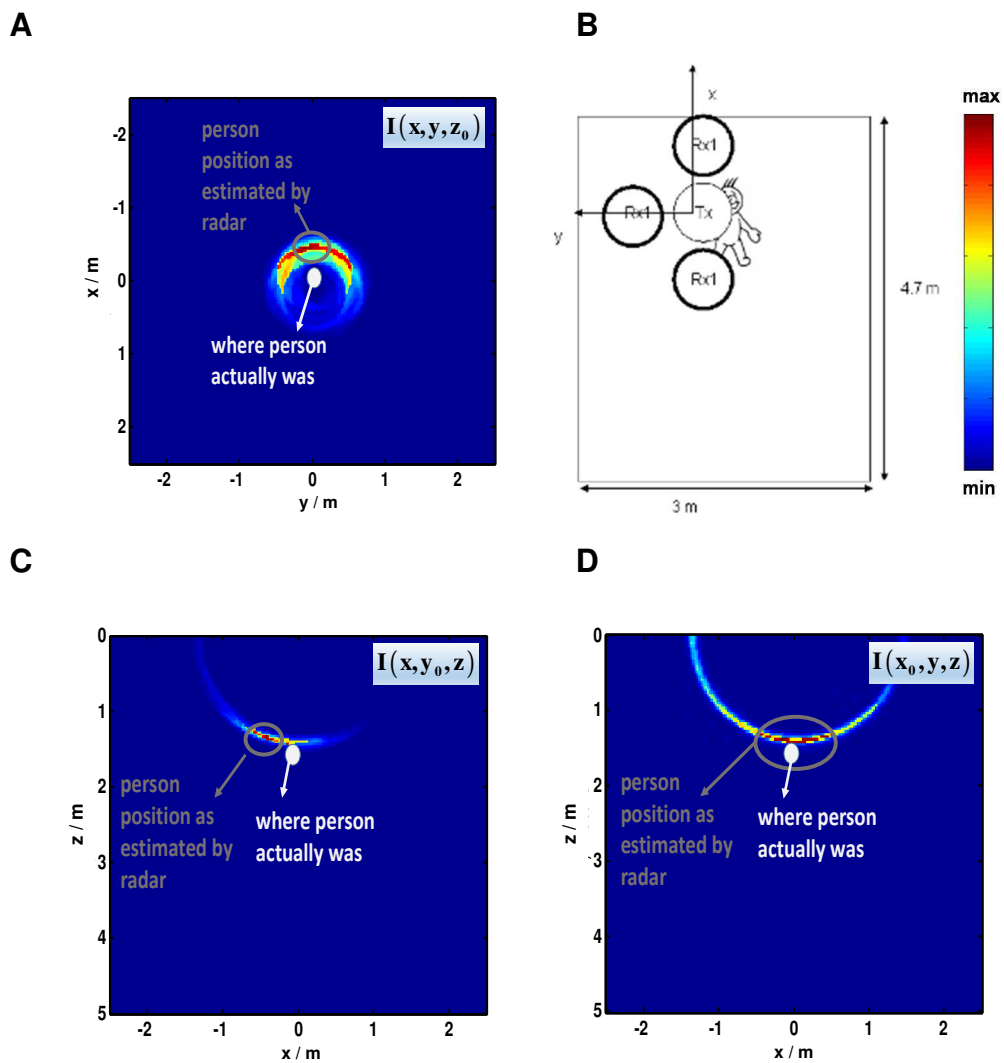


Figure 5.5: Detection and 3d localization of breathing person: measurement scenario (A) and results (B, C and D).

## 6 Radar unit for breathing detection

In the breathing detecting radar system used in this work pseudo-noise random code serves as a stimulus signals. More specifically, Maximal Length Binary Sequence (MLBS or, for brevity, M-sequence) is used.

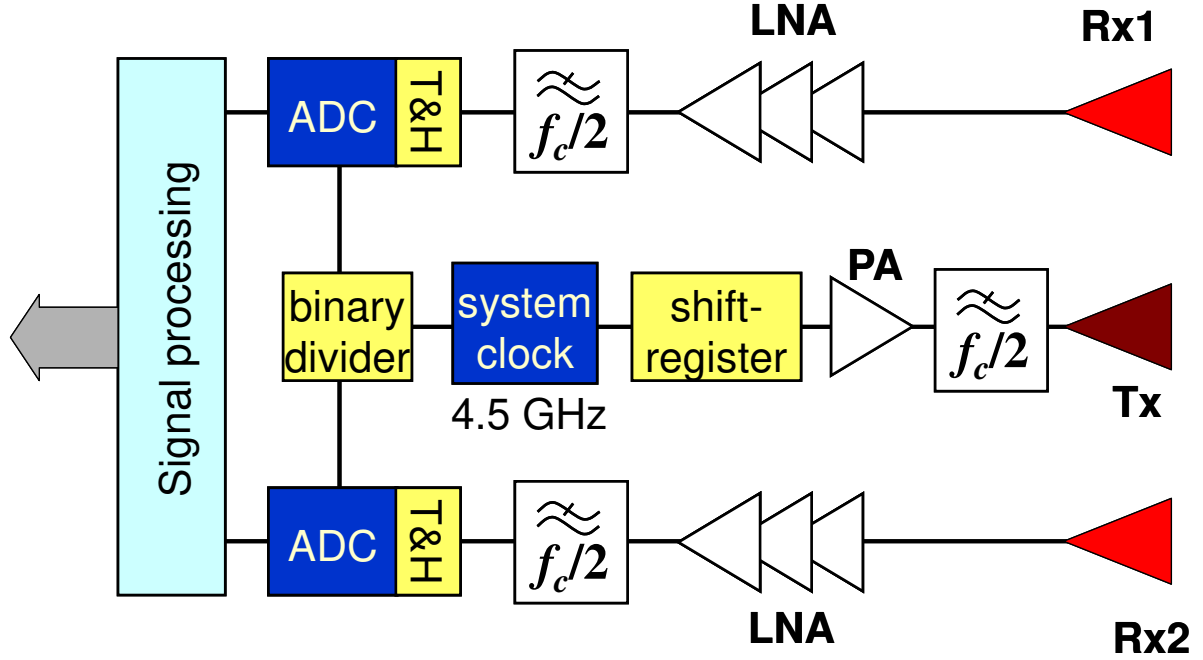


Figure 6.1: System structure an M-Sequence radar with one transmitter and two receivers.

Structure of pseudo-noise radar is shown in figure 6.1. Shift-register, pulsed by the RF-clock, provides the M-sequence, which serves as a stimulus signal transmitted by the Tx-antenna. On the receiver side signal is converted into the digital domain by a sub-sampling controlled by binary divider. Received signal is a pseudo-random one; part of it is shown in figure 6.2. Pulse-like time-domain radar signal  $\hat{X}_M(t)$  is reconstructed by means of calculating cross-correlation function of received pseudo-random signal  $\hat{W}_M(t)$  and ideal M-sequence  $W_M(t)$ :

$$\hat{X}_M(t) = \hat{W}_M(t) * W_M(-t) \quad (6.1)$$

After that,  $\hat{X}_M(t)$  is available for further processing in the form similar to that of the impulse radar signals.

Technical parameters of the radar device that was extensively used to acquire test data for this work are summarized in table 6.1.

Parameter name	Value
Clock frequency	4.5 GHz
Frequency bandwidth	0.005—2.25 GHz
M-sequence order	9
IRF length in samples	511
IRF length	114 ns

Table 6.1: Technical details of the radar device

Let us point out advantages of M-sequence radar device. First, using only simple and stable digital components (digital shift register controlled by a single oscillator) to produce probing signal of such high frequency bandwidth results in fast (real-time) and stable performance of radar electronics.

Second, RF electronics of M-sequence radar allows monolithic implementation in SiGE technology. Due to small binary voltage amplitudes switching of M-sequence happens extremely fast which property guarantees low jitter (this is especially important for detecting survivals beneath rubble how it was shown in chapter two). Besides, by its nature M-sequence has low crest factor which ensures high SNR.

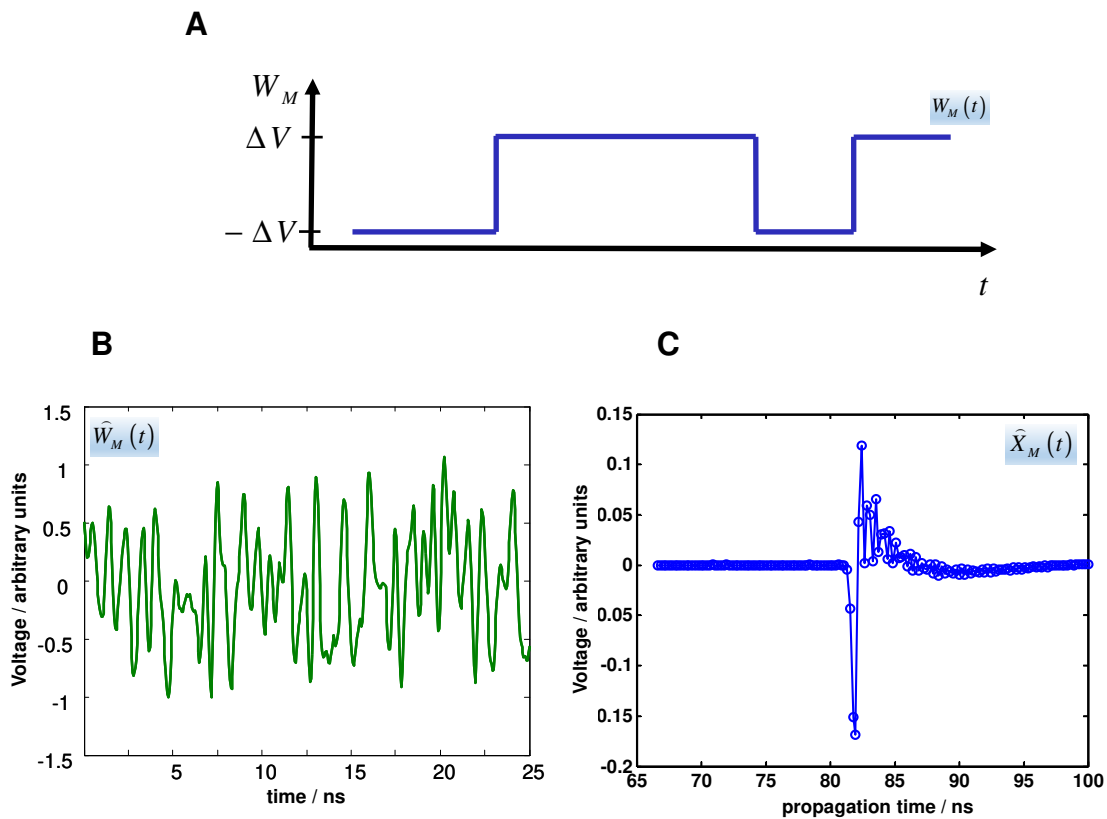


Figure 6.2: M-sequence radar, signals. Idealized M-sequence (A), measured M-sequence (B), measured IRF (C).



## 6.1 SNR of the radar unit and different ways to increase target detection range

Let us look at how noise level and signal level (measured as main peak, maximum of the IRF) change depending on the amount of attenuation introduced between transmitting and receiving channel of the radar ( $L_{in}$ ). Results of such measurement are shown in figure 6.3.

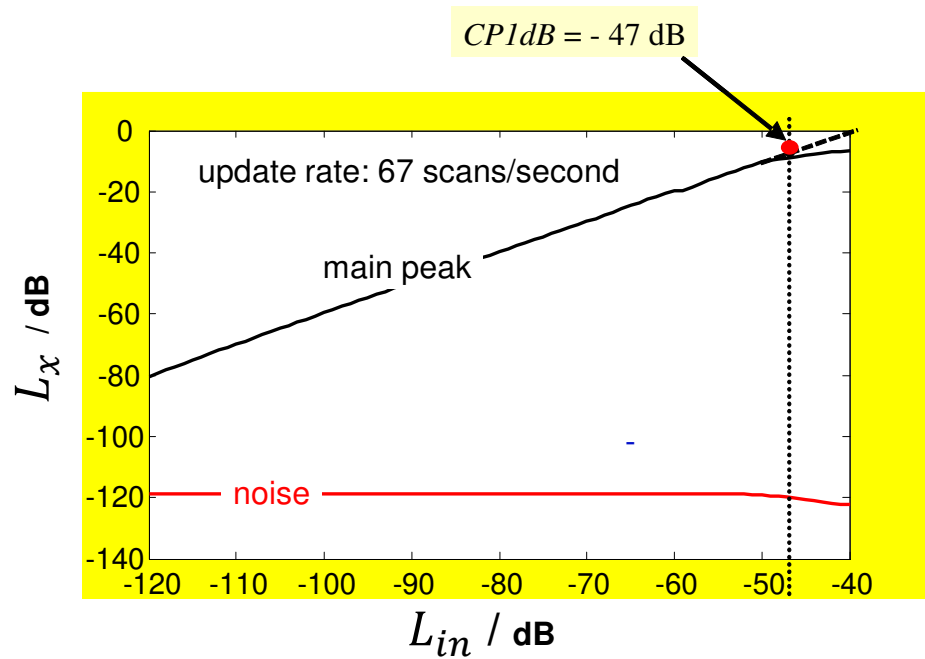


Figure 6.3: Radar signal components measured in receiving channel of the breathing-detecting radar unit through different number of attenuators.

One thousand of IRFs were averaged to estimate each parameter. Main peak grows linearly together with input power. Since noise level is flat on input power, from the first view it looks easy to improve SNR by increasing transmit power of radar device. However, we cannot increase transmit power endlessly. Limiting factor is that with increasing received power radar receiver becomes saturated and thus it works in nonlinear mode. In practice it means that received signal becomes distorted in an unpredictable way and it is hard to speak about detecting useful signal under such conditions. The state when radar receiver becomes nonlinear is characterized by 1 dB compression point (1 dB compression in comparison with linear dependency) In figure 6.3 this point is denoted as CP1dB. Of course when developing the radar one should try to keep transmit power as high as possible given that system remains in linear mode.

If we take into account that due to averaging noise level is 30 dB lower in figure 6.3 than it actually was we can state that SNR of the radar unit used in this work is about 80 dB with maximal update rate possible (67 IRFs per second). Due to additional averaging it becomes 97 dB if we collect 1 IRF per second.

One should also take into account that useful signal is often not the reason for saturating receiver since there are stronger parasitic signal components that determine the received power. In case their contribution is minimized one can improve SNR by transmitting stronger signal. Usually the strongest of parasitic contributors is antenna crosstalk-- direct wave between transmitting and receiving antenna. Crosstalk can be weakened via choosing antennas of the proper types, by placing absorbing materials between and around them, or by separating transmitter and receiver by larger distance. (the latter, however, weakens useful signal as well at least in some scenarios).

Besides, when developing or choosing the radar one should take care of course about how much noise is added on the receiver part of radar electronics. Noise figure is one of the key radar parameters and it has to be kept as low as possible.

Minor motion detectability can also be improved due to increasing recording time (followed by proper type of averaging) in case motion happens at the same place and for long. Significant part of this work is about how exactly it can be done and what are the consequences. However, in real radar systems amount of data that could be averaged is reduced because of using subsampling.

Let us briefly introduce it. Since probing signal is sent repeatedly, we can take one sample from first received signal, the second from another and so on and after that to reconstruct one IRF. Working without subsampling (reconstructing one IRF per one probing signal sent) means using very fast and expensive electronics and thus, in practice subsampling is widely applied.

Potential SNR increase in case of practical realization of a radar as used in this work without subsampling is significant: 511 averages, or 27 dB in SNR. Very roughly we can think of 1 dB as of 1 centimetre of rubble material in terms of detection range. Potential SNR rise due to other hardware-related aspects mentioned above seem to be less (in the order of several dB). However, in total potential gain due to hardware development is huge: it is not less than several dozens of centimetres in detection range.

If we speak about how much SNR is increased by algorithms, 27 dB is in ideal case approximately equivalent to SNR improvement due to calculating horizontal spectrum (with typical recording time of one minute and typical sampling speed of 10 IRFs per second) with state-of the art radar in use. Other data processing approaches, like

averaging in propagation time, bring ideally several dB more. However, we can state that unlike in case of hardware there seems to be no much space left for increasing the detection range by using newer algorithms. But we should remember of course that even small advance can save somebody's life.

If we speak about increasing detection range when non-stationary clutter is present software and hardware methods can bring essential gain of one meter and more. Yet,, this is an increase from zero level since as we have seen non-stationary clutter can destroy radar ability to see respiratory motion almost completely.

It should also be mentioned that SNR improvements by hardware and software modifications are additive. Besides, algorithms described in this work are not firmly connected to specific radar or radar type; they are applicable in combination with any UWB device.

## Summary

In this work, all essential software aspects of the detection of human being beneath rubble are considered: SNR enhancement due to signal periodicity and due to respiration signature being range-spread, stationary and non-stationary clutter removal and localization.

In the beginning, necessary conditions for detecting minor motion by means of UWB radar are formulated. One of such conditions is low jitter level and in order to fulfill this requirement M-sequence radar was used in the experimental part of this work. Original prove of M-sequence radar having low jitter level is given. It is derived that the weakest target shift detectable with the radar system used in this work is below ten micrometers, which makes it possible to detect even very slight respiratory activity.

It should be noted that signal enhancement and localization methods were not developed specifically for M-sequence radar and they would perform with approximately equal quality independently of the type of UWB radar in use.

After discussing general sensitivity of the radar device to minor motion, respiratory signature within radargram is considered theoretically. Breathing activity appears in the radar data as a very specific pattern which pattern is distinct from typical noise and clutter signals. Model of respiratory motion allowed discovering and analyzing harmonics of type two that appear in the radar data at nonlinear parts of the signal pulse. It is shown that in case of weak single tone breathing Fourier transform yields optimal signal processing with respect to enhancing useful signal due to its periodicity. Typical deviations of breathing signal from being stationary single-tone periodical are found in measured radar data. In this context Welch periodogram and bispectrum slice method are proposed as alternatives to Fourier transform.

In the part of denoising due to integration in propagation time, optimal data processing by correlation detector is considered in two ways. First, as a theoretical border of SNR improvement that cannot be reached by other methods. Second, as a viable data processing technique in case reference main tone respiration signature can be evaluated in some way. Besides, original method for respiratory signature enhancement is proposed. The method is based on the specific properties of slow-time cross-correlation functions that allow us to take advantage of coherence existing between respiratory periodicals. It is shown by means of theoretical considerations that slow-time cross-correlation function method outperforms its competitor, incoherent summation in all possible cases.

Proposed SNR-improving methods are compared with one another and state of the art technique via processing diverse simulated datasets and measured data. Simulations are carried out for different SNR levels and they are repeated many times in order to make comparison of different methods statistically significant. Simulations confirm all theoretical predictions about cross-correlation detector, slow time cross-correlation functions method and incoherent summation.

Besides, SNR improvement via modified Welch method in combination with slow-time cross-correlation function method is implemented in the measurement software for online breathing detection. In the field tests by using this software it was possible to detect breathing person reliably through 1.3 meters of diverse rubble mainly consisted of reinforced concrete.

Non-stationary clutter (strongly moving unwanted object in the radargram) can be considered as a critical limiting factor for the breathing-detecting radar. In this work for removing non-stationary clutter two original algorithms are proposed. Both of them rely on the simple idea that clutter usually appears outside frequency window of breathing and make use of adaptive data processing to get clutter estimate from measured radargram by analyzing its slow version. Performance of both methods is evaluated by means processing measured and simulated radar data. Comparison with state of the arts method is given.

Ability to provide information about the position of a victim due to his/her respiratory activity is the main advantage of UWB radar in rescue scenario. In this work simple method of localizing the victim is proposed. In practice, this method allowed successful localization of a person in radar data through more than one meter of reinforced concrete.

## List of symbols

In this work following notation was used: italic ( $Z$ )-- variables of continuous quantities; bold( $\mathbf{Z}$ )-- variables of discrete quantities(matrix, vector); underlined ( $\underline{Z}$ )—complex-valued quantities; ( $\hat{Z}$ )— randomized variables (influenced by random perturbations).

$A(t)$  -- Probing signal generated by radar electronics

$A_0$  -- Zero term coefficient in Taylor series approximating respiration-caused pulse variation

$A_1$  -- First term coefficient in Taylor series approximating respiration-caused pulse variation

$A_2$  -- Second term coefficient in Taylor series approximating respiration-caused pulse variation

$B_1(t)$  -- Impulse response function of antenna in receive mode

$B_2(t)$  -- Impulse response function of antenna in transmit mode

$B$  -- Frequency bandwidth

$B_r$  -- Frequency bandwidth of antennas

$C(t)$  -- Impulse response function that characterizes reflection from the object

$c$  -- Speed of light

$d$  -- Varying part of the distance between antenna system and target ( $r - r_0$ )

$\Delta d$  -- Pulse shift expressed as a distance

$d_k$  -- Amplitudes of harmonic components in respiratory motion

$d_{t1}$  -- Amplitude of the main tone of respiratory motion used in simulation

$d_{t2}$  -- Amplitude of the first-type harmonic of respiratory motion used in simulation

$D$  -- Amplitude of the main tone of respiration

$DSNR_0$  -- 'Differential' SNR of moving object without blockwise averaging

$DSNR_{ba}$  -- 'Differential' SNR of moving object after blockwise averaging

$E_s$  -- signal energy

$E_n$  -- noise energy

$E_t$  -- total signal energy in main-tone respiration signature

$E_m$  -- signal energy at one time instant in main-tone respiration signature maximal with respect to other time instants

$f$  -- Frequency (in fast time direction)

$f_{ad}$  -- Adjusting function in modified Welch method

$f_G$  -- Gaussian wavelet

$g_f$  -- Filtering function to match antenna frequency bandwidth with frequency bandwidth of radar device

$G$  -- Horizontal bispectrum

$h = \xi_{ver}$  -- Coordinate of the vertex of parabola in Taylor series approximation of reflected pulse

$\underline{H}_{SVD}$  -- Estimate of non-stationary clutter as a combination of maximal principal components of the horizontal spectrum

$\underline{H}_{SVD2}$  -- Estimate of non-stationary clutter as a projection of original horizontal spectrum onto clutter components located in slow radargram

$I$  -- Spatial image of breathing person calculated from the radargram

$j$  -- Number of particular singular value (and corresponding principal component)

$J$  -- Total number of principal components that need to be considered to find respiratory motion

$k$  -- Sinusoidal micro Doppler rate index

$k_\sigma$  -- Number of standard deviations in tolerance interval

$k_d$  -- Signal 'degradation' coefficient  
 $k_r$  -- Ratio between signal energies of the samples in two-point pulse  
 $K_{CC/IS}$  -- SNR outperformance of cross-correlation method over incoherent summation  
 $K_{CD/\max}$  -- SNR outperformance of correlation detector method over maximum search  
 $l$  -- Propagation time index  
 $L$  -- Maximal propagation time index  
 $L_m$  -- Amount of attenuation between transmitting and receiving channel of the radar device  
 $m$  -- Observation time index  
 $M$  -- Maximal observation time index  
 $M_c$  -- Number of principal components used to estimate clutter  
 $M_d$  -- Number of 'deterministic' principal components in simulated  
 $n_T$  -- Thermal noise in the radargram  
 $n_q$  -- Quantization noise in the radargram  
 $n$  -- Total additive noise in the radargram  
 $n_{cl}$  -- Non-stationary clutter in the radargram  
 $n_1$  -- Noise at the first instant of two-point pulse  
 $n_2$  -- Noise at the second instant of two-point pulse  
 $N_T$  -- Number of transitions in M-sequence  
 $N_M$  -- M-sequence length  
 $N_e$  -- Number of experiments(simulations)  
 $N_d$  -- Number of successful detections  
 $P$  -- Number of blocks when using blockwise averaging  
 $P_d$  -- Probability of detection  
 $q$  -- Position index in main tone respiration signature  
 $Q$  -- Size of a block when using blockwise averaging  
 $Q$  -- Size of main tone respiration signature  
 $r$  -- Distance between antenna system and target  
 $r_u$  -- Radar unambiguous range  
 $r_0$  -- Distance between antenna system and target at the beginning of observation  
 $r_i$  -- Distance between one of the antennas and target  
 $\underline{R}$  -- Main tone respiration signature  
 $s$  -- Velocity of the moving object  
 $s_0$  -- Object velocity in case of forward motion  
 $S$  -- Diagonal matrix of singular values  
 $S_{i,i}$  -- Singular value  
 $SNR_0$  -- SNR of static object without averaging  
 $SNR_a$  -- SNR of moving object after averaging when aligning was used  
 $SNR_{FFT}$  -- SNR of respiration after horizontal FFT  
 $SNR_{CD}$  -- SNR of respiration after using correlation detector  
 $SNR_{CC}$  -- SNR of respiration after using cross-correlation method  
 $SNR_{IS}$  -- SNR of respiration after using incoherent summation  
 $SNR_m$  -- SNR of respiration without signal enhancement due to respiration signature elongation (only maximum search)

$t$  -- Propagation time (fast time)  
 $\Delta t$  -- Propagation time sampling interval  
 $t_c$  -- Length of the elementary chip of M-sequence  
 $t_w$  -- (Gaussian) pulse width  
 $t_s$  -- Time shift  
 $t_p$  -- Pulse duration  
 $t_m$  -- Instant when pulse reaches it maximum  
 $t_e$  -- Instant on the pulse edge  
 $t_r$  -- Pulse rise time  
 $t_0$  -- Fixed instant of  $t$   
 $t_{\min}$  -- Lower border of propagation time interval for the pulse reflected from the moving chest.  
 $t_{\max}$  -- Upper border of propagation time interval for the pulse reflected from the moving chest.  
 $T_p$  -- Period of radar pulse in the pulse train  
 $U$  -- Matrix of eigenimages  
 $u_i$  -- eigenimage  
 $v_i$  -- principal component  
 $V$  -- Matrix of principal components  
 $\Delta V$  -- M-sequence 'amplitude'  
 $V_G$  -- Maximal value of the Gaussian pulse  
 $w_m$  -- windowing function (Welch method)  
 $w$  -- windowing function in propagation time  
 $W$  -- Radargram (consisted of IRFs) without additional data processing  
 $W_s$  -- Radargram, shifted to the target position  
 $W_{rb}$  -- Radargram, after removing stationary background  
 $W_{st}$  -- Estimate of stationary clutter in the radargram  
 $W_f$  -- Radargram, after vertical filtering (after matching the bandwidth of measured signal to the operational bandwidth of antenna system) and removing stationary background  
 $W_{SVD}$  --  $W_f$ , after using SVD-based reference algorithm for denoising and clutter removal  
 $W_l$  -- Radargram part that depends linearly on respiration-caused motion  
 $W_{nl}$  -- Radargram part that depends nonlinearly on respiration-caused motion  
 $W_{low}$  -- Slow part of the radargram that contains non-stationary clutter  
 $W_{f0}$  -- Radargram after its 'cluttered' regions are set to zero due to big variations in  $W_{low}$   
 $W_{SVD2}$  -- Radargram after non-stationary clutter is removed by using SVD of  $W_{low}$   
 $W_{ba}$  -- Radargram, averaged blockwisely in horizontal direction  
 $W_M$  -- Probing signal of M-sequence radar  
 $W_a$  -- Aligned radargram  
 $W_1$  -- Particular example of a radargram  
 $W_2$  -- Particular example of a radargram  
 $(x, y, z)$  -- Cartesian coordinates of the target  
 $X_M$  -- Received signal of M-sequence radar after pulse compression  
 $X_G$  -- Received signal of (Gaussian) pulse radar  
 $X_1$  -- Particular example of an IRF



$X_2$  -- Particular example of an IRF  
 $Y_{WVD}$  -- Wigner-Ville distribution of the radargram  
 $z_1$  -- Signal at the first instant of two-point pulse  
 $z_2$  -- Signal at the second instant of two-point pulse  
 $\underline{Z}$  -- Horizontal FFT spectrum of the radargram  
 $\underline{Z}_f$  -- Horizontal FFT spectrum of filtered radargram  
 $Z_w$  -- Horizontal spectrum that we get by Welch method  
 $Z_{CD}$  -- Horizontal spectrum after applying correlation detection  
 $Z_{IS}$  -- Horizontal spectrum after applying incoherent summation  
 $Z_{CC}$  -- Horizontal spectrum after applying cross-correlation data processing  
 $Z_{SVD}$  -- Horizontal spectrum after using SVD-based reference algorithm for denoising and clutter removal  
 $Z_B$  -- Horizontal spectrum that we get by using bispectrum-slice method  
 $Z_{MW}$  -- Horizontal spectrum that we get by (modified) Welch method  
 $\underline{Z}_{low}$  -- Horizontal spectrum after low-pass horizontal filtering  
 $\underline{Z}_{cl}$  -- Horizontal spectrum of non-stationary clutter estimate  
 $\underline{Z}_p$  -- Horizontal spectrum of the p-th segment of the radargram  
 $\underline{Z}_{f0}$  -- Horizontal spectrum of the radargram after its 'cluttered' regions are set to zero due to big variations in corresponding regions of slow part of the radargram  
 $\underline{Z}_{SVD2}$  -- Radargram horizontal spectrum where clutter estimate  $\underline{H}_{SVD2}$  is subtracted  
  
 $\beta$  -- ratio between the absolute values of maximal signal pixel and maximal noise pixel  
 $\Gamma_i$  -- geometry matrix used for localization of breathing person  
 $\varepsilon$  -- dielectric permittivity of the medium  
 $\nu$  -- Sinusoidal micro Doppler rate  
 $\nu_0$  -- Breathing rate  
 $\nu_s$  -- Sampling rate in horizontal direction  
 $\nu_{t1}$  -- Frequency of the main tone of respiratory motion used in simulation  
 $\nu_{t2}$  -- Frequency of the first-type harmonic of respiratory motion used in simulation  
 $\xi$  -- Respiration-caused pulse position variation  
 $\sigma_T$  -- Thermal noise standard deviation  
 $\sigma_q$  -- Quantization noise standard deviation  
 $\sigma$  -- Total additive noise standard deviation  
 $\sigma_j$  -- Jitter standard deviation  
 $\tau$  -- Observation time (slow time)  
 $\Delta\tau$  -- Observation time sampling interval  
 $\tau_{obs}$  -- Duration of the whole observation time interval  
 $\varphi_k$  -- Initial phases of harmonic components in respiratory motion  
 $\chi$  -- M-sequence order  
 $\Delta\psi$  -- Sampling jitter  
 $\omega$  -- Sinusoidal micro Doppler rate (angular)

## Reference list

- [1] Aftanas, M. ; Crabbe, S. ; Drutarovsky, M. ; Klukas, R. ; Kocur, D. ; Nguyen, T.T. ; Peyerl, P. ; Rovnakova, J. ; Zaikov, E., Detection and tracking of moving or trapped people hidden by obstacles using ultra-wideband pseudo-noise radar, *Proceedings of European Radar Conference, 2008.( EuRAD 2008)*, pp. 408—411, ISBN: 978-2-87487-009-5, Amsterdam, Netherlands, October 2008, IEEE
- [2] Arai, I. (2001). Survivor search radar system for persons trapped under earthquake rubble, *Proceedings of APMC 2001*, pp 663-668 vol.2, ISBN: 0-7803-7138-0, Taipei, Taiwan, December 2001
- [3] Barkat M., "Signal Detection and Estimation", ISBN: 978-1580530705, Artech House; 2nd edition, 2005.
- [4] BBC, 2012, "Earthquake rescue: How survivors are found"; <http://news.bbc.co.uk/2/hi/americas/8459653.stm>
- [5] Bechtel Special Technologies Laboratory Ground Penetrating Radar (STL GPR) (2003). Operational Test and Evaluation Report of Ground Penetrating Radar for Casualty Location in Rubble, November 2003
- [6] BOS - Sondermaschinenbau GmbH. Locate to Live — Save of Live (Bioradar BR402) <http://www.bos-berlin.de/en/products-technologies/safety-equipment/bioradar.html>
- [7] Chernyak, V. (2006). Signal Processing in Multisite UWB Radar Devices for Searching Survivors in Rubble, *Proceedings of EuRAD 2006*, pp. 190 - 193, ISBN: 2-9600551-7-9, Manchester, September 2006
- [8] Geophysical Survey Systems, Inc. (2005). Technical Note 103: Using the SIR-3000 as a Breathing Detector with the “Breathe” Setup, February 2005
- [9] Haddad, W.S., "The Rubble Rescue Radar (RRR): A low power hand-held microwave device for the detection of trapped human personnel", 1997, Technical report of Lawrence Livermore National Lab., CA (United States)
- [10] Hock Kai M., “Narrowband Weak Signal Detection by Higher Order Spectrum”, *Signal Processing, IEEE Transactions on*, vol. 44, no. 4, April 1996
- [11] Knott E. F., "Radar Cross Section," in *Radar Handbook*, edited by Skolnik M. I., McGraw-Hill, New York, 1990, Chapter 11
- [12] Lai, J.C.Y.; Ying Xu; Gunawan, E.; Chua, E.C.; Maskooki, A.; Yong Liang Guan; Kay-Soon Low; Cheong Boon Soh and Chueh-Loo Poh, "Wireless Sensing of Human Respiratory Parameters by Low-Power Ultrawideband Impulse Radio Radar", *Instrumentation and Measurement, IEEE Transactions on*, vol. 60, no. 3, pp. 928-938, 2011
- [13] Levitas, B. & Matuzas, J. (2006). UWB Radar for Human Being Detection Behind the Wall, *Proceedings of IRS 2006*, pp. 1 - 3, ISBN: 978-83-7207-621-2, Krakow, Poland, May 2006

- [14] Levitas, B. Matuzas, J. & Drozdov, M. (2008). Detection and separation of several human beings behind the wall with UWB Radar, *Proceedings of IRS 2008*, pp. 1 - 4, ISBN: 978-83-7207-757-8, Wroclaw, Poland, May 2008
- [15] Lidicky, L. (2008). Fourier Array Processing for Buried Victims Detection Using Ultra Wide Band Radar with Uncalibrated Sensors, *Proceedings of Geoscience and Remote Sensing Symposium, 2008. IGARSS 2008. IEEE International*, pp. II-831 - II-834, ISBN: 978-1-4244-2807-6, Boston, MA, July 2008
- [16] Lin Yaying; Jianchao Yao and Yap-Peng Tan (2010). Respiratory rate estimation via simultaneously tracking and segmentation, *Proceedings of Computer Vision and Pattern Recognition Workshops (CVPRW), 2010 IEEE Computer Society Conference on*, pp. 170 - 177, ISBN: 978-1-4244-7029-7, San Francisco, CA, June 2010
- [17] Loschonsky, M.; Feige, C.; Rogall, O.; Fisun, S. and Reindl, L.M.; (2009). Detection technology for trapped and buried people, *Proceedings of Wireless Sensing, Local Positioning, and RFID, 2009. IMWS 2009. IEEE MTT-S International Microwave Workshop on*, pp. 1 - 6, ISBN: 978-1-4244-5060-2, Cavtat, Croatia, September 2009
- [18] S.L. Marple, Jr, *Digital Spectral Analysis with Applications*, Prentice-Hall, Englewood Cliffs, NJ 1987.)
- [19] Narayanan, R.M. (2008). Through wall radar imaging using UWB noise waveforms, *Proceedings of ICASSP 2008*, pp. 5185 - 5188, ISBN: 978-1-4244-1483-3, Las Vegas, NV, April 2008
- [20] A. Nezirovic, A. G. Yarovoy, and L. P. Ligthart, "Signal Processing for Improved Detection of Trapped Victims Using UWB Radar", *Geoscience and Remote Sensing, IEEE Transactions on*, vol. 48, no. 4, pp. 2005-2014, 2010.
- [21] Ossberger, G.; Buchegger, T.; Schimback, E.; Stelzer, A. & Weigel, R., Non-Invasive Respiratory Movement Detection and Monitoring of Hidden Humans Using Ultra Wideband Pulse Radar, *Proceedings of the International Workshop on Ultrawideband Systems and Technologies*, pp. 395-399, ISBN: 0-7803-8373-7, May 2004
- [22] J. Sachs, M. Helbig, R. Herrmann, M. Kmec, K. Schilling, E. Zaikov Trapped Victim Detection by Pseudo-Noise Radar, *ACWR '11 Proceedings of the 1st International Conference on Wireless Technologies for Humanitarian Relief ACWR '11*, pp. 265—272, ISBN: 978-1-4503-1011-6, 2011
- [23] Sachs J., "Handbook of Ultra-Wideband Short-Range Sensing", ISBN 978-3-527-40853-5, Wiley-VCH; 1st edition, 2012.
- [24] J. Sachs, M. Helbig, R. Herrmann, M. Kmec, K. Schilling, E. Zaikov. "Remote vital sign detection for rescue, security, and medical care by ultra-wideband pseudo-noise radar" *Ad Hoc Networks, Part A((1)Special Issue : Wireless Technologies for Humanitarian Relief & (2)Special Issue: Models And Algorithms For Wireless Mesh Networks)*, vol.13, part A, pp. 42–53, 2014

- [25] UltraVision Security Systems, Inc. Product Backgrounder: LifeLocator™  
[http://www.imrex.sg/phpform/use/AddaProduct/files/UVSS\\_LifeLocatorBrochure.pdf](http://www.imrex.sg/phpform/use/AddaProduct/files/UVSS_LifeLocatorBrochure.pdf)
- [26] United States Geological Survey 2014, "Earthquakes with 1,000 or More Deaths since 1900", [http://earthquake.usgs.gov/earthquakes/world/world\\_deaths.php](http://earthquake.usgs.gov/earthquakes/world/world_deaths.php)
- [27] Wei Chong Yu and Wang Da Quan. (2010). On the Signal Processing in the Life-Detection Radar Using an FMCW Waveform, Proceedings of Information Processing (ISIP), 2010 Third International Symposium on, pp. 213 - 216, ISBN: 978-1-4244-8627-4, Qingdao, China, October 2010
- [28] Yarovoy, A.G. & Ligthart, L.P. (2007). UWB Radars: Recent Technological Advances and Applications, Proceedings of Radar Conference, 2007 IEEE, pp. 43 - 48, ISBN: 1-4244-0284-0, Boston, MA, April 2007
- [29] Zaikov, E.; Sachs, J.; Aftanas, M.; & Rovnakova J. (2008). Detection of trapped people by UWB radar, German Microwave Conference, GeMiC 2008, pp 240-243, ISBN: 978-3-8007-3086-5, Hamburg, Germany, March 2008
- [30] Zaikov, E. and Sachs, J., "UWB radar for detection and localization of trapped people," In book: *Ultra Wideband*, B. Lembrikov, ed., Rijeka, Croatia: Sciyo, 2010.
- [31] E. Zaikov: UWB radar for detection and localization of trapped people, *Proceedings of 11th International Radar Symposium (IRS), 2010*, pp. 1—4. ISBN: 978-1-4244-5613-0, Vlinius, Lithuania, June 2010, IEEE
- [32] E. Zaikov. "M-Sequence Radar Sensor for Search and Rescue of Survivors Beneath Collapsed Buildings" In book: *Handbook of Ultra-Wideband Short-Range Sensing: Theory, Sensors, Applications*, pp.745—762, Editors: J. Sachs, Wiley-VCH, 2012
- [33] Zakrzewski, M. and Vanhala, J.; (2010). Separating respiration artifact in microwave doppler radar heart monitoring by Independent Component Analysis, Proceedings of Sensors, 2010 IEEE, pp. 1368 - 1371, ISBN: 978-1-4244-8170-5, Kona, HI, November 2010
- [34] Zhang Yang; Jing Xijing; Jiao Teng; Zhang Zhu; Lv Hao and Wang Jianqi. (2010). Detecting and Identifying Two Stationary-Human-Targets: A Technique Based on Bioradar, *Proceedings of Pervasive Computing Signal Processing and Applications (PCSPA), 2010 First International Conference on*, pp. 981 - 985, ISBN: 978-1-4244-8043-2, Harbin, China, September 2010
- [35] A. Nezirovic (2010) Trapped-victim Detection in Post-Disaster Scenarios using Ultra-Wideband Radar. PhD thesis, Delft University of Technology
- [36] B. Karlsen, J. Larsen, K. Jakobsen, H. Sorensen and S. Abrahamson: Antenna characteristics and air-ground interface deembedding methods for stepped-frequency ground penetrating radar measurements. *In Proc. of SPIE, Aero- Sense 2000*, vol. 4038, April 2000

- [37] T. Thayaparan, S. Abrol and E. Riseborough, Micro-Doppler radar signatures for intelligent target recognition, *Defence R&D Canada-Ottawa, TECHNICAL MEMORANDUM*, DRDC Ottawa TM 2004-170, September 2004; <http://www.dtic.mil/dtic/tr/fulltext/u2/a427483.pdf>
- [38] J.Sachs, R.Herrmann, M-sequence-based ultra-wideband sensor network for vitality monitoring of elders at home, *IET Radar, Sonar & Navigation*, vol. 9 no. 2, pp. 125-137, 2015